

**Dynamic Behavior of Primary Structures attached with
Flexibly Connected Secondary Systems**

THESIS

Submitted in partial fulfilment
of the requirements for the degree of

DOCTOR OF PHILOSOPHY

by

**CHALLAGULLA SURYA PRAKASH
2015PHXF0407H**

Under the Supervision of
Dr. Chandu Parimi




BITS Pilani
Pilani | Dubai | Goa | Hyderabad

**BIRLA INSTITUTE OF TECHNOLOGY AND SCIENCE,
PILANI
2020**

BIRLA INSTITUTE OF TECHNOLOGY AND SCIENCE, PILANI

CERTIFICATE

This is to certify that the thesis titled **Dynamic Behavior of Primary Structures attached with Flexibly Connected Secondary Systems** and submitted by **Challagulla Surya Prakash**, ID. No. **2015PHXF0407H** for award of Ph.D. of the Institute, embodies original work done by him under my supervision.

Signature of the Supervisor: 

Name in capital letters: Dr. CHANDU PARIMI

Designation: Assistant Professor

Date: 16-10-2020

Acknowledgements

Words cannot express my thanks to all those who contributed to the success of this study and made this journey an unforgettable experience for me. Nevertheless, here is an effort.

Firstly, I express my honest appreciation for my supervisor **Dr. Chandu Parimi**, who provided inspiration throughout my research work. His experience in the industry helped me formulate a relevant problem statement in the area of nuclear power. I offer him my sincere gratitude for his continuous support, patience, motivation, and his immense knowledge.

I also thank my Doctoral Advisory Committee members; **Dr. Mohan S.C.** and **Dr. Arkamitra Kar** not only for their insightful comments and encouragement, but also for their hard questions, which helped me to widen my perspective. I thank the present DRC Convener, **Dr. Prasanta Kumar Sahu**, and former DRC Conveners, **Dr. Anasua GuhaRay** and **Dr. Murari R.R. Varma** for their valuable suggestions and encouragement throughout my doctoral studies.

I offer my humble regards to **Prof. Sridhar Raju**, current HOD and **Prof. Jagadeesh Anmala**, former HOD, Department of Civil Engineering, BITS Pilani, Hyderabad Campus for permitting me to carry out my research work and providing facilities in the department.

I have a deep sense of gratitude towards **Prof. G. Sundar**, Director, BITS Pilani, Hyderabad campus and to **Prof. Souvik Bhattacharya**, Vice Chancellor, BITS Pilani for giving me this opportunity and for providing research facilities that offered an excellent platform for undertaking doctoral work.

I am thankful to **Prof. Vamsi Krishna V**, current Associate Dean, AGSRD, **Prof. Vidya Rajesh**, former Associate Dean, ARD, BITS-Pilani, Hyderabad campus for their continuous support throughout the tenure of my doctoral work.

I would like to acknowledge the support and suggestions received from **Prof. Vasan** from the early days of my research. I offer my sincere thanks to the **all the faculty members** of the Department of Civil Engineering, BITS-Pilani, Hyderabad campus for their kind support and assistance.

I am thankful to **Dr. Vikranth Kumar S** for offering the software facilities in the Central Computing Laboratory, BITS-Pilani, Hyderabad campus. I would like to extend my thanks to **Mr. Ramachandra Sharma**, and **Mr. Vamsi** (CAD lab) for their support during software installation and laboratory-related tasks. I would also like to thank **Mr. P. Hemanth Kumar**, **Mr. Basha**, and **Mr. Shankar** for their assistance during the various laboratory sessions and department related tasks.

I thank **Dr. Kalyana Rama J.S.**, and **Mr. Prakash Mohan M.M** for their support and cooperation since my early days of research. I would also like to thank **Mr. CH.B.V.Hareen**, and **Mr. U. Rama Krishna** for their valuable technical inputs and suggestions while carrying out this work.

I also offer my sincere gratitude to **Dr. Mohan S.C** for his valuable inputs and suggestions in numerical analyses, **Prof. Jagadeesh Anmala** for his guidance in using artificial neural networks in this study and **Prof. P.K.Thiruvikraman** for support with MATLAB coding. I would also like to acknowledge **Dr. Ehsan Noroozinejad Farsangi** for his insights and collaboration.

I am grateful for the work and inputs from **Mr. Ranjit Patil**, and **Mr. Ajinkya Naringe**. I would also like to thank **Mr. Akhil**, **Mr. Ramsagar M**, **Mr. Pradeep**

Reddy S, Mr. Bhargav M, and Mr. Pritish Dey Sarkar for their assistance with the numerical studies.

I offer my heartfelt appreciation to all my friends- they have been more than family during my doctoral time. My sincere thanks to **Mr. Ashok Kumar S, Mr. Naveen Naidu M, Mr. Jayateja M, Mr. Zoheb Nawaz, Mrs. Vineesha Ch, Mrs. Swathi M, Mrs. Madhuri R, Mr. Syed Mazhar,** and **Mr. Vamsi I.** for their infinite support and cooperation. I express my warm thanks to all my Ph.D. colleagues at BITS Pilani, Hyderabad campus who have made my doctoral journey an enjoyable and memorable experience. Though I am not mentioning all the names, I am very grateful to all my friends for their intensive care and moral support.

I would like to thank my well-wisher, **Dr. V Ramesh,** V.R. Siddhartha Engineering College, for mentoring me towards research and his continuous enquiry about the work.

I owe thanks to a very special person, my wife, **Mounika** for her continued and unflinching love, support and understanding during my pursuit of Ph.D. degree that made the completion of my thesis possible. She was always around at times I thought that it is impossible to continue, she helped me to keep things in perspective. I greatly value her contribution and deeply appreciate her belief in me. My heartfelt regard goes to my father-in-law, **Venkateswarlu Manne** mother-in-law, **Leelavathi Manne** for their love and moral support.

Finally, this would be incomplete without acknowledging my parents, **Smt. Nirmala Challagulla & Shri. Murali Srinivasa Rao Challagulla,** for showing faith in me and giving me the liberty to choose what I desired. I salute them for the selfless love, care, pain and sacrifices they made to shape my life. Although they hardly understood my research, they were willing to support any decision I made. I would never be able to

pay back the love and affection showered upon me by my parents. I also express my thanks to my sister, **Bhavani V** and brother in law, **Hari Krishna V** for their support and valuable prayers.

I thank the **God Almighty** for giving me the strength and patience to work through all these years so that today I can stand proudly with my head held high.

ABSTRACT

The object of this thesis was to investigate the effect of Non-Structural Components (NSCs) on the dynamic behavior of a primary structure (PS) under harmonic and earthquake excitations. In this thesis, the NSCs were classified into two types, namely, hanging NSCs, and multiple sliding NSCs. Again, multiple sliding NSCs were divided into the multiple bodies resting side-by-side and one over the other in the form of stacks. An analytical model of the hanging NSC and the single-degree-of-freedom (SDOF) structure was used to demonstrate the structure's performance under harmonic and earthquake excitations. In this study, hanging NSC was termed as flexibly attached secondary system (FSS). An FSS affects the main structure during ground excitation differently than a secondary system that is rigidly attached to it. The equations of motion describing the behavior of the PS and the FSS were derived by considering small displacements in the FSS. Mass ratio, tuning frequency ratio, and excitation frequency ratio were considered to study their effect on the dynamic behavior of the PS. The dynamic response of the structure was found to be independent of the mass ratio at a low tuning frequency ratio of FSS. A methodology was presented to estimate the spectral acceleration of the primary structure with FSS. Using statistical non-linear regression (NLR) and artificial neural network (ANN), an expression was developed to calculate the spectral acceleration of such a structure.

The seismic behavior of the SDOF structure with multiple sliding NSCs was also investigated in this thesis. Sliding NSCs were termed as secondary bodies (SBs). Governing equations of motion were derived for the structure and multiple SBs that were side-by-side and one over the other (in the form of stacks) by considering the Coulomb's friction model. The analysis was limited to a linear elastic SDOF structure with two sliding SBs. The model developed in this study of the SDOF structure with the sliding SBs was validated with a Finite Element (FE) model. Two Indian seismic hazard levels were considered consistent with the medium (Zone III) and highest (Zone V) conditions. A parametric study was performed to analyze the variation in the displacement of the structure by varying the structural period, the mass ratio, and coefficients of friction. The results demonstrate that multiple sliding bodies resting side-by-side on the structure with the same coefficients of friction were shown to behave identically to a single body with their combined mass. In the case of a structure with stacked sliding secondary bodies, the displacement estimates of the structure were found to be conservative if the energy dissipation due to friction within the stack was neglected. A novel methodology was proposed to calculate the modified structural period (T_{new}) with such secondary bodies. Finally, design equations were proposed to determine the T_{new} as a function of structural period, mass ratios, and coefficients of friction by means of an NLR and ANN. Further study on the performance of NSCs on the dynamic response of multi-degree-of-freedom structures is required before the implementation of design expressions for actual structures.

DECLARATION

I certify that

- a. The work contained in the thesis is original and has been done by me under the guidance of my supervisor;
- b. The work has not been submitted to any other Institute for any degree or diploma;
- c. I have followed the guidelines provided by the Institute in preparing the thesis;
- d. I have conformed to ethical norms and guidelines while writing the thesis and;
- e. Whenever I have used materials (data, figures, and text) from other sources, I have given due credit to them by citing them in text of the thesis, and taking permission from the copyright owners of the sources, whenever necessary.

Challagulla Surya Prakash

TABLE OF CONTENTS

| | |
|---|-------------|
| Acknowledgements | iii |
| Abstract | vii |
| Declaration | viii |
| Table of Contents | ix |
| List of Tables | xiii |
| List of Figures | xv |
| List of symbols and abbreviations | xx |
| 1 Introduction | 1 |
| 1.1 Background of the Work | 1 |
| 1.2 Objectives of the Study | 6 |
| 1.3 Methodology Adopted for the Study | 7 |
| 1.4 Scope of the Study | 9 |
| 1.5 Organization of the Thesis | 10 |
| 2 Literature Review | 11 |
| 2.1 Introduction | 12 |
| 2.2 Non-Structural Components | 12 |
| 2.2.1 Hanging Non-Structural Components (NSCs) | 16 |
| 2.2.2 Influence of hanging NSCs on the structural seismic response | 18 |
| 2.2.3 Sliding Non-Structural Components (NSCs) | 24 |
| 2.2.4 Influence of sliding NSCs on the structural seismic response | 29 |
| 2.3 Summary from literature review and limitations of existing research | 33 |
| 2.4 Research Significance | 34 |
| 2.5 Summary | 34 |
| 3 Hanging Non-Structural Components | 35 |

| | | |
|----------|---|-----------|
| 3.1 | Analytical Model Hanging NSC and SDOF Structure | 35 |
| 3.1.1 | The SDOF Structure | 35 |
| 3.1.2 | Hanging NSC | 36 |
| 3.1.3 | Combined Model for Structure and Hanging NSC | 38 |
| 3.1.4 | Validation of the Model | 42 |
| 3.2 | Dynamic response of a SDOF structure coupled with hanging NSC under Harmonic Excitations | 43 |
| 3.2.1 | Effect of excitation frequency ratio | 45 |
| 3.2.2 | Effect of tuning frequency ratio | 46 |
| 3.2.3 | Effect of mass ratio | 47 |
| 3.2.4 | Mass effect ratio | 48 |
| 3.3 | Dynamic response of a SDOF structure coupled with hanging NSC under Earthquake Excitations | 51 |
| 3.3.1 | Effect of tuning frequency ratio | 53 |
| 3.3.2 | Effect of mass ratio | 55 |
| 3.4 | Effect of hanging NSC on the design response spectrum | 56 |
| 3.4.1 | Methodology to determine the modified spectral acceleration for the structure | 61 |
| 3.4.2 | Effect of the mass ratio and tuning frequency ratio | 63 |
| 3.4.3 | Validation of the proposed design methodology | 68 |
| 3.4.4 | Design expressions to determine the spectral acceleration of the structure by Non-Linear Regression (NLR) and Artificial Neural Network (ANN) | 69 |
| 3.5 | Summary | 77 |
| 4 | Sliding Non-Structural Components | 78 |
| 4.1 | Mathematical Formulation of Sliding Side-by-Side NSCs and SDOF Structure | 78 |
| 4.1.1 | Validation of the Model | 83 |
| 4.1.1.1 | Comparison with the existing study | 83 |

| | | | |
|----------|---------|---|------------|
| | 4.1.1.2 | Comparison with the Finite Element (FE) study | 84 |
| 4.2 | | Dynamic response of a SDOF structure with sliding side-by-side NSCs | 87 |
| | 4.2.1 | Displacement Response | 87 |
| | 4.2.2 | Parametric Study | 91 |
| | 4.2.3 | Modified structural period due to sliding NSCs | 94 |
| | | 4.2.3.1 Algorithm for determination of modified structural period | 95 |
| | | 4.2.3.2 Validation of the proposed algorithm | 96 |
| | 4.2.4 | Parametric study on modified structural period | 98 |
| | 4.2.5 | Design expression for modified structural period by Non-Linear Regression and Artificial Neural Network | 100 |
| 4.3 | | Mathematical Formulation of Sliding Stacked NSCs and SDOF Structure | 104 |
| | 4.3.1 | Validation of the Model | 110 |
| 4.4 | | Dynamic response of a SDOF structure with stacked sliding NSCs | 112 |
| | 4.4.1 | Displacement Response | 113 |
| | 4.4.2 | Parametric Study | 114 |
| | 4.4.3 | Modified structural period due to sliding NSCs | 117 |
| | | 4.4.3.1 Algorithm for determination of modified structural period | 118 |
| | 4.4.4 | Parametric study on modified structural period | 120 |
| | 4.4.5 | Design expression for modified structural period by Non-Linear Regression and Artificial Neural Network | 123 |
| 4.5 | | Summary | 124 |
| 5 | | Damping Behavior of the Structure with NSCs | 126 |
| | 5.1 | General | 126 |
| | 5.2 | Damping effect of the sliding NSCs | 128 |

| | | |
|----------|--|------------|
| 5.2.1 | Methodology to determine the additional equivalent damping ratio due to slide effect | 129 |
| 5.2.2 | Parametric Study | 131 |
| 6 | Summary and Conclusions | 135 |
| 6.1 | Summary | 135 |
| 6.1.1 | Combined Model for Structure and Hanging NSC | 135 |
| 6.1.2 | Combined Model for Structure and Sliding NSCs | 137 |
| 6.2 | Conclusions | 138 |
| 6.2.1 | Combined Model for Structure and Hanging NSC | 138 |
| 6.2.2 | Combined Model for Structure and Sliding NSCs | 141 |
| 6.2.2.1 | Combined Model for Structure and Side-by-Side Sliding NSCs | 141 |
| 6.2.2.2 | Combined Model for Structure and Stacked Sliding NSCs | 143 |
| 6.2.2.3 | Damping Effect of Sliding NSCs | 144 |
| 6.3 | Further Scope of Work | 146 |
| 6.3.1 | Combined Model for Structure and Hanging NSC | 146 |
| 6.3.2 | Combined Model for Structure and Sliding NSCs | 146 |
| | References | 147 |
| | Appendices | 155 |
| | List of Publications and Presentations | 161 |
| | Biography | 162 |

List of Tables

| Table No. | Description | Pg. No. |
|------------------|--|----------------|
| 3.1 | Dynamic parameters of the coupled SDOF-Hanging NSC System | 43 |
| 3.2 | Details of earthquakes considered for this study | 52 |
| 3.3 | Response reduction at optimal tuning frequency ratios | 55 |
| 3.4 | Details of earthquakes | 57 |
| 3.5 | Dominant frequencies of the excitations | 58 |
| 3.6 | Response of PS with and without FSS, and <i>RARR</i> | 61 |
| 3.7 | Variation of <i>DAR</i> as per IS 1893:2016 and ASCE-41-13 response spectra (5% damping) | 66 |
| 3.8 | Correlations between the length of the FSS and tuning frequency ratio | 66 |
| 3.9 | Optimal tuning frequency ratios of FSS | 69 |
| 3.10 | Performance of ANN 3-6-1 Model | 73 |
| 3.11 | Weights and biases of ANN 3-6-1 Model | 75 |
| 3.12 | Limits of Input and Output Parameters of the ANN 3-6-1 Model | 76 |
| 4.1 | Specifications of the strong ground motions used in the current study | 82 |
| 4.2 | Performance of the regression models | 101 |
| 4.3 | Performance of the ANN 5-6-1 Model | 103 |
| 4.4 | Weights and biases of ANN 5-6-1 model for Zone III | 103 |
| 4.5 | Weights and biases of ANN 5-6-1 model for Zone V | 103 |

| | | |
|-----|---|-----|
| 4.6 | Limits of Input and Output Parameters for the ANN 5-6-1 Model | 104 |
| 4.7 | Maximum displacement of the PS with and without stack | 114 |
| 4.8 | Performance of the models | 124 |
| 5.1 | Additional damping ratio (ξ_a) added to the structure | 134 |

List of Figures

| Figure No. | Title | Pg.No. |
|-------------------|--|---------------|
| 1.1 | Investments for three common construction types | 3 |
| 1.2 | Structure with (a) Sliding; (b) Overturning components under horizontal motion | 5 |
| 1.3 | Structure with hanging (flexible) components under horizontal motion | 5 |
| 1.4 | Research methodology | 8 |
| 2.1 | NSCs on a SDOF structure: (a) PS; (b) PS with P-NSC; (c) PS with S-NSC | 14 |
| 2.2 | Suspended structure on Mega structure | 17 |
| 2.3 | Idealization and model of structure-contents sliding system | 28 |
| 2.4 | Structure with sliding live load object (Pile-supported container terminal) | 31 |
| 3.1 | SDOF structure model | 36 |
| 3.2 | Free-body diagram of SDOF structure | 36 |
| 3.3 | The simple pendulum | 37 |
| 3.4 | Scaffolding with hanging lead blankets | 40 |
| 3.5 | Free-body diagram of the considered 2-DOF system | 40 |
| 3.6 | Comparison of displacement of PS with finite element model | 43 |
| 3.7 | Displacement response of the PS with and without FSS | 44 |
| 3.8 | Displacement response of the PS for different lengths of FSS | 44 |

| | | |
|------|--|----|
| 3.9 | Comparison of peak structural displacement with and without FSS for different excitation frequencies | 46 |
| 3.10 | Variation of peak structural displacement for different tuning frequency ratios | 47 |
| 3.11 | Variation of peak structural displacement for different mass ratios | 48 |
| 3.12 | Variation of mass effect ratio (ϵ) with forcing frequency (ω_f) | 49 |
| 3.13 | Average mass effect ratio (ϵ^+ and ϵ^-) against μ for different β | 51 |
| 3.14 | Ground acceleration time histories of selected earthquakes | 52 |
| 3.15 | FFT amplitudes of selected earthquakes | 53 |
| 3.16 | Peak structural response versus tuning frequency (a) El Centro (1940); (b) Kobe (1995); (c) Chi-Chi (1999) | 54 |
| 3.17 | Peak structural response versus mass ratio (a) El Centro (1940); (b) Kobe (1995); (c) Chi-Chi (1999) | 56 |
| 3.18 | IS 1893:2002 Zone III design spectra and response spectra of the ground motions | 58 |
| 3.19 | IS 1893:2002 Zone V design spectra and response spectra of the ground motions | 58 |
| 3.20 | Acceleration response of PS with and without FSS for hard soil excitation (a) Zone III; (b) Zone V | 59 |
| 3.21 | Acceleration response of PS with and without FSS for medium soil excitation (a) Zone III; (b) Zone V | 59 |
| 3.22 | Acceleration response of PS with and without FSS for soft soil excitation (a) Zone III; (b) Zone V | 59 |
| 3.23 | Target design spectra for different soil conditions (a) Zone III; (b) Zone V | 61 |

| | | |
|------|--|----|
| 3.24 | Effect of a smaller length and a higher mass ratio of an FSS on the design spectrum (a) Zone III; (b) Zone V | 62 |
| 3.25 | Effect of a longer length and a smaller mass ratio of an FSS on the design spectrum (a) Zone III; (b) Zone V | 62 |
| 3.26 | Variation of <i>DAR</i> with mass ratio (μ_{SS}) for different structural periods (T_p) | 64 |
| 3.27 | Variation of <i>DAR</i> with mass ratio (μ_{SS}) and tuning frequency ratio (β) | 66 |
| 3.28 | Variation of <i>DAR</i> with mass ratio (μ_{SS}) for a selected tuning frequency ratio (β) | 66 |
| 3.29 | Variation of Fourier amplitude response of PS for different tuning frequency ratios (β) | 67 |
| 3.30 | Actual <i>DAR</i> vs. predicted <i>DAR</i> by Non-linear Regression | 70 |
| 3.31 | MSE against number of hidden nodes | 72 |
| 3.32 | Architecture of the ANN 3-6-1 Model | 72 |
| 3.33 | Predicted <i>DAR</i> and Actual <i>DAR</i> of (a) Training set; (b) Testing set; (c) Complete database | 74 |
| 3.34 | Values of <i>DAR</i> predicted by ANN and Non-linear Regression versus the actual <i>DAR</i> value | 75 |
| 4.1 | Flow chart showing research methodology | 79 |
| 4.2 | Idealization of primary structure with two sliding SBs | 81 |
| 4.3 | Target and mean acceleration spectra | 82 |
| 4.4 | Velocity responses (a) primary structure; (b) rigid block | 84 |
| 4.5 | ABAQUS model of a PS with two sliding SBs | 85 |
| 4.6 | Acceleration time history used for validation of PS with two SBs model | 86 |

| | | |
|------|--|-----|
| 4.7 | Comparative response of Runge-Kutta Method and FE model for $\alpha_1 = \alpha_2 = 0.5$: (a) $T_p = 0.39$ s, $\mu_1 = 0.2$, $\mu_2 = 0.3$; (a) $T_p = 0.5$ s, $\mu_1 = 0.2$, $\mu_2 = 0.2$ | 87 |
| 4.8 | Displacement of PS with single and two SBs (a) Zone III; (b) Zone V | 88 |
| 4.9 | Displacement of the PS for same coefficients of friction (a) Zone III; (b) Zone V | 89 |
| 4.10 | Displacement of primary structure (a) Zone III; (b) Zone V | 90 |
| 4.11 | Displacement ratio (<i>DR</i>) for Zone III (a) $\mu_1 = 0.1$; (b) $\mu_1 = 0.3$ | 93 |
| 4.12 | Displacement ratio (<i>DR</i>) for Zone V (a) $\mu_1 = 0.1$; (b) $\mu_1 = 0.3$ | 94 |
| 4.13 | Determination of the modified structural period by proposed algorithm | 96 |
| 4.14 | Determination of the modified structural period for OLE hazard level | 97 |
| 4.15 | Validation of the Proposed algorithm | 98 |
| 4.16 | Modified structural period (T_{new}) for Zone III (a) $\mu_1 = 0.1$; (b) $\mu_1 = 0.3$ | 99 |
| 4.17 | Modified structural period (T_{new}) for Zone V (a) $\mu_1 = 0.1$; (b) $\mu_1 = 0.3$ | 100 |
| 4.18 | MSE against Number of hidden nodes for both the zones | 102 |
| 4.19 | Architecture of the ANN 5-6-1 model | 102 |
| 4.20 | Clusters formation | 108 |
| 4.21 | The flowchart of the numerical analysis procedure | 109 |
| 4.22 | Idealization of single-degree primary structure with two level stack of SBs | 109 |
| 4.23 | ABAQUS model of a structure with a two-level stack of SBs | 110 |
| 4.24 | Acceleration time history used for validation | 112 |

| | | |
|------|---|-----|
| 4.25 | Comparative response of Runge-Kutta method and FE model for $\alpha_1 = \alpha_2 = 0.5$, $\mu_1 = 0.3$, $\mu_2 = 0.1$, and: (a) $T_p = 0.5$ s, (b) $T_p = 1$ s | 113 |
| 4.26 | Displacement response of the PS with stacked SBs (a) Zone III; (b) Zone V | 114 |
| 4.27 | Displacement response ratio (<i>DRR</i>) for primary structure under medium seismic damage risk zone (Zone III) | 116 |
| 4.28 | Displacement response ratio (<i>DRR</i>) for primary structure under highest seismic damage risk zone (Zone V) | 118 |
| 4.29 | Determination of the T_{new} of a PS with a stack of sliding SBs | 120 |
| 4.30 | T_{new} against T_p for medium seismic hazard level (Zone III) | 121 |
| 4.31 | T_{new} against T_p for highest seismic hazard level (Zone V) | 122 |
| 5.1 | Displacement of a structure (a) with and without sliding SB; (b) with and without FSS | 128 |
| 5.2 | Displacement spectra for various damping ratios | 130 |
| 5.3 | Estimation of additional equivalent damping ratio (ξ_a) | 131 |
| 5.4 | Variation of ξ_a with coefficient of friction for different mass ratios (a) $T_p = 0.5$ s; (a) $T_p = 1$ s | 132 |
| 5.5 | Variation of ξ_a with the damping ratio for $\mu = 0.2$ and $\alpha = 0.75$ | 133 |

List of Symbols and Abbreviations

| Symbol/Abbreviation | Description |
|---------------------|---|
| $(u_p)_{rigid}$ | Displacement of the structure with rigidly attached bodies |
| $(u_p)_{stack}$ | Displacement of the structure with stacked bodies |
| $\ddot{u}_g(t)$ | Ground acceleration |
| L_s | Length of the suspended rod |
| M_0 | Mass of the 1 st cluster |
| M_l | Mass of the l^{th} cluster |
| S_D | Spectral displacement |
| S_a | Spectral acceleration |
| T_{new} | Modified structural period |
| T_p | Structural period |
| T_{rigid} | Structural period when the secondary body is rigidly attached |
| U_p | Displacement of the 1 st cluster |
| c_p | Damping coefficient |
| f_r | Excitation frequency ratio |
| k_p | Stiffness of the Primary structure |
| k_s | Stiffness of the hanging structure |
| m_{bi} | Mass of the i^{th} secondary body |
| m_n | Mass of the n^{th} secondary body |
| m_p | Mass of the primary structure |
| m_s | Mass of the suspended/hanging system |
| u_{bi} | Displacement of the i^{th} secondary body |
| u_g | Ground displacement |
| u_p | Displacement of the primary structure relative to the ground |
| u_s | Displacement of hanging mass relative to the ground |

| | |
|-------------|--|
| u_{ss} | Displacement of hanging mass relative to the primary structure |
| α_i | Mass ratio of the i^{th} secondary body |
| μ_{ss} | Mass ratio of hanging secondary structure |
| μ_k | Coefficient of kinetic friction |
| μ_s | Coefficient of static friction |
| ξ_a | Additional equivalent damping ratio of the structure |
| ξ_{eqf} | Equivalent damping ratio of the structure when the live load is rigidly attached |
| ξ_{eqs} | Equivalent damping ratio of the structure when the live load object slides |
| ξ_p | Damping ratio of the structure |
| ω_1 | First natural frequency of the combined structure and hanging NSC model |
| ω_2 | Second natural frequency of the combined structure and hanging NSC model |
| ω_f | Excitation frequency |
| ω_p | Natural frequency of the primary structure |
| ω_s | Natural frequency of hanging secondary structure |
| ANN | Artificial Neural Network |
| CHT | Combined Horizontal and Tilting |
| <i>DAR</i> | <i>Design acceleration ratio</i> |
| <i>DDR</i> | <i>Drift Demand Ratio</i> |
| DHS | Direct hung suspended |
| <i>DR</i> | <i>Displacement ratio</i> |
| <i>DRR</i> | <i>Displacement response ratio</i> |
| FE | Finite Element |
| FFT | Fast Fourier Transform |
| FSS | Flexibly attached secondary system |
| MDOF | Multi-degree of freedom |
| NLR | Non-linear Regression |

| | |
|-------------|--|
| NSCs | Non-Structural Components |
| NSEs | Non-Structural Elements |
| PGA | Peak ground acceleration |
| PS | Primary structure |
| PTMD | Pendulum tuned mass damper |
| QC | Quadratic combination |
| <i>RARR</i> | <i>Response acceleration reduction ratio</i> |
| RP | Reference point |
| SBs | Secondary bodies |
| SDOF | Single-degree of freedom |
| SEs | Structural Elements |
| SMP | Suspended mass pendulum |
| SSS | Suspended structural system |
| TTMD | Translational tuned mass damper |
| α | Mass ratio |
| β | Tuning frequency ratio |
| ξ | Damping ratio of the structure |
| ϵ | Mass effect ratio |

CHAPTER 1: INTRODUCTION

1.1 Background of the Work

Seismic design of a structure requires a good understanding of its dynamic behavior. It involves the calculation of various loads to be included in the seismic analysis and design. Various masses such as heavy machinery, chandeliers, and unrestrained components on the floor etc., are usually not considered in the study of this dynamic behavior. When considered, they are usually lumped as a part of the main structure, which is conservative for design. These masses are called secondary structures or non-structural components (NSCs).

Sometimes these components are not fully attached to the main structure. In such cases, they move out of phase with respect to the building motion. Few examples of such components are lead blankets draped on the scaffolding in the nuclear industry, suspended coal buckets in coal power industry, heavy chandeliers and cranes inside the industrial buildings with heavy hoist masses. Furthermore, some components which are not at all attached to the main structure and simply rest on the floor levels and are called unrestrained components. Heavy machinery, power generators, heavy storage containers on pile supported structures are few examples of such unrestrained components. When the mass of such a secondary mass comparable to the supporting structure, their effect cannot be ignored.

Such flexible and unrestrained components do not add extra stiffness to the structure whereas rigid secondary components like infills and cladding panels alter the stiffness of the structure. Hence, a structure with rigid NSCs can be modelled as a single structure by taking the complete mass of the NSCs into consideration. A structure with flexible NSCs can be modelled as a multi-degree of freedom (MDOF) system. Structural design becomes

conservative if the mass of components is fully considered in the structural design. The design can be unsafe if these components are completely ignored. Hence, proper quantification is required for the economic seismic design of the main structure with such secondary structures. Therefore, this study made a preliminary attempt to incorporate the effect of the secondary structure and its dynamic parameters in the seismic analysis of the structure under harmonic and real earthquake ground motions.

A building structure consists of a primary structural system that is designed to resist a variety of loads. Structural Elements (SEs) in buildings carry all earthquake-induced inertia forces generated in the building down to its foundations. There are many components of buildings supported by SEs, which only generate inertia forces, but are not directly connected to the foundations, e.g., in-fill walls, contents of buildings, appendages to buildings, and services & utilities. Their inertia forces are also carried down to foundations by structural elements. Such items are generally referred to as Non-structural elements (NSEs) (Murty et al. 2012). In existing literature, NSEs are referred to by various names, such as “non-structural components”, “secondary systems”, and “secondary structures”. From herein NSEs are termed as Non-Structural Components (NSCs) in this study. Generally, these NSCs are classified into three categories: architectural components, mechanical and electrical equipment, and building contents (Villaverde 1997a). Architectural components include stairways, walls, parapets, penthouses, appendages and ornamentations, veneer, cladding systems, suspended ceiling, and sign boards. Cranes, boilers, storage tanks, piping systems, fire protection systems, ducts, escalators, antennas, generators, and engines are considered mechanical and electrical components. Building contents include components such as bookshelves, storage racks, furniture, and file cabinets.

During severe earthquakes, secondary systems attached to primary structures are also subjected to earthquake forces. In standard design practice, non-structural components are not modelled due to a perception that they do not carry any load. The seismic behavior of the secondary structures has been studied extensively for many decades under harmonic and real earthquake excitations. Although mostly these NSCs are ignored in the current seismic design methodology of the supporting structures, they constitute a major part of failure of the structure in the event of major earthquake (Myrtle et al. 2005; Perrone 2012). About 60-70% of the total cost of the buildings being built in urban India is of NSCs (Murty et al. 2012). Percentage of economic losses due to non-structural damage is greater to the percentage of the construction cost (Taghavi and Miranda 2004). Fig. 1.1 below shows the relative costs of contents, structural, and non-structural components for three common construction types (Whittaker and Soong 2003) .

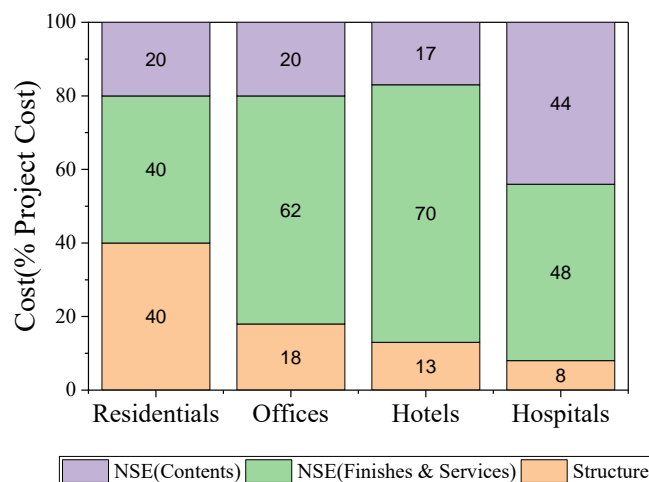


Fig. 1.1 Investments for three common construction types (Whittaker and Soong 2003).

Based on their types of failure, NSCs can be classified as acceleration sensitive components and displacement sensitive components (Pardalopoulos and Pantazopoulou 2015). The deformation failure is due to excessive inter-story building drift. They can also be caused by the improper detailing between the structure and the component. The

acceleration failure is due to the inertial forces produced in the component or rocking/sliding due to unanchored or marginally anchored conditions. Non-structural components can also be classified as rigid and flexible NSCs. Rigid component is attached to the building such that it is in phase with the structural movement and does not vibrate independently of the supporting structure. Flexibly mounted NSCs are the components which can displace independently from its point of attachment to the building (Kehoe 2014). ASCE 7-10 (Committee 2010) provides a definition for determining whether an NSC is rigid or flexible based on the vibrational period of the component. If the period of the component is less than or equal to 0.06 sec (16.7 Hz), it is termed as a rigid NSC. Flexible NSCs are those with a vibrational period greater than 0.06 sec.

The seismic response of secondary structures has been studied extensively for the last five decades. Engineers widely use floor response spectra to design secondary structures. They assumed that the primary and secondary structures do not affect each other. But the study (Kelly and Sackman 1978) concluded that secondary-primary interaction cannot be neglected in some cases. When a structure vibrates during an earthquake, the unrestrained or marginally restrained (flexible) components connected to that structure may slide, swing, roll, or overturn. File cabinets, generators, suspended items, office equipment, free-standing bookshelves are the few examples to experience such failure modes. Fig. 1.2 and Fig. 1.3 show the sliding, overturning, and swinging of the unrestrained and marginally restrained components connected to the structure.

In the seismic analysis of structures with NSCs, it is necessary to consider the flexibility of the component. In the case of rigid component, their accelerations are the same as the supporting structure's acceleration on which they are installed, while in the case of flexible components, the components' accelerations do not depend on the acceleration of structure.

The flexibility of the structure affects these accelerations. Some researchers have identified the effect of the non-structural components

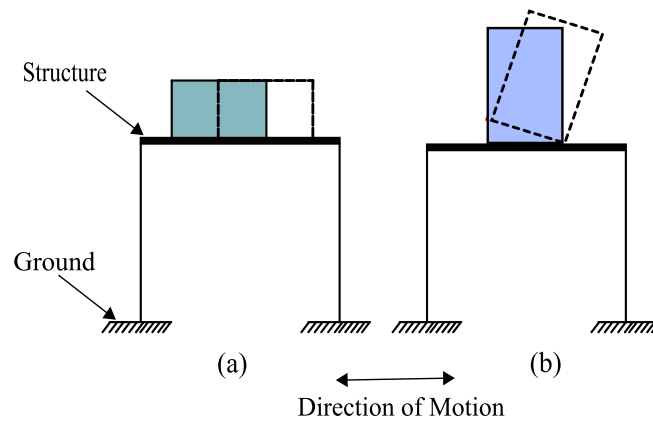


Fig. 1.2 Structure with (a) Sliding; (b) Overturning components under horizontal motion.

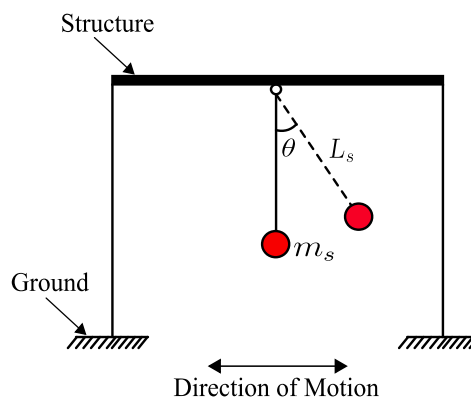


Fig. 1.3 Structure with hanging (flexible) components under horizontal motion.

on the overall structural performance (Li et al. 2009, 2011). The dynamic interaction between the structure and rigid NSCs like infills and cladding panels have been reported in past studies (Dolšek and Fajfar 2008; Li et al. 2010; Morfidis and Kostinakis 2016; Palermo 2012). There are some studies conducted on the effect of the hanging/suspended mass on the overall performance of the structure (Belleri et al. 2017; Wang et al. 2009; Wei et al. 2016). The dynamic interaction between the supporting structure and unanchored contents

(sliding failure mode) is proved to be significant under earthquake excitations for higher mass ratios (Chandrasekaran and Saini 1969; Smith-Pardo et al. 2014).

Consideration of damping and calculation of the damping coefficient gives a crucial insight into the dynamic behavior of structure. Especially in the cases where NSCs are present such studies are critical. If the damping ratio of the primary structure or the NSC were over-estimated, this would produce the unconservative response for both the PS and NSC. The damping of the combined primary-secondary structure system has to be carefully considered if the dynamic interaction is deemed significant in the analysis. When the damping characteristics of the primary and secondary structures are different, then the combined system is non-classically damped (Gupta and Bose 2017). The damping characteristics of the primary structure were improved due to dissipation in energy by NSCs attached to the structure at single/multiple points (Lu et al. 2018; Welch et al. 2014).

In view of the importance of the dynamic interaction between the primary and secondary structures, there is a need to carry out additional research on the seismic response of the primary/supporting structure with secondary structures. This study contributes to the aforementioned purpose by developing design expressions for evaluating the seismic response of the primary structure as a function of the primary and secondary structural parameters. The present study also deals with the quantifying of energy dissipation by the NSCs attached to the primary structure at a single point. The focus is on primary building structure with the unrestrained and hanging components shown in Figs 1.2(a) and 1.3 respectively.

1.2 Objectives of the Study

The global objective of this study is to arrive at a methodology for the estimation of the effect of flexibly attached secondary structures on the seismic design of the primary

structure. This will involve studying such a structure under real earthquake excitations. Development of such a methodology requires an understanding of the governing dynamic equations of motion of the structure and the secondary components. Although vast amounts of information are available for estimating the seismic demands on the secondary structure by considering the primary-secondary structure dynamic interaction, only few studies had attempted to estimate the demands on the primary structure. Hence, the approach in the study is geared towards establishing an equation to estimate the seismic response of the structure with hanging and sliding live load objects. The specific objectives of the study are summarized as follows:

- Investigation on the effect of flexibly attached secondary systems on the seismic behavior of the primary structures by an analytical study.
- Development of a numerical model to corroborate the above study.
- To examine the damping effect of secondary systems on the primary structures.
- Development of mathematical expressions for economical seismic design of primary structures attached with flexible secondary systems.

1.3 Methodology adopted for the Study

The methodology adopted in the present research work is shown as a flow chart in Fig. 1.4.

As shown in the below figure, the following study tasks were successfully completed to achieve the objectives of the present study

1. Primary structure (PS) is considered as a single-degree of freedom (SDOF) structure. The PS with a hanging component and sliding live load objects with their mass comparable to the mass of the PS was considered. The combined

structure (PS+NSC) was modelled as a multi-degree of freedom (MDOF) system.

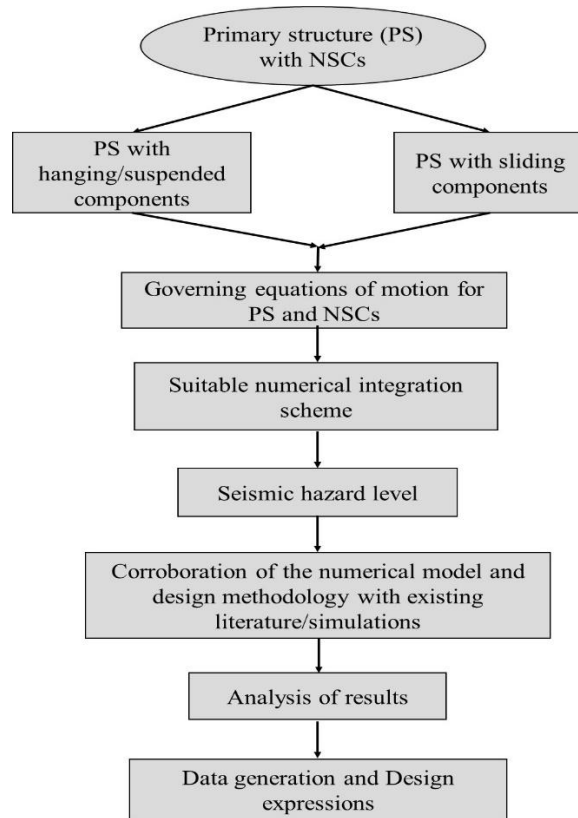


Fig. 1.4 Research methodology.

2. Governing equations of motion for the PS and corresponding non-structural component were derived by considering the dynamic interaction between PS and NSCs.
3. The developed governing equations of motion were solved by numerical integration technique. The equations of motion of the structure with hanging NSC and sliding live load objects were solved by Duhamel integral and Runge-Kutta 4th order method respectively.
4. The seismic response of the structure was investigated by varying the secondary structure parameters for a given seismic hazard level.

5. The numerical model and the proposed design methodology was corroborated with the existing literature or simulations.
6. An extensive parametric study has been conducted on the numerical model by varying the primary and secondary structure dynamic properties and the seismic hazard levels.
7. Design expressions have been developed to estimate the seismic response of the primary structure as a function of its dynamic properties, secondary structure dynamic parameters for a given seismic hazard level.

1.4 Scope of the Study

In this study the effect of hanging and sliding NSCs on the dynamic behavior of a structure under earthquake excitations is investigated. Hanging NSCs were modelled as simple pendulums. Sliding NSCs were modelled as rigid blocks. The present study is limited to a single hanging NSC with small displacements and rigid blocks which show only sliding mode of vibration. The primary structure was limited to a linear elastic model. The natural frequency of the hanging secondary mass was adjusted by changing the length of the simple pendulum similar to a tuned mass damper. The sliding live load objects were considered to be resting side-by-side or stacked one over the other. While the equations developed in this study are for any number of such masses, the results and analyses performed are for two masses at a time.

The combined structure (PS+NSCs) was subjected to spectrum compatible earthquake excitations. Design methodologies were developed to determine the dynamic properties of one-story structures with secondary masses sliding on and hanging from it. The design methodology developed in this study is suitable for evaluation of the influence of NSCs on the dynamic behavior of actual complex multi-degree of freedom (MDOF) structures in the

non-linear range. Accordingly, the proposed design equations can be modified. These equations can be used to design such structures seismically.

1.5 Organization of the Thesis

The description of the work carried out is listed below.

Chapter 1. An introduction of the research is explained in this chapter by highlighting the background, and motivation to carry out this research. The research objectives, methodology to carry out the research and scope of the study are also listed out in this chapter.

Chapter 2: An extensive review of literature by emphasizing on the seismic response of the secondary structures. Dynamic interaction between primary structure and the NSCs is presented. The limitations and the research gaps on the dynamic interaction of the primary and flexible secondary system bring out the objectives of the present study.

Chapter 3: The analytical modelling of the primary structure with hanging non-structural component is presented. Seismic analysis results of the primary structure are reported in this chapter. The validation of the model and the proposed design methodology are also presented.

Chapter 4: The analytical modelling of the primary structure with sliding non-structural component is presented. Seismic analysis results of the primary structure are reported in this chapter. The validation of the model with the Finite Element (FE) study is presented.

Chapter 5: In this chapter, the damping effect of sliding non-structural components on the primary structure's response is investigated.

Chapter 6: Summary and the relevant conclusions of the study from chapter 1 to 5 and the scope for further research are presented in this chapter.

The next chapter presents the extensive review of literature on the seismic response of the secondary structures. Dynamic interaction between the primary structure and the NSCs relevant to present research work is also presented.

CHAPTER 2: LITERATURE REVIEW

2.1 Introduction

Significant research has been done in an effort into investigate the seismic response of the non-structural components over many decades. Much of the research has focused on the understanding of seismic demands on the secondary structures under seismic events. Such understanding can be utilized in the seismic design of NSCs to overcome the huge economic loss created by them. Recently, researchers have studied the dynamic interaction between the primary and secondary structures to understand their seismic behavior. When the mass of a secondary structure is comparable to the mass of the primary structure, the seismic behavior of the primary structure is affected considerably. Therefore, this chapter presents a thorough review of the existing research on the seismic response of the non-structural components. Since the focus of the present study is on hanging and unrestrained NSCs, this chapter presents a review of their seismic demands under harmonic and real earthquake excitations. This chapter also discusses the dynamic interaction between the hanging and unrestrained NSCs and the supporting structure.

2.2 Non-Structural Components

Significant progress has been made over decades in the seismic analysis and performance of secondary systems anchored or attached to primary structural systems under seismic excitations (Filiatrault *et al.* 2018; Miranda *et al.* 2018; Zhai *et al.* 2016; Magliulo *et al.* 2012; Martinelli and Faella 2012). Secondary systems are not commonly designed to resist external loads such as earthquakes or impact loads. Hence, these systems are vulnerable to damage even during minor earthquakes. Therefore, seismic analysis and design of secondary structures is important to withstand external loads. State-of-the-art reviews on the seismic response of secondary structures have been presented by the studies (Chen and

Soong 1988; Villaverde 1997a). Initial studies on the response of the NSCs were focused on the safety of critical secondary components in nuclear power plants (Biggs and Rosset 1970; Villaverde 1997a). These studies were used to develop the US Nuclear Regulatory Guide 1.22 (Commission 1976). In current practice, two basic approaches exist which provide the seismic demands on secondary structure. They are, floor response spectrum approach and combined primary-secondary system approach (Chen and Soong 1988). In practice, the floor response spectrum is often adopted for the estimation of the seismic demands on the secondary structure (Biggs and Rosset 1970; Sackman and Kelly 1979; Singh *et al.* 1986; Medina *et al.* 2006).

In the floor response spectrum approach, primary and secondary structures are decoupled and analyzed individually. The response of the primary structure at the support points of the secondary structure is determined. In this process, the effect of the secondary structures is neglected. The response spectra at the support points or floor response spectra are then applied to the secondary structure as an input from which response of the secondary mass is determined. The use of this method results in inaccurate prediction of the response of secondary structure, since it neglects the primary- secondary structure interaction. This deficiency in this method can be overcome by performing a coupled analysis by combined primary-secondary system (PS-system) approach suggested in the study (Chen and Soong 1988).

The response of a secondary structure depends not only on the characteristics of the ground motion, but also on the dynamic properties of the supporting structure. Also, there exists a significant amount of interaction between the primary and secondary structure, which alters the response of both of them (Villaverde 1997a). Matta and Stefano (Matta and De Stefano 2015) classified non-structural components (NSCs) as “in-parallel” (P-NSCs) and “in series” (S-NSCs) according as they work with the main structure. Few

examples of P-NSCs mentioned in their study are masonry infills, pavements in bridges. Suspended ceilings, piping systems, chimneys, storage tanks and antennas are few S-NSCs listed out in the study. They reported that S-NSCs significantly modify the overall modal behavior of the structure if accidentally tuned to the structural mode.

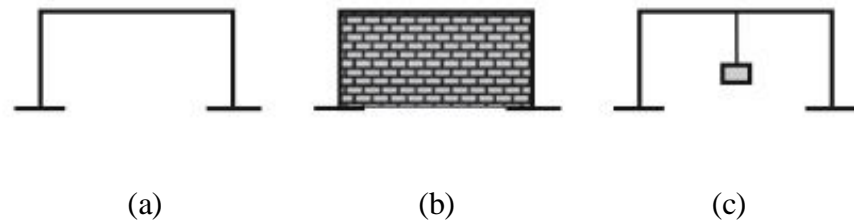


Fig. 2.1 NSCs on a SDOF structure: (a) PS; (b) PS with P-NSC; (c) PS with S-NSC

(Matta and De Stefano, 2015)

Currently, the effect of P-NSCs on the dynamic behavior of the main structure appears to be well documented (Chandel and Yamini Sreevalli 2019; Morfidis and Kostinakis 2016; Paper *et al.* 2006; Perrone 2012; Pokhrel *et al.* 2019; Sofi *et al.* 2017; Uva *et al.* 2012). The studies on the effects of S-NSCs on the overall behavior of the primary structure are yet to be explored. On the other hand, some research has dealt with the dynamic interaction between S-NSCs and primary structure to assess the dynamic response or seismic vulnerability of the non-structural elements (Lim and Chouw 2018; Martinelli and Faella 2012; Salman *et al.* 2019; Villaverde 1991; Wang *et al.* 2009; Wang and Liu 2008; Zhai *et al.* 2016).

Another important class of non-structural components include building contents and mechanical/electrical equipment. Most of these components are free standing or unrestrained. The seismic response of this class of components is very complex and shows non-linear characteristics. Generally, these components are modelled as a rigid bodies under external excitations (Kafali 2006). When free standing structures are subjected to

base excitation, they may undergo a number of failure modes. They may slide, rock or shows combined slide-rock failure modes (Lopez Garcia and Soong 2003; Shao and Tung 1999). Heating, ventilation and air-conditioning (HVAC) units, spent nuclear fuel storage casks, critical and laboratory equipment, heavy lead blankets draped on scaffolding structures are few examples of such free standing structures (*Challagulla et al. 2020; Lin et al. 2015; Shie et al. 2007*). The sliding displacement of the rigid bodies under base excitation is investigated by many studies (Choi and Tung 2002; Demosthenous and Manos 2005; Lopez Garcia and Soong 2003; Westermo and Udwadia 1983; Younis and Tadjbakhsh 1984).

In conventional design of structural systems, the sliding response during earthquake excitations, either at the foundation level or at the various structural components, is generally ignored. However, there are structural systems where sliding at the interface of different structural components is significant of their earthquake response and overall stability. Several research shows that the sliding-friction devices can be used for protecting the structures from a developing undesirable performance during earthquake excitations (*Etedali et al. 2020; Mohammadi 2017; Mohammadi et al. 2011; Mostaghel and Tanbakuchi 1983; Swain et al. 2016; Vafai et al. 2001*).

The following sections discuss the response of the hanging and sliding secondary structures under harmonic and earthquake excitations. Dynamic interaction between the primary and secondary structure is also discussed. Extensive literature on the effect of these secondary structures on the seismic response of the structure under harmonic and seismic ground excitations is presented.

2.2.1 Hanging Non-Structural Components

NSCs can be classified as rigid, flexible and hanging type components based on how they contribute to the dynamics of the structure. The research in this sub-section primarily is focused on the hanging type NSC, which is connected to the primary structure at single point as shown in Fig. 3. Such non-structural components are connected to their supporting structure (i.e., hung from above) with a hinge. They may be modelled as a simple pendulum. Examples of such NSCs are lighting systems, cable trays and heavy chandeliers. The problem in this study is motivated by the heavy hanging lead blankets from the supporting scaffolding structure in the nuclear power industry. Few NSCs which are connected at single point or at multiple points and hung from the supporting structure are widely used as a pendulum tuned mass dampers (PTMDs) by adjusting their frequency equal to the fundamental frequency of the supporting structure to reduce the unwanted vibrations.

Suspended structural system (SSS) can be considered as a pendulum tuned mass damper (PTMD) and the equations of motion of the structure and the suspended system can be developed similar to the equations of structure with PTMD. Under small oscillations of the PTMD, it can be considered equivalent to a translational tuned mass damper (TTMD). The suspended systems are intended to design in a way that ensures that the suspended system move within a small range. Therefore, they can be analyzed as a TTMD system instead of a PTMD system (Chulahwat 2013).

Yao (2000) investigated the vibrational characteristics and capacity of direct hung suspended (DHS) ceiling system analytically and experimentally in an earthquake environment. This study concluded that the natural frequency of the DHS system could be estimated using the pendulum formula. Analytically obtained natural frequencies and mode shapes of the combined structural system were verified by modal experiments (Yao 2000).

Wang and Liu (2008) studies the dynamic response of the suspended structures. They found out that the dynamic response of the suspended structures is very complex and there is no opportunity to derive the nonlinear behavior of the dynamic responses if only linear restoring force is considered. They also reported that the substructures can play an important role in the mitigation of the dynamic response of the mega structure. The dynamic response of the suspended structure is hypersensitive to the length of the suspenders (Wang and Liu 2008).

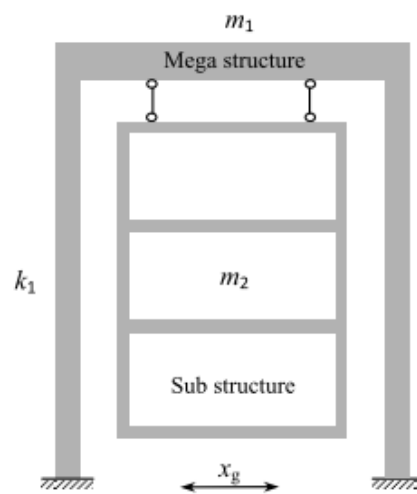


Fig. 2.2 Suspended structure on Mega structure (Wang and Liu 2008)

Coal buckets suspended on the higher levels of the structure in coal-fired power plant serve as equivalent pendulum tuned mass dampers. A large mass ratio of the coal buckets leads to bigger coal bucket displacements under external excitations. By increasing the supplementary damping to the suspended buckets, the inert-story drifts increase and the buckets displacements decrease (Shu *et al.* 2017). The seismic response of the coal-fired power plant with multiple suspended coal buckets as PTMDs is investigated. The use of multiple coal buckets as a PTMDs in improving the seismic performance of the coal-fired power plant structures was confirmed by the study (Peng *et al.* 2018).

In this section, studies about seismic response of suspended secondary structures under external excitations are presented. The following section explains the studies about the effect of such secondary structures on the dynamic response of primary structure under seismic excitations.

2.2.2 Influence of hanging NSCs on the structural seismic response

In this section, the literature that studied the effect of suspended/hanging NSCs, which are un-tuned to the structural frequency on the seismic response of the supporting structure is presented. In order to study the effect of a secondary mass on a structure, understanding the dynamic interaction between the secondary and primary masses needs to be examined.

The input load to the secondary structure is calculated using floor response spectrum. This method is also known as the cascade approach. This method assumes that the primary and secondary structure do not affect each other. When the secondary structure has comparable mass to the primary structure, this assumption does not hold good. In such cases, combined system has to be considered in the analysis since primary and secondary structures may affect the response of each other (Kelly and Sackman 1978). Amin *et al.* (1971) also indicated that the interaction between the primary and secondary structure is not significant when the mass ratio is less than 1% (Amin *et al.* 1971).

Murty *et al.* (2012) reported that when the mass of the NSCs is less than the 1% of the supporting building, the dynamic oscillation of the NSC does not alter the response of the building. In such cases, the dynamic interaction can be neglected. The interaction between the response of the NSC and the building increases when the mass of the NSC increases. The seismic demands of the NSCs computed are too conservative in some cases and even un-conservative in others when the dynamic interaction is neglected (Murty *et al.* 2012).

Ignoring the interaction between the secondary masses and the primary structure leads to overestimation of demands on the systems (Taghavi and Miranda 2008).

Understanding of the characteristics of ground motion and dynamic properties of the primary and secondary structures is essential for dynamic interaction studies. Proper design of the secondary structure can be done only if dynamic interaction effects are considered. During the excitations, the response of the primary structure is greatly reduced due to the presence of a secondary structure. Under different excitation frequencies, secondary structure can affect the primary structure differently (Lim and Chouw 2014). Seismic behavior of the primary structure can be altered by the presence of secondary structure if dynamic interaction effects are considered in the analysis (Meersschaert and Chouw 2016).

Lim and Chouw (2015), in their study concluded that primary-secondary structure interaction (PSSI) is more pronounced in the response of the secondary structures. They also pointed out that the floor response spectrum method for the analysis of secondary structures is only applicable for the secondary structures with difference in natural frequencies, and with masses much smaller than those of the supporting structures. They considered primary and secondary structures as a combined system i.e., the secondary structure is considered as an additional degree-of-freedom to the primary structure (Lim and Chouw 2015).

Lim and Chouw (2018) provided an empirical formula to predict the displacement of the secondary structure by incorporating the dynamic interaction effects in their analysis. They concluded that the formulae can predict the displacement more accurately, in comparison with the conventional floor response spectrum method (Lim and Chouw 2018).

The above studies have highlighted the importance of dynamic interaction between the primary and secondary structures. From these studies, we can infer that the response of the

primary structure is significantly affected due to the presence of a secondary structure. The following studies exclusively explain the effect of hanging masses on the seismic response of the primary structure.

When a primary structure is attached with the suspended mass, the effect of such mass on the response of the structure is significant. Wei *et al.* (2016) investigated the seismic response of structures with a suspended mass subjected to combined horizontal and tilting (CHT) ground motions by both shake table tests and theoretical analyses. In the experimental model, the secondary mass was suspended by four steel cables or four steel springs. An earthquake excitation was applied to the primary structural frame. Frames without and with a suspended mass were used as the test models for comparison. They found that due to the tilting component in ground motion, the suspended mass has significant effect on the seismic response of the structures. They also reported that seismic response of the structures may also be affected by the vibration parameters of the suspended mass and need further investigation (Wei *et al.* 2016).

Belleri *et al.* (2017) studied the influence of hoist load on the seismic response of the industrial building under earthquake loading. The results of the parametric analyses showed that the hoist mass is significant under some conditions, particularly on the type of ground motions and type of the buildings. They also proposed a simple design methodology to account for the hoist load in response spectrum analysis (Belleri *et al.* 2017).

Huang *et al.* (2018) performed an analysis on the control performance of a suspended mass pendulum (SMP) on the displacement response of the structure under earthquakes. In order to verify the effectiveness of an SMP on the vibrational control of a structure, a transmission tower was chosen as the primary structure. The suspended mass pendulum was considered as a spatial model in the study. The SMP model was connected to the structure through a massless rope. From the numerical results conducted under eight

earthquakes, the study concluded that the spatial model can predict the dynamic response of the structure more accurately than a planar model. From the results of this study, authors concluded that the SMP has a significant mitigation effect on the seismic response of the tower (Huang *et al.* 2018).

Tian *et al.* (2012) conducted a study on the mitigation of vibration of a transmission tower using suspended mass pendulum under earthquakes using the finite element computer program SAP 2000. A parameter called, vibration decreasing ratio is defined to quantify the effect of the pendulum on the response of the tower. Seismic response of the tower with and without pendulum on different site soils were obtained from the numerical analysis. The analysis results revealed that the suspended mass can mitigate the response of the structure under seismic excitations (Tian *et al.* 2012).

Saudy *et al.* (1994) proposed stochastic analysis by including the dynamic interaction between primary and secondary structures. They concluded that dynamic interaction shows two effects and they are, effect of the interaction forces at the attachment points and the changes in the primary structure properties due to the attachment of the secondary structure. When the secondary structure is rigidly attached to the primary structure, the effect of the dynamic interaction is associated with the change in primary structure properties. The effect of interaction forces is more significant when the secondary structure is connected through flexible supports to the primary structure (Saudy *et al.* 1994).

Few works examined the percent of critical damping in the combined primary and secondary structure system. Villaverde assumed very low damping ratios (0% and 0.1%) for non-structural components (Villaverde 1997a). If the light NSC is tuned with a dominant mode of the supporting structure and has the damping values lower than those of the supporting structure, neglecting non-classical damping effect would result in non-conservative results (Singh and Suarez 1987). If the fundamental frequency of the NSC is

away from that of the primary structure, then the system is classically damped. If the system is tuned, and interaction must be considered, then the system is non-classically damped (Igusa and Kiureghian 1985). Rayleigh damping can cause significant error in the calculation of the damping matrix if the damping ratios of the primary structure and NSC differ by orders of magnitude (Villaverde 1997b).

The vibration effects of the non-classically damped building-piping system subjected to ground motions were studied (Gupta and Bose 2017; Ryu *et al.* 2016). In their studies, SDOF primary-SDOF secondary systems were considered. From the analysis results, they concluded that the vibration effects of non-classical damping are significant when the natural frequencies of the two systems were nearly tuned. If the structural system consists of two or more systems with different levels of damping, e.g., a soil-building system or a structure with energy dissipating devices or equipment, the system damping is non-proportional (non-classical) (Chopra 2011).

Singh and Suarez (1987) studied the effect of dynamic interaction and non-classicality of the damping in evaluating the equipment response. The authors concluded that large errors in the equipment response might occur when the non-classical damping effects are ignored. They also observed that this effect is considerable for tuned structures and light equipment. This was more pronounced when there were varying damping ratios (Singh and Suarez 1987).

Qin and Lou (2000) investigated the effects of non-proportional damping on the seismic response of suspension bridges. Modern suspension bridges exhibit non-classical damping because different members such as steel decks, steel cables, concrete towers have different damping properties. They concluded that classical damping is not sufficient to capture the response of such bridges. A non-classical damping model was found to be more appropriate in this case (Qin and Lou 2000).

Raheem (2016, 2014) explored the dynamic response of non-classically damped hybrid structures. In a hybrid structure, the upper and lower part of the structure comprise of different materials like steel and concrete. When the dynamic interaction between the tower and supporting footing structure is considered, then the damping in the combined system needs to be non-classical. Rayleigh's damping exhibits significant error in constructing the damping matrix if the combined structure has different damping ratios (Abdel Raheem 2016; Raheem 2014).

Ryu et al. (2016) studied the vibration effects of non-classically damped building-piping system under extreme loads. They considered SDOF primary structure and SDOF secondary system and employed finite element analysis to evaluate the response of the combined system. The effect of non-classical damping model on the combined system was insignificant when the modal mass ratios are small (Ryu et al. 2016).

Gupta and Bose (2017) discussed the significance of non-classical damping in the coupled primary-secondary structural system. The authors utilized a simple primary-secondary structural system. The analysis concluded that, in nearly tuned primary-secondary structural systems, classical damping could give conservative results. The classical damping underestimates the response in perfectly tuned primary-secondary systems (Gupta and Bose 2017).

A structural system is classically damped when it has uniform damping properties. The system is said to be non-classically damped when it is attached with secondary equipment, supplemental damping devices, or base isolation (De Domenico and Ricciardi 2019).

In this section, few studies about the effect of suspended secondary structures on the seismic response of primary structure under external excitations are presented. Classical and non-classical damping are also reviewed in this section. The following section explains the studies about the seismic response of sliding secondary structures.

2.2.3 Sliding Non-Structural Components

Various loads need to be considered in the seismic design of a structure. Determination of the self-weight of the structure is easy but the calculation of live loads is a difficult task (Smith-Pardo *et al.* 2014). Among various live loads on the structure, the unanchored or free standing structures have received some attention from researchers over the past few decades. Past observations from seismic events have shown that sliding of contents caused injuries and damage even though primary structure suffered little damage (Dhakal 2010). Generally, in many structures, equipment and systems are not anchored to the base. For example, building contents, sensitive laboratory equipment and the spent nuclear fuel storage casks, are not fixed to the base. In the case of a base excitation, these equipment or systems are prone to different failure modes. Hence, it is important to study the behavior of freestanding structures subjected to base excitations. The following studies explain the seismic response of the unanchored or free-standing structures under harmonic and earthquake excitations.

An unanchored body can move in any of the three modes of motion. It may remain at rest, slide or rock. It may also slide and rock at the same time if the vertical motion of the base is large. Non-structural components such as utility based equipment, freestanding and unanchored building contents can be modelled as rigid blocks in the analysis (Kafali 2006; Lopez Garcia and Soong 2003). Shenton presented graphs that enable one to determine the mode of response (Shenton 1996). When a freestanding object is subjected to sliding mode of response, the extent of sliding can be obtained by solving the equation of motion numerically (Aslam *et al.* 1975).

Kaneko *et al.* (1999) proposed a new formula to estimate the sliding displacement of furniture during earthquakes. By using this formula, they evaluated the sliding displacement of the furniture for various conditions. The formula indicates that the sliding

displacements are inversely proportional to the coefficients of friction. Finally, from the analysis results, they concluded that the sliding displacements are significantly influenced by coefficients of friction and soil conditions (Kaneko *et al.* 1999).

Lopez and Soong (2003) developed the fragility curves for the sliding block-type non-structural components under seismic excitations. They concluded that fragility estimates obtained without taking into account vertical base accelerations can be significantly non-conservative. They classified fragility curves according to the friction coefficient and peak horizontal ground acceleration (Lopez Garcia and Soong 2003). Newmark (1965) proposed a formula for estimating the distance the body slides when the structure is subjected to a rectangular acceleration pulse (Newmark 1965).

Shao and Tung (1999) presented a chart in their study which enabled to determine the maximum sliding distance of an unanchored body (Shao and Tung 1999). The sliding displacement of a freestanding rigid block can be estimated by the Newmark's formula if an adjustment factor to the friction coefficient and horizontal base acceleration was applied (Choi and Tung 2002). Taniguchi and Miwa proposed the use of horizontal sinusoidal acceleration to find the slip displacement of a freestanding body. They proposed modification factors for determining the design slip displacements from the basic slip displacements (Taniguchi and Miwa 2007).

Lin *et al.* (2013, 2015) proposed a simple mechanics based method to determine the sliding displacement of contents on a structure subject to an impulse ground motion. The sliding displacement of the contents as a function of the normalized friction coefficient was obtained. The authors concluded that sliding displacement for elastically responding SDOF structures from a suite of earthquakes was found to be similar to that of from the impulse ground motion for the same normalized coefficient (Lin *et al.* 2013, 2015).

Yeow *et al.* (2014) conducted an experimental study on the sliding behavior of the building contents. They conducted experiments on the sliding behavior of a desk on carpet flooring under sinusoidal floor excitations using a shake table. The analysis results showed that the peak floor acceleration is not a consistent parameter to correlate against the maximum sliding displacement. They derived a parameter called the modified peak total floor velocity which had a strong correlation with the sliding displacement for the sinusoidal loading considered (Yeow *et al.* 2014).

Saraswat *et al.* (2016) investigated the effect of the excitation frequency on the stability of a freestanding rigid block. Sliding motion of the rigid block is analyzed for the harmonic base excitation for a given coefficient of friction and amplitude of ground acceleration. Their analysis showed that the sliding displacement of the block decreased with an increase in the excitation frequency. They found a relation between the excitation frequency and the stability of a rigid block (Saraswat *et al.* 2016).

Taniguchi (2002) analyzed the non-linear response of the rectangular rigid bodies subjected to horizontal and vertical ground motions. The governing equations of motion of the rigid block were derived for the lift off, slip and lift off-slip interaction. The time history responses of the rigid body show that the body is sensitive to small changes in the coefficients of friction and intensity of ground motions. The study concluded that the overturning is not significant on the low-grip foundation even at the high intensity base excitations, while the slip displacement is high. Rigid body subjected to large sliding displacement and overturn failure when it is subjected to long-period earthquake (Taniguchi 2002).

Chaudhuri and Hutchinson (2005) characterized the frictional behavior for the prediction of seismic response of the unattached equipment. In their study, small and sensitive equipment found in biological and chemical science laboratories were considered.

Static and kinetic coefficients of friction were experimentally measured. They concluded that the response can be reasonably estimated analytically by using the average frictional resistance values (Chaudhuri and Hutchinson 2005).

Konstantinidis and Makris (2010) have conducted experimental and analytical studies on response of the freestanding objects subjected to strong earthquake motion. A numerical model was first validated by experimental results conducted on the 1/4-scale models. The model was then used for analytical analysis on the full-scale free standing equipment under strong earthquakes. Their analysis results showed that the sliding mode is dominant and the sliding displacement reaches up to 70 cm. Finally, they developed the ready-to-use fragility curves (Konstantinidis and Makris 2010).

In nuclear power plants, spent fuel storage facility is unanchored to the base and show sliding or overturning when subjected to external loading like earthquakes. If it slides too far, it may collide with other fixed or freestanding equipment. Therefore, understanding the sliding phenomena of the spent fuel storage facility is important to the design of such freestanding equipment (Furuta *et al.* 2008; Ito *et al.* 2018; Iwasaki *et al.* 2012; Shie *et al.* 2007). A large coefficient of friction will retard the sliding of the cask. The sliding displacement of a freestanding body is greatly affected by the intensity of the earthquake loading and the frictional resistance. Sliding distance increases when the acceleration of the earthquake increases and/or the coefficient of friction is small (Shie *et al.* 2007). These studies focused on the dynamic response of the sliding bodies under base excitations. Such studies are required to design suitable fixing mechanisms for freestanding structures. Very few studies have looked into the behavior of structures on which freestanding bodies rest.

Younis and Tadjbakhsh (1984) found significant slippage for smaller frequency ratios and resonance bands of frequencies. It is also deduced that this phenomenon was amplified when the mass of the sliding body is comparable to that of the structure. Also in their study,

they found that a limiting frequency ratio exists which when exceeded the response will be the stick-mode (Younis and Tadjbakhsh 1984).

Matsui. *et al.* (1991) presented a study to understand the dynamic behavior of a rigid block resting on a footing supported by a spring and a dashpot. The response of the rigid block is studied carefully by exciting base with a harmonic force. They concluded that periodic motion can be possible in three forms: stick-stick, stick-slip and slip-slip. The conditions that initiate the stick-stick and stick-slip modes are derived in explicit forms. The main findings in this study include that the condition for the slippage is independent of the mass ratio. Slippage of the rigid block is minimum when the external frequency ratio increases beyond one (Matsui *et al.* 1991). The initiation times for stick and slip behaviors for the rigid mass resting on the SDOF oscillator are analytically obtained (Larson and Fafitis 1995).

Lin. *et al.* (2013, 2015) investigated the seismic demands of the building contents in elastically responding structures subjected to ground motion excitation as shown in Fig. 2.3. In their study, elastic SDOF structure was considered. Response spectra due to sliding were developed as functions of normalized friction coefficients. From the analysis results, they concluded that, as structural period increases, the sliding displacement of the contents decreases as result of lower floor accelerations (Lin *et al.* 2013, 2015).

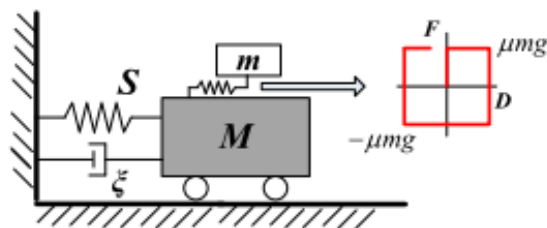


Fig. 2.3 Idealization and model of structure-contents sliding system (Lin *et al.* 2013)

The seismic response of sliding equipment and contents in base-isolated buildings subjected to ground motions was studied (Konstantinidis and Nikfar 2015; Nikfar and Konstantinidis 2013). For the analysis, they considered a SDOF superstructure. The response was investigated by varying the frictional coefficients and the isolation system properties. This study found the isolation to be effective in reducing seismic demands on the sliding equipment. The study also showed that the demand on the equipment increased for low coefficient of friction and high earthquake intensities.

Nikfar and Konstantinidis (2017) examined the seismic demands of the unanchored equipment in the base-isolated buildings under pulse excitation. They idealized the unanchored equipment as freestanding rigid bodies by considering the Stribeck friction model between the floor and the equipment. The analysis results concluded that the simple Coulomb friction model with the single coefficient of friction value is adequate for estimating the peak sliding displacements. The sliding response of the equipment is high for certain combinations of the isolation design parameters, compared to the fixed-base building (Nikfar and Konstantinidis 2017).

In this section, studies about seismic response of sliding secondary structures under external excitations are presented. The following section explains the studies about the effect of such secondary structures on the dynamic response of primary structure under seismic excitations.

2.2.4 Influence of sliding NSCs on the structural seismic response

In the previous section, the studies about the seismic response of the freestanding rigid bodies/equipment or building contents subjected to harmonic and earthquake excitations are presented. Few studies about the response of the rigid bodies resting on the supporting structures are also presented. In all these studies, mass of the equipment is very less

compared to the mass of the supporting structure and hence dynamic interaction between them is neglected. But, the dynamic interaction should not be neglected if heavy bodies are resting on the structure, since they affect the structural response (Konstantinidis and Nikfar 2015; Lin *et al.* 2013, 2015; Nikfar and Konstantinidis 2017; Yeow *et al.* 2015). Depending on the coefficient of friction and the mass ratio, the building content may affect the dynamic response of the building. Heavy content with high coefficient of friction increased the period of the building. Equipment with the low coefficients of friction increased the damping of the structure by dissipating the input seismic energy through friction (Nikfar and Konstantinidis 2017). Therefore, it can be postulated that structural response can be altered due to the presence of heavy sliding non-structural components.

Chandrasekaran and Saini (1969) studied the dynamic response of a SDOF structure due to live load. From the results of their analyses, they concluded that the increase in mass ratio decreases the response of the rigid block. For design purposes, average values of the response based on seven ground motions could be adopted (Chandrasekaran and Saini 1969). The resonance response of steel structure with sliding floor loads is investigated under harmonic and earthquake excitations (Okada and Takanashi 1992). They concluded that the response of an oscillator with a sliding load system is influenced by the mass ratio and coefficient of friction. For a heavy load and small value of the coefficient of friction, a reduced structural displacement and acceleration were observed.

Takanashi and Xiaohang (1989) conducted experimental studies on a single story and three story frame models supporting sliding floor loads using a shake table. Numerical and theoretical analysis are verified using these experimental results. From the analysis results, they concluded that the response of the frame reduces when the floor loads slide during vibration. They suggested that the live loads can be estimated to be lower than the actual values in seismic design of the frames (Xiaohang 1989).

Ardila-Giraldo *et al.* (2013) developed a finite element model to depict the interaction between a sliding block and a structure. They found that the finite element (FE) model estimated the displacement response of the supporting structure within 2% on average of the values obtained through the numerical integration of the equations of motion. Finally, they concluded that the FE model will serve to conduct parametric studies to develop the design recommendations in regards to the fraction of sliding mass that should be added to the dynamic mass in structures supporting sliding rigid blocks (Ardila-Giraldo *et al.* 2013).

Smith-Pardo *et al.* (2014) made an attempt to develop a model to depict the interaction between a sliding block and the structure. Two levels of seismic risk were studied. They introduced a new parameter called *Drift Demand Ratio (DDR)* for quantification of the effect on the behavior of the structure. A parametric study was presented to show the variation of *DDR* by varying the structural period (T_p), mass ratio (α), and coefficients of friction (μ_s and μ_k) for a given seismic hazard level. Their analysis results show that the portion of live load that should be included as inertia in the primary structure design/analysis depends upon the properties of the structure, magnitude of earthquake and the coefficient of friction (Smith-Pardo *et al.* 2014).

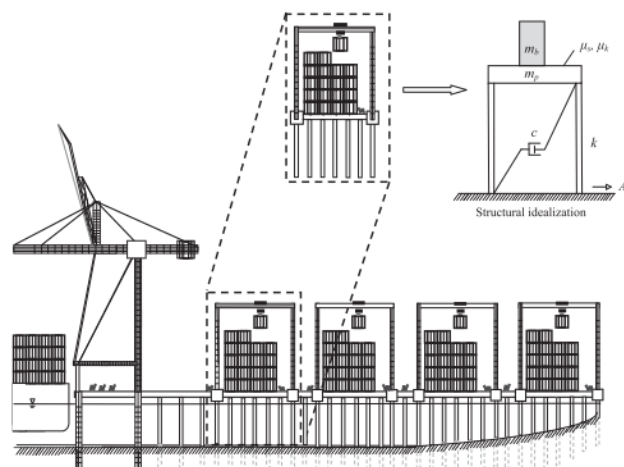


Fig. 2.4 Structure with sliding live load object (Pile-supported container terminal)

(Smith-Pardo *et al.* 2015)

The effect of live load on the seismic design of a single-story storage structures (Fig. 2.4) under horizontal ground motions was studied (Smith-Pardo *et al.* 2015). An algorithm was developed to determine the fraction of sliding load as dynamic mass (λ) under operational and contingency seismic hazard levels. A thorough study was conducted to find the change in λ by varying the structural period, mass ratio and coefficient of friction. Parametric study results show that the λ increases significantly with T_p , α , and μ for both the seismic hazard levels. A simple design expression was developed to estimate the λ as a function of the maximum acceleration of the structure, α , and μ . A design expression was developed and verified by an experimental study (Reyes *et al.* 2016).

The studies (Reyes *et al.* 2016; Smith-Pardo *et al.* 2015) were conducted on SDOF primary structures supporting rigid sliding blocks. The methodology proposed in these studies was to estimate the fraction of sliding load as dynamic mass. This was extended to the multi-degree of freedom (MDOF) systems. A design expression was proposed to estimate the λ and tested through the seismic analysis of two-story and four-story three dimensional models (Reyes *et al.* 2018).

In the present study, Artificial Neural Networks (ANNs) were used for the generation of design expressions. ANNs have been used extensively in various fields to relate the input and output data (Briki and Lahbari 2018; Wang et al. 2011).

In this section, few studies about sliding secondary structures and their effect on the seismic response of a primary structure under external excitations are presented. The following section explains the summary of the literature review and limitations of existing research.

2.3 Summary from literature review and limitations of existing research

After a thorough study of available literature, it is understood that the dynamic interaction between the primary and the heavy secondary structures is significant to the both primary and secondary structural dynamic analysis under external excitations. Based on the review of literature summarized in the preceding sections, the following limitations were identified for this study:

1. Limited research has been reported on the effect of suspended mass on the seismic response of the primary structure under harmonic and seismic excitations. None of the studies have incorporated the vibrational and interactional properties of suspended NSCs and their effects on the overall dynamic response of primary structures.
2. Research on the effect of sliding NSCs on the primary structure has been limited to single sliding live load objects. But in reality, multiple sliding live load objects exist in the form of stacks. The effect of such multiple sliding live load objects and their interaction properties on the dynamic behavior of primary structure has not been reported yet.
3. None of the studies from the review of literature study the effect of vibrational and interactional properties of NSCs on the structural damping.
4. Relevant design expressions for the seismic design of primary structure with flexible attached secondary systems and multiple sliding NSCs are not developed. This study is to be carried out since present codal provisions have not given any guidelines covering these NSCs especially in an Indian scenario.

2.4 Research Significance

Non-structural components like suspended/hanging NSCs and the multiple sliding live load objects change the dynamic response of the structure. This change in dynamic response will be analyzed and quantified in this study. This research will show the importance of the dynamic interaction between the primary and secondary structure in the primary structural design. Moreover, this research will provide design methodologies on how to incorporate the vibrational and interactional properties of the secondary structure in the primary structure equations of motion. This study will also be beneficial to design the simple elastic primary structure in more economical way. Since there are no existing design standards for the design of the structure with such secondary structures, the outcomes of this study can be a first step towards the formulation of the standard code of practice especially for Indian scenario. It should be noted that this research will be especially helpful for industrial structures with heavy secondary loads and light primary structures such as scaffolding frames.

2.5 Summary

In this chapter, the research on the dynamic behavior of non-structural components and the effect of such components on the dynamic behavior of the primary structure have been discussed. The following chapters will describe the analytical models of the structure with various types of NSCs (hanging and sliding).

CHAPTER 3: HANGING NON-STRUCTURAL COMPONENTS

The analytical model to be presented is an idealized version of the structure with a hanging NSCs. The motivation is to describe the effect of a hanging NSC on the motion of a structure under external excitations. Additionally, the implementation of the analytical model will demonstrate the results of the parametric study for a given vibrational and dynamic properties of the NSC and the primary structure, respectively.

3.1 Analytical Model of Hanging NSC and SDOF Structure

3.1.1 The SDOF Structure

The particular problem studied here is based on the lead-shielding application in nuclear power plants. Lead-shielding in power plants is primarily provided by lead blankets hanging from and laid on lightweight scaffolding. Due to the high risk associated with the interior of the nuclear power plants, these scaffolding structures need to be designed for seismic loads. Since the lead blankets are considerable in weight with respect to the light frame and are hanging from the scaffolding structure, it is a good example of the problem statement. For simplicity, the scaffolding is assumed to be on the ground and single-storied.

The structure is modelled as a single-degree-of-freedom (SDOF) scaffolding structure with a lumped mass (m_p). The motion of the mass is defined by the displacement relative to the ground, $u_p(t)$. The lateral stiffness of the structure is modelled as a linear spring with constant stiffness k_p . The energy contained in the system is dissipated with a viscous damper having a damping coefficient c_p . The structure is excited by a harmonic and real earthquake type ground motions. The ground acceleration is represented by $\ddot{u}_g(t)$. A schematic of the model is shown in Fig. 3.1.

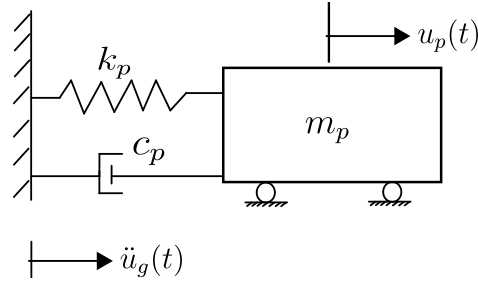


Fig. 3.1 SDOF structure model

D'Alembert's principle of dynamic equilibrium is employed to formulate the equations of motion for the system. A free-body diagram of the structure is shown in Fig. 3.2.

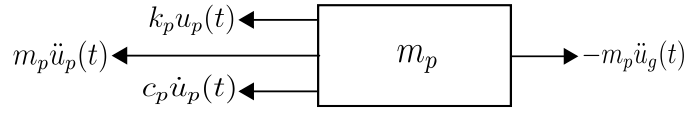


Fig. 3.2 Free-body diagram of SDOF structure

The dynamic equation of motion for the structure model is given by Eq. (3.1).

$$m_p \ddot{u}_p(t) + c_p \dot{u}_p(t) + k_p u_p(t) = -m_p \ddot{u}_g(t) \quad (3.1)$$

The undamped natural frequency and the damping ratio of the structure are denoted by ω_p and ξ_p respectively. They are defined as follows:

$$\omega_p = \sqrt{\frac{k_p}{m_p}} \quad (3.2)$$

$$\xi_p = \frac{c_p}{2\sqrt{k_p m_p}} \quad (3.3)$$

3.1.2 Hanging NSC

The lead blankets are considerable in weight with respect to the light frame and are hanging from the scaffolding structure. The hanging lead blankets can be modelled as a simple pendulum with a point mass m_s supported by a massless rod of length L_s . The rod pivots about a single point. The hanging mass is restricted to move horizontally. The differential equation of motion of a simple pendulum is derived by assuming the pendulum with a single

degree of freedom. The variables used in deriving the equation are time (t) measured in seconds and angle (θ) measured in radians. The length of the pendulum (L_s) is measured in meters and mass of the pendulum (m_s) measured in kilograms. A force diagram of the simple pendulum is shown in Fig. 3.3. From Fig. 3.3, it can be seen that the driving force of the pendulum is:

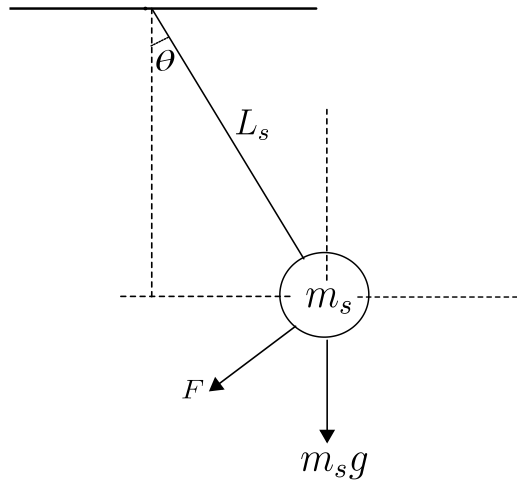


Fig. 3.3 The simple pendulum

$$F = -m_s g \sin\theta \quad (3.4)$$

Remember that the acceleration g is moving downwards, hence the negative sign. If we take the displacement of the pendulum mass from its equilibrium state to be s , then the acceleration of the mass is \ddot{s} .

Newton's second law of motions states that:

$$F = m_s a \quad (3.5)$$

Where F denotes a force, m denotes a mass and a denotes acceleration. So, therefore:

$$-m_s g \sin\theta = m_s \ddot{s} \quad (3.6)$$

$$-g \sin\theta = \ddot{s} \quad (3.7)$$

When the massless rod makes an angle θ with the vertical, then the displacement s of the bob is given by:

$$s = L_s \theta \quad (3.8)$$

Differentiating Eq. (8) twice with respect to time t gives us:

$$\ddot{s} = L_s \ddot{\theta} \quad (3.9)$$

Substituting Eq. (9) into Eq. (7) and rearranging:

$$L_s \ddot{\theta} = -g \sin \theta \quad (3.10)$$

Thus:

$$\ddot{\theta} + \frac{g}{L_s} \sin \theta = 0 \quad (3.11)$$

For small angles of θ , the differential equation of simple pendulum motion can be obtained from Eq. (11) as:

$$\ddot{\theta} + \frac{g}{L_s} \theta = 0 \quad (3.12)$$

3.1.3 Combined Model for Structure and Hanging NSC

In this chapter, the two systems from the previous two sub-sections are coupled. This is the next step to arrive at the final analytical model. In this model, the interaction between the two systems will be studied. One system is the SDOF structure with a damper and a spring, and another system is a pendulum with its massless rod. As the combined system has two different motions, two equations are obtained.

Before deriving the differential equations, the following critical assumptions are mentioned in order to establish the analytical model.

1. The length of the pendulum rod is not variable.

2. The mass of the SDOF system is only moved in one direction, i.e., in horizontal direction.

In this study, the structure model is considered as an undamped SDOF system. Flexibly connected hanging loads on the supporting structure during seismic events, as shown in Fig. 3.4, are considered in the current study. A typical scaffold frame with hanging lead blankets through carabiners is shown in Fig. 3.4a. A typical frame with hanging lead blankets subjected to ground acceleration is shown in Fig. 3.4b. The system is idealized, as shown in Fig. 3.4c. The hanging lead blankets are assumed as simple pendulums. The mechanical model for the simplified system is shown in Fig. 3.4d. In this study, a lead blanket hanging from the center of the frame through carabiners is considered. A simple primary structure and the pendulum attached to it is a problem statement considered in this study. Since the original problem that we tried to study was of such a simple structure (single story scaffolding), such assumptions are adequate for the structure and the hanging mass. The scaffolding is considered as a 2D steel frame of a column height of 2.74 m with a circular pipe section of 48.26 mm diameter and a thickness of 3.04mm. Each hanging lead blanket is 1.05 m long and 0.3 m wide with a weight of 80 kg/m². These measurements are taken from actual scaffolding structures that were installed in real power plants. This mass is modelled as a simple pendulum with smaller angular displacements.

The chosen degrees of freedom are the horizontal displacement of the structure relative to the ground and the rotational displacement of the flexibly connected secondary structure (FSS). The free-body diagram of the considered 2DOF combined system is represented in Fig. 3.5.

The hanging mass is connected to the structure by a massless member. The resisting force (F_{res}) acting on the primary structure (PS) by the pendulum can be expressed as follows:

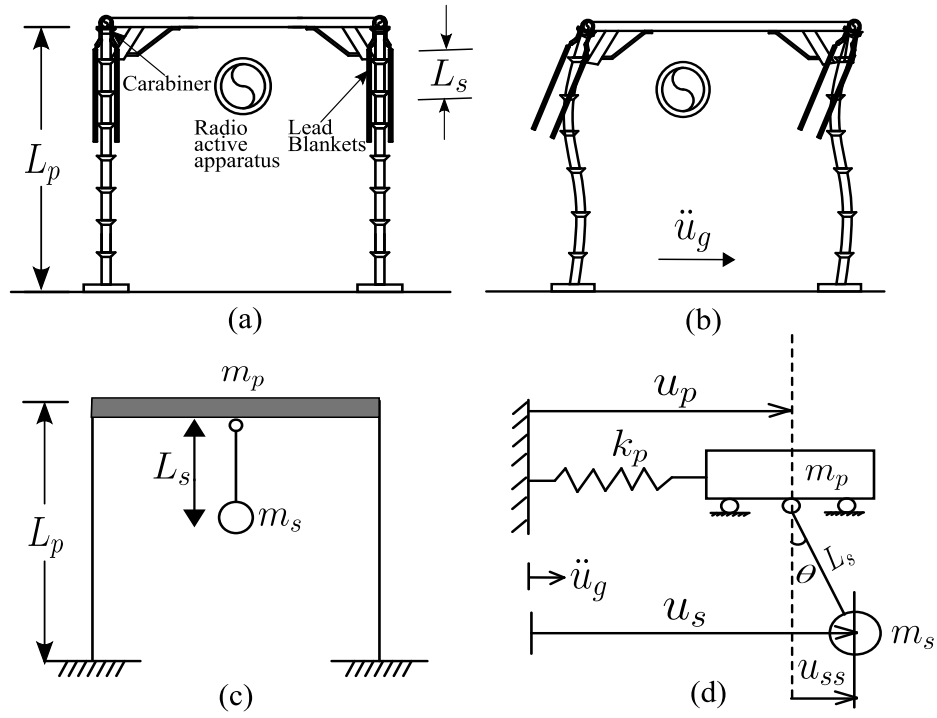


Fig. 3.4 Scaffolding with hanging lead blankets

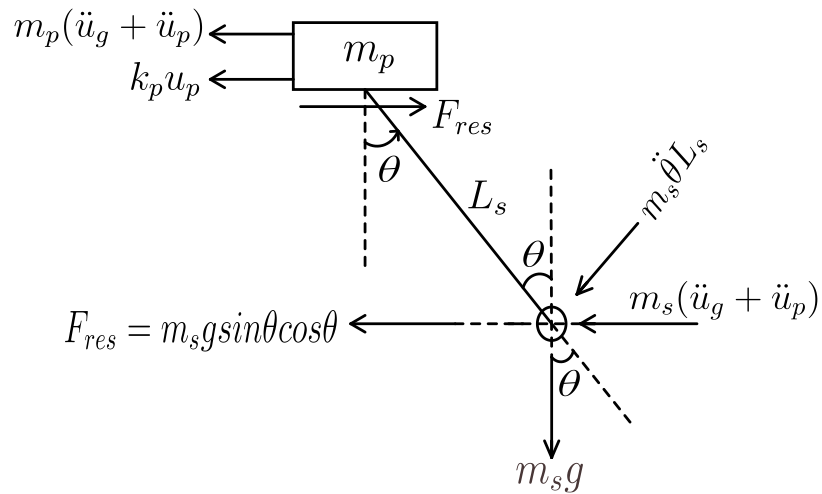


Fig. 3.5 Free-body diagram of the considered 2-DOF system

$$F_{res} = m_s g \sin \theta \cos \theta \quad (3.13)$$

From Fig. 3.5, the horizontal equilibrium of the primary structure gives the governing equation of motion of the PS when coupled with the FSS:

$$m_p(\ddot{u}_p + \ddot{u}_g) + k_p u_p - F_{res} = 0 \quad (3.14)$$

The differential equation governing the motion of the pendulum (FSS) is given by

$$m_s(\ddot{u}_p + \ddot{u}_g)L_s \cos\theta + m_s \ddot{\theta} L_s^2 + m_s g L_s \sin\theta = 0 \quad (3.15)$$

The Eq. (3.15) can be rewritten as:

$$m_s(\ddot{u}_p + \ddot{u}_g) \cos\theta + m_s \ddot{\theta} L_s + m_s g \sin\theta = 0 \quad (3.16)$$

If the amplitude of the external excitation is small, the response of the system will be small. Hence, in this study, small displacements are assumed for the pendulum to simplify the mathematical model by removing the non-linear terms in the differential equations. By assuming the small displacements of the pendulum ($\sin\theta = \theta, \cos\theta = 1$), the resisting force/control force by the pendulum given by Eq. (3.13) reduces to:

$$F_{res} = m_s g \theta \quad (3.17)$$

Eqs. (3.14), (3.16) and (3.17) reduce to:

$$\begin{bmatrix} m_p & 0 \\ m_s & m_s \end{bmatrix} \begin{Bmatrix} \ddot{u}_p \\ \ddot{\theta} L_s \end{Bmatrix} + \begin{bmatrix} k_p & -\frac{m_s g}{L_s} \\ 0 & \frac{m_s g}{L_s} \end{bmatrix} \begin{Bmatrix} u_p \\ \theta L_s \end{Bmatrix} = -\ddot{u}_g \begin{Bmatrix} m_p \\ m_s \end{Bmatrix} \quad (3.18)$$

The above system of equations (Eqs. (3.18)) looks very similar to the equations of motion governing the classical 2DOF system given by:

$$\begin{bmatrix} m_p & 0 \\ m_s & m_s \end{bmatrix} \begin{Bmatrix} \ddot{u}_p \\ \ddot{u}_{ss} \end{Bmatrix} + \begin{bmatrix} k_p & -k_s \\ 0 & k_s \end{bmatrix} \begin{Bmatrix} u_p \\ u_{ss} \end{Bmatrix} = -\ddot{u}_g \begin{Bmatrix} m_p \\ m_s \end{Bmatrix} \quad (3.19)$$

The similarity is attained from replacing u_{ss} and k_s (in Eq. (3.19)) with θL_s and $\frac{m_s g}{L_s}$ respectively (to obtain Eq. (3.18)). Hence, the hanging mass/secondary mass can be accounted for by means of a horizontal spring with stiffness $\frac{m_s g}{L_s}$ connected to a mass

corresponding to the secondary mass (*i. e.*, m_s). The motions of the system are analyzed in the time domain. Duhamel's Integral is used to solve the differential equations in MATLAB.

3.1.4 Validation of the Model

The validation of the analytical model was performed using finite element analysis software SAP 2000. An SDOF frame 2.74 m high and 2 m wide span was considered. The floor beam was considered to be infinitely rigid. The column sections were taken from the actual scaffolding structure with moment of inertia ($I = 11 \times 10^{-8} \text{ m}^4$). The columns total stiffness was calculated to be 25924 N/m. The frame mass is assumed to be lumped at the beam level and the mass is assigned to the special node defined at that level. The ends of the columns are fixed at the base level. With this data, the time period of the primary frame is calculated as 0.263 s. Now, a 2D lumped frame model with a flexibly attached secondary structure is considered in the simulation. The flexibly attached secondary structure is modeled as a simple pendulum. One end of the pendulum is connected to the single story frame mass. The secondary mass (m_s) is lumped at the other end (free end) of the pendulum. A flexible connection between PS and secondary system is achieved by releasing the end moment at the connected end of the pendulum to the frame mass.

Dynamic analysis is performed with a fixed step size of 0.01 sec. The harmonic base motion of acceleration 0.05g with a forcing frequency of 2 Hz is the input given to the support of the primary structure. A representative comparison of displacement time histories by the proposed model and the SAP model is shown in Fig. 3.6.

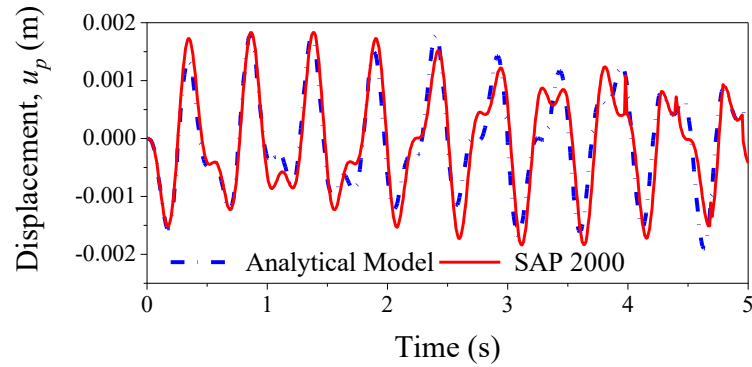


Fig. 3.6 Comparison of displacement of PS with Finite Element model

3.2 Dynamic response of a SDOF structure coupled with a hanging NSC under Harmonic Excitations

In this chapter, the primary structure is coupled with an FSS and is studied for harmonic ground motion. The harmonic ground excitation with the excitation frequency of 4 Hz and amplitude of acceleration as 0.05g is considered. Unless stated otherwise, the dynamic parameters of the PS and FSS used in this section are based on actual values of the lead shielding application from Sec. 3.1.3 and are listed in Table 3.1.

Table 3.1 Dynamic parameters of the coupled SDOF-Hanging NSC system

| Parameter | Value |
|---|--------|
| SDOF mass, m_p (kg) | 45.668 |
| FSS mass, m_s (kg) | 25 |
| Lateral stiffness of the structure, k_p (N/m) | 25924 |
| Length of the FSS, L_s (m) | 0.5 |
| Mass ratio (μ_{SS}) | 0.547 |

A set of equations shown in Eq. (3.19) are used in the simulation in MATLAB. In the first simulation, the displacement time history response of the PS with and without FSS is

plotted, as shown in Fig. 3.7. It can be seen that the relative displacement response of the PS with FSS is different from the PS alone. Thus, flexible secondary systems show a significant effect on the response of the primary structures and cannot be ignored in the design of light structures.

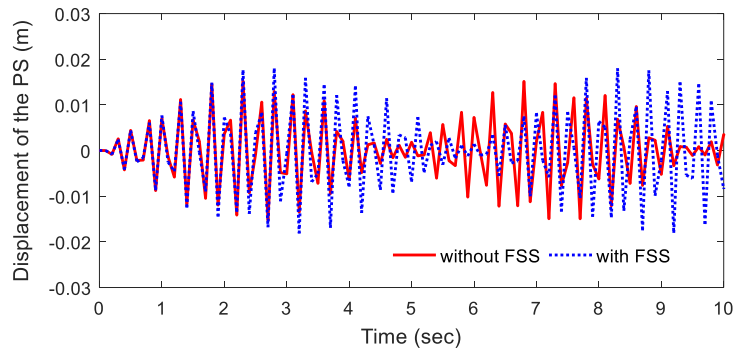


Fig. 3.7 Displacement response of the PS with and without FSS

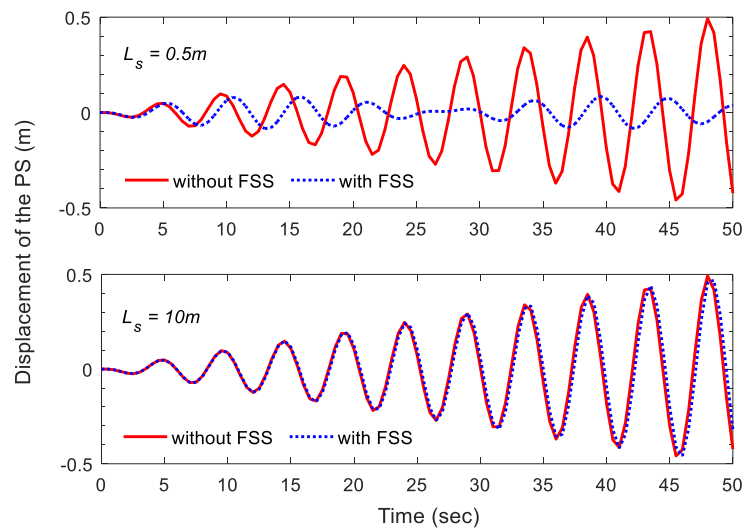


Fig. 3.8 Displacement response of the PS for different lengths of FSS

To further confirm the effect of FSS on the response of the structure, a resonating frequency (forcing frequency equal to the natural frequency of the primary structure) is given to the combined system for two different lengths of FSS say 0.5m and 10m as shown in Fig. 3.8. It can be seen that for length 0.5m, the response of the PS without FSS is more. The response of PS with FSS is subdued since the addition of the FSS creates an extra DOF

on the system, thus changing the vibrating frequencies. For a longer length say 10m, the response of the PS with and without FSS is nearly equal. This is due to the low-frequency pendulums and their non-participation in the vibration of the PS. An extensive parametric study was conducted on the response of the primary structure by varying the excitation frequency, the natural frequency of the FSS and, the mass of the FSS. New parameters called excitation frequency ratio (f_r), tuning frequency ratio (β), and the mass ratio (μ_{SS}) are introduced in this section. The excitation frequency ratio is defined as the ratio of excitation frequency (ω_f) to the natural frequency of the PS (ω_p). Tuning frequency ratio is defined as the ratio of the natural frequency of the FSS (ω_s) to the natural frequency of the PS (ω_p). The mass ratio is the ratio of the mass of the FSS (m_s) to the mass of PS (m_p). In the parametric study, the dynamic properties of the PS are kept constant. The dynamic properties of the FSS and the excitation frequency are varied.

3.2.1 Effect of excitation frequency ratio

To study the effect of the forcing frequency, the value of ω_p is kept constant, and the value of ω_f is varied. Fig. 3.9 depicts the comparison of peak displacement of the PS with and without FSS for different values of β . The results show that the PS with FSS behaves almost as a PS without FSS for a very small tuning frequency ratio ($\beta=0.1$). Thus, the response of the PS with FSS is similar to the response of a PS without FSS, and hence only one peak of the response occurs at $f_r=1$. This is because a very long length of FSS leads to very small tuning frequency ratios. Similarly, in the case of a combined system with a very high tuning frequency ratio ($\beta=2$), only one peak is observed at lower resonant frequency ($f_r=0.8$). Thus, FSS acts as an additional mass which modifies the SDOF system. Similarly, in the case of tuning frequency ratios ($\beta=0.5$ and $\beta=1$), the response curve of the system shows two peaks. The system behaves as a two-degree of freedom system. For certain frequencies,

the system behaves as a single-degree of freedom system, and response is higher than the two-degree of freedom system. Therefore, it can be deduced that the response of the PS with FSS can be controlled by the modified SDOF structure at some excitation frequencies range. For all other cases it acts as a two-degree of freedom system.

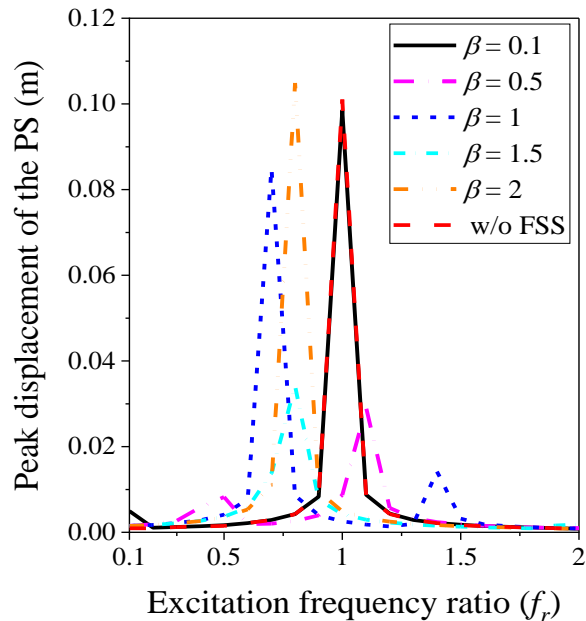


Fig. 3.9 Comparison of peak structural displacement with and without FSS for different excitation frequencies

3.2.2 Effect of tuning frequency ratio

To study the effect of frequency of the secondary system, the value of ω_p is kept constant, and the value of ω_s is varied. The effect of β on the structure is shown in Fig. 3.10. For a given excitation, it is observed that at very small tuning frequency ratios, the response of the structure is independent of the mass of the pendulum. This can be attributed to the fact that a longer length of pendulum causes a lower tuning frequency ratio. The response of the structure increases with an increase in tuning frequency ratio to some point and then gradually decreases with a further increase in the tuning frequency ratio. It can be deduced that, when the frequency of the FSS is in the neighborhood of the primary structural frequency, irrespective of mass ratio, the peak structural response reduces considerably. For

all the mass ratios considered, the range of optimal tuning frequency ratio found out to be 0.8-1, as observed from Fig. 3.10. Thus, for certain tuning frequency ratio, the response reduces significantly.

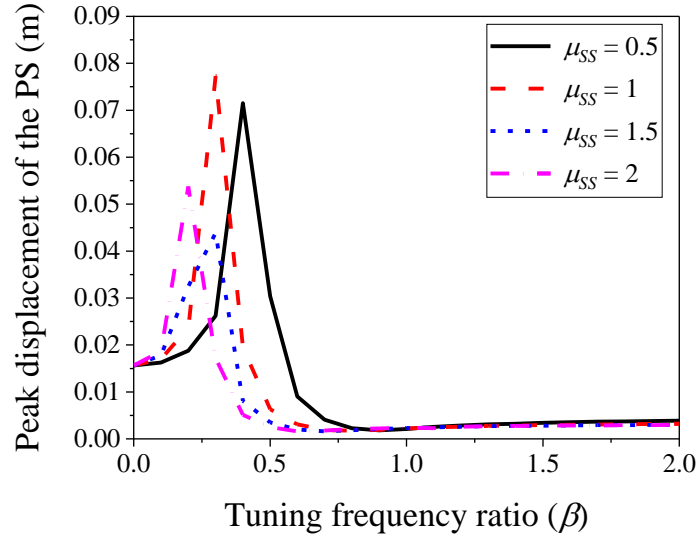


Fig. 3.10 Variation of peak structural displacement for different tuning frequency ratios

3.2.3 Effect of mass ratio

This study is primarily for secondary structures that have a comparable mass to the primary structure. In this section, the effect of mass ratio on the peak displacement response of the PS is studied. The response of the structure is plotted versus the mass ratio (μ_{SS}) as shown in Fig. 3.11. Resonance is observed for $\beta=1$ and $\mu_{SS}=0.7$ if the excitation frequency is equal to either of the natural frequencies of the combined system (Fig. 3.11c). At a higher tuning frequency ratio ($\beta=2$), the variation in the response of the PS with mass ratio depends upon the f_r . For $f_r=0.5$, the response of the PS increases with an increase in μ , whereas the opposite behavior can be observed for $f_r=1$. At a lower tuning frequency ratio ($\beta=0.1$), the response of the PS is not affected by the mass ratio of the FSS for a given excitation frequency ratio (f_r). Therefore, it can be concluded that the response of the PS varies significantly with a mass ratio for a given excitation frequency ratio and tuning frequency ratio.

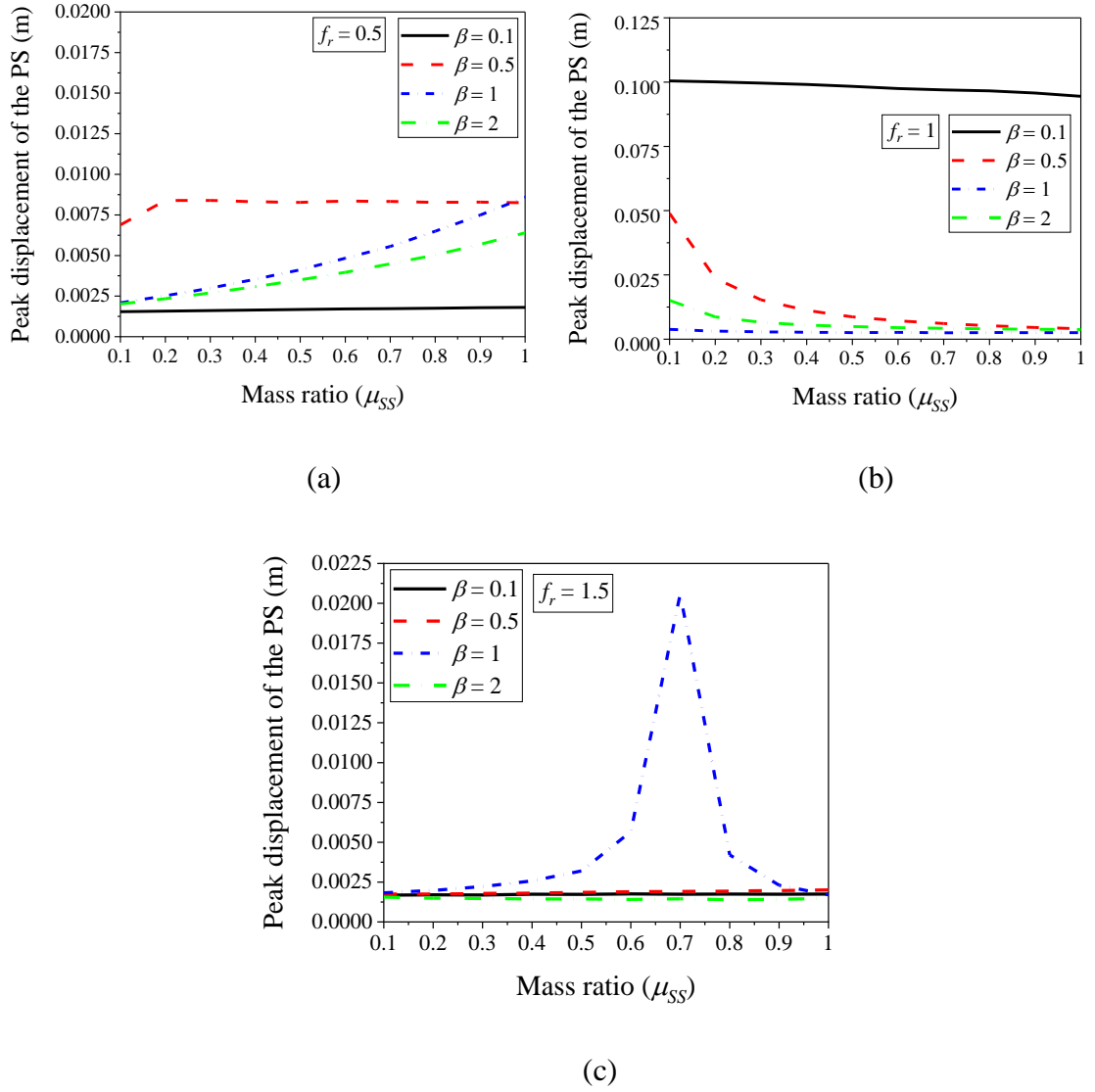


Fig. 3.11 Variation of peak structural displacement for different mass ratios

3.2.4 Mass effect ratio

To understand the participation of secondary mass in the dynamic behavior of the primary structure, the inertial forces on the primary structure need to be looked at. A parameter ϵ is defined to quantify this participation. The mass effect ratio (ϵ) compares the effect of hanging mass on the structure to a structure without a pendulum. It is defined as follows:

$$\epsilon = \frac{m_p \ddot{u}_p (m_p, m_s)}{m_p \ddot{u}_p (m_p, 0)} \quad (3.20)$$

where, $\ddot{u}_p(m_p, m_s)$ is the acceleration of the primary mass as a function of the primary mass (m_p) and secondary mass (m_s).

Considerable values of ϵ gives a clear indication of the significance of this study. When $\epsilon > 1$, the mass participation of the hanging mass cannot be ignored. In the same breath, when $\epsilon < 1$, the hanging mass can be ignored in the design as the effect is less than its actual mass. Fig. 3.12 shows the variation of ϵ with forcing frequency (ω_f) for a particular mass ratio ($\mu_{SS} = 0.547$) and length of FSS, $L_s = 0.5m$ which corresponds to tuning frequency ratio (β) as 0.185.

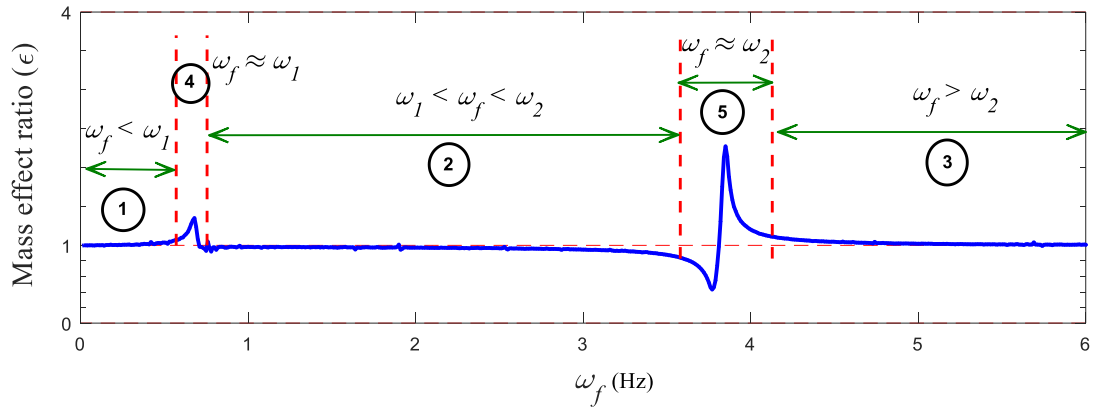
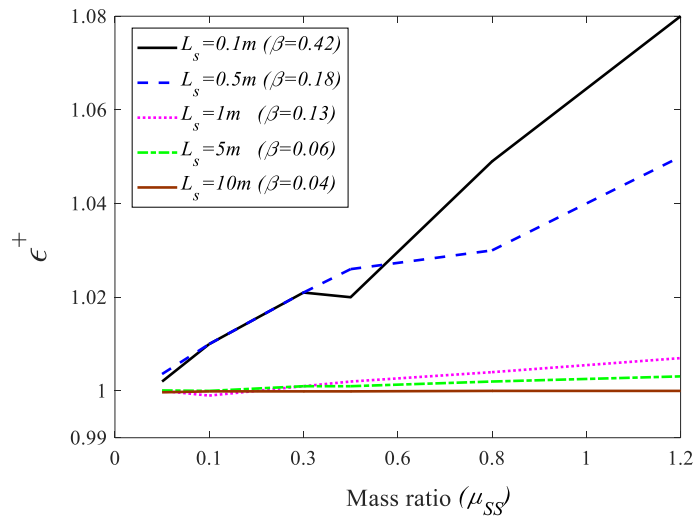


Fig. 3.12 Variation of mass effect ratio (ϵ) with forcing frequency (ω_f)

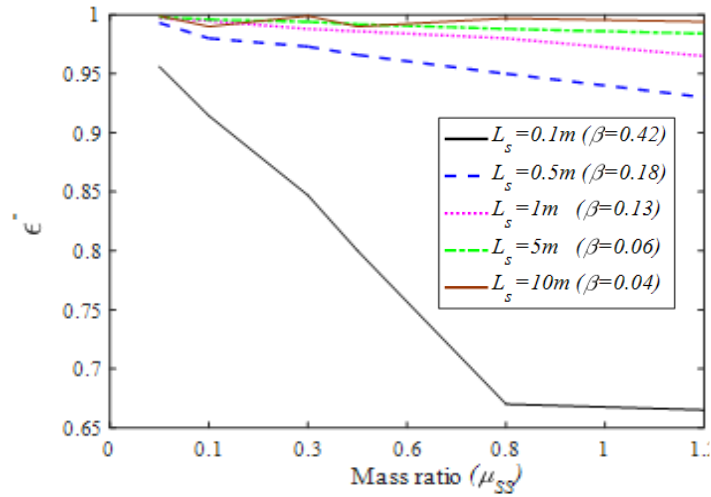
The behavior of ϵ as a function of ω_f is observed to fall into 5 regions, as shown in Fig. 3.12. Regions 4 and 5 show resonance and hence spikes in the value of ϵ . These regions are noted to be in the proximity of natural frequencies of the pendulum and the primary structure, respectively. Since coupled frequencies of the system are close to the individual components frequencies, this behavior is observed. It is also noted that $\epsilon > 1$ in region 1, where $\omega_f < \omega_1$. The average ϵ in this region is defined as ϵ^+ . ϵ is found to be less than unity when the forcing frequency falls between ω_1 and ω_2 . Let the average ϵ in this region be ϵ^- . When the forcing frequency is greater than ω_2 , the value of ϵ tends to 1. In region 1, since the frequency is very low, secondary mass participates in the vibration and hence

$\epsilon^+ > 1$. In region 2, since $\omega_1 < \omega_f < \omega_2$, out of phase motion between the components causes the pendulum to damp the response of the primary structure ($\epsilon^- < 1$). For $\omega_f > \omega_2$ (region 3) the pendulum stops participating in the structural vibration ($\epsilon = 1$). The pendulum, in this case, will stay at rest and not participate in the motion. These observations are in consistent with the plots shown in Fig. 3.11.

The variation of ϵ^+ and ϵ^- against different masses and lengths of the FSS is shown in Fig. 3.13. From Fig. 3.13a, it can be seen that for smaller lengths, as the mass of the FSS increases, the inertial forces on the structure increase. As the length of pendulum increases, the effect of FSS on the PS is considerably reduced and ϵ^+ tends to unity. The pendulum starts damping the response of the PS when the system is vibrating with a forcing frequency in between ω_1 and ω_2 . This effect can be clearly observed from Fig. 3.13b. At smaller lengths, the mitigation in the response of the PS is more as mass increases. As the length of FSS increases, the mitigation effect on the response of the PS decreases and ϵ^- tends to unity.



(a)



(b)

Fig. 3.13 Average Mass effect ratio (ϵ^+ and ϵ^-) against μ_{SS} for different β

3.3 Dynamic response of a SDOF structure coupled with a hanging NSC under Earthquake Excitations

While applying harmonic ground motions to the problem gives us insights in to its behavior, real earthquake motion should be applied before formulating a design methodology for such structures. This gives us a better understanding of the dynamic behavior of the structure. To study the effect of a flexible secondary system on the response of the primary structure, a set of recorded earthquake ground motions are considered. These motions are characterized by their differing frequencies and intensity levels. The details of earthquake motions that are studied here, their time histories and Fast Fourier Transforms are shown in Table 3.2, Fig. 3.14, and Fig. 3.15, respectively.

In this section, a primary structure with and without the secondary mass is subjected to the excitations shown in Fig. 3.14. The characteristics such as mass and tuning frequency ratios are presented here. While the characteristics of the primary structure are not varied, the properties of the secondary system are changed.

Table 3.2. Details of earthquakes considered

| Earthquake | Station name | Component | PGA (g) | Duration (s) |
|-----------------|--|-----------|---------|--------------|
| El Centro(1940) | Imperial valley, Southern California, USA. | N-S | 0.348 | 53.74 |
| Kobe(1995) | Nishi-Akashi, Japan | 0° | 0.509 | 41 |
| Chi-Chi(1999) | Taichung, Taiwan | 0° | 0.537 | 93 |

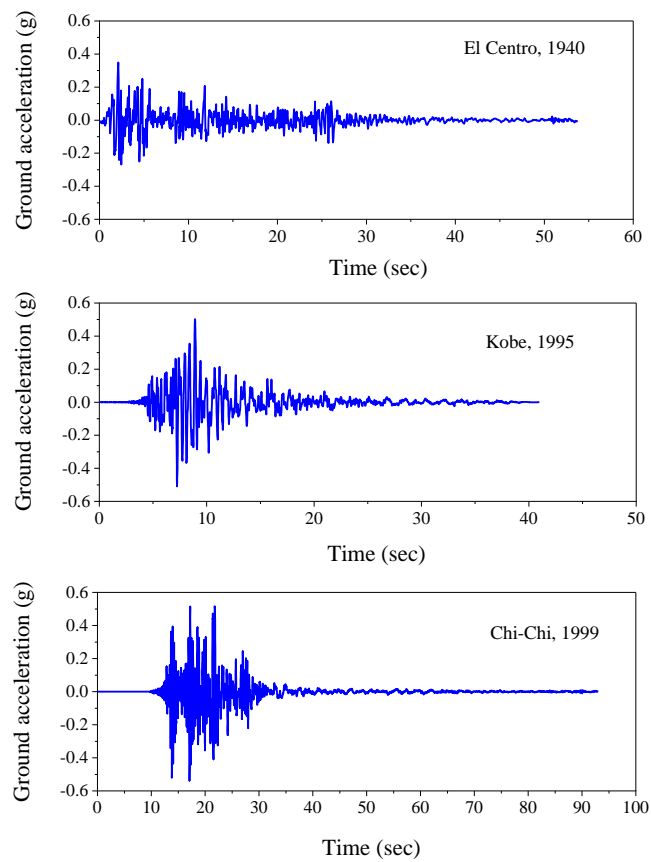


Fig. 3.14 Ground acceleration time histories of selected earthquakes

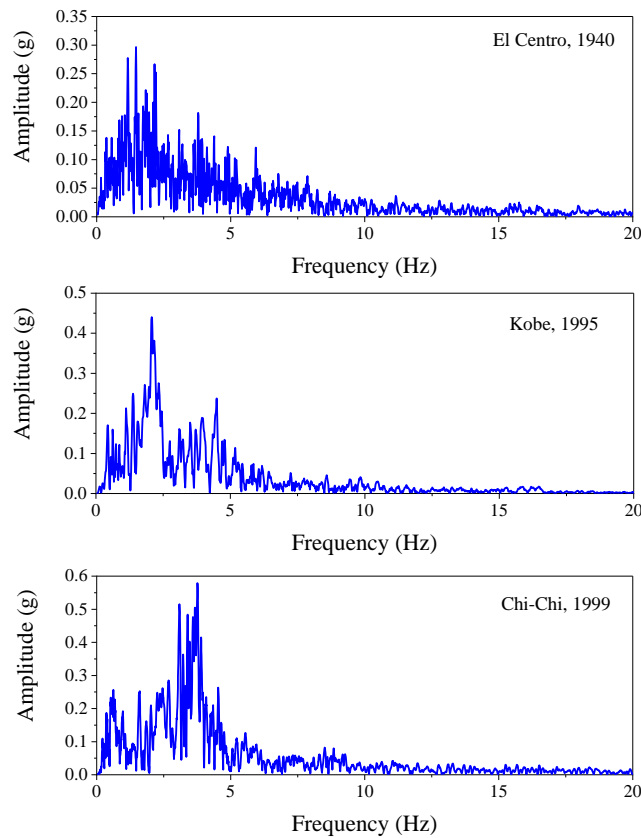


Fig. 3.15 FFT amplitudes of selected earthquakes

3.3.1 Effect of tuning frequency ratio

Fig. 3.16 shows the peak displacement response of the PS when the tuning frequency ratio varies. For this purpose, ω_p is kept constant and ω_s is varied. It is observed that the response of the PS with FSS depends upon the excitation frequency. As earthquakes have random forcing frequencies and the selected earthquakes differ by frequency content, widely varying behavior is seen for each earthquake. It was found in Fig. 3.16 that the response of the structure varies significantly with the tuning frequency ratio for a given mass ratio. The large masses resulted in optimum tuning frequency ratios deviating from the resonance condition ($\beta=1$). For lower mass ratios of FSS, the optimum tuning frequency ratio is in the vicinity of the 1.0 but not certainly in the resonance condition.

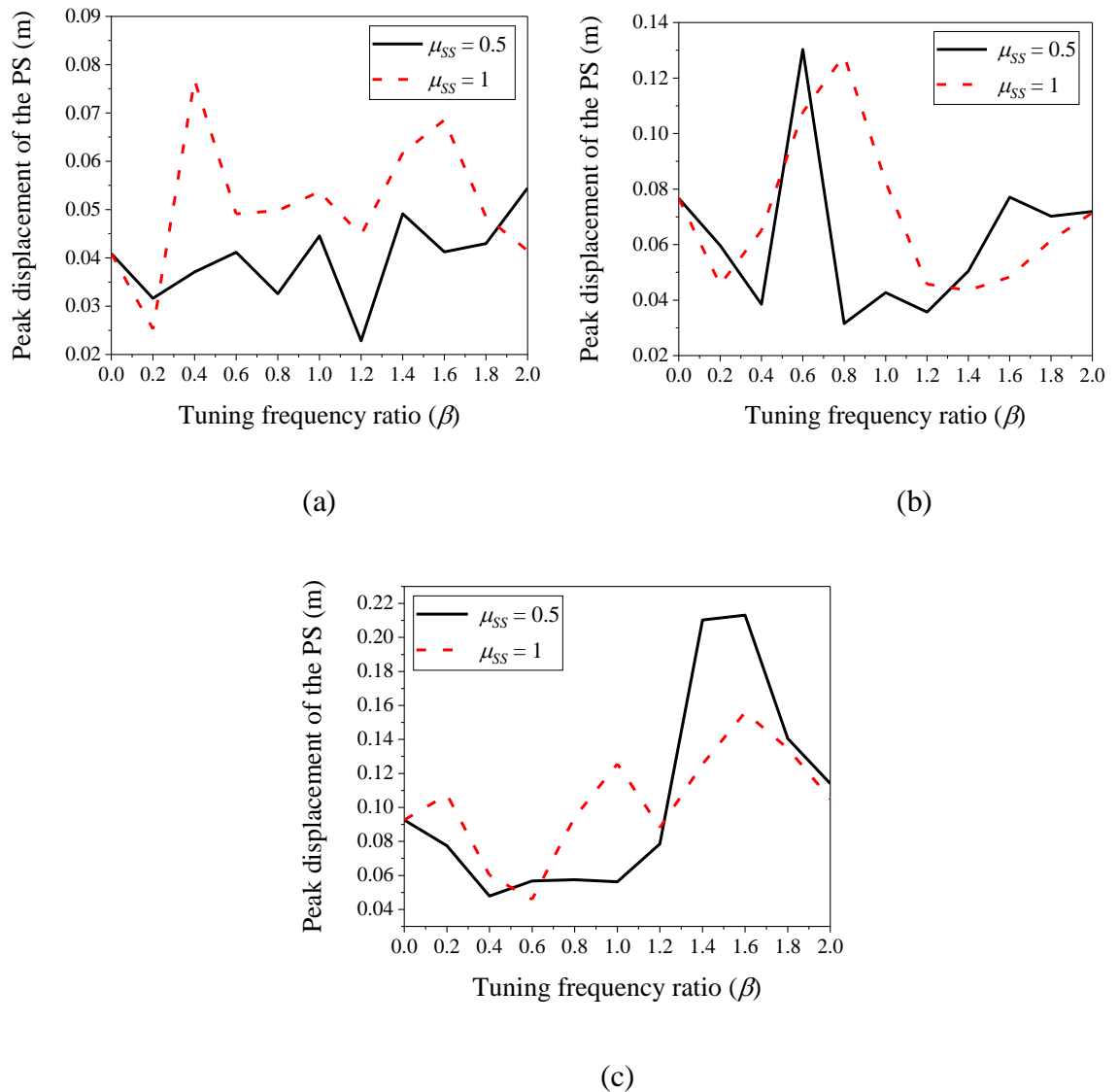


Fig. 3.16 Peak structural response versus tuning frequency (a) El Centro (1940); (b) Kobe (1995); (c) Chi-Chi (1999)

The response of the system with and without FSS under each earthquake is shown in Table 3.3 for better understanding. Optimal tuning frequency ratio is the ratio at which the structural response is minimum. For El Centro and Kobe earthquakes, the percentage reduction in the response of the PS with FSS is more when the β is in the vicinity of the resonance condition. The reduction in response is significant when the tuning frequency ratio is not in the vicinity of the resonance condition at larger mass ratios of FSS. For the Chi-Chi earthquake, the reduction in the response of the structure is high for a larger mass

ratio. This reveals that at larger mass ratios of FSS, the structural response reduces significantly when the tuning frequency ratio is not within the vicinity of the resonance condition. It can also be deduced that the optimal tuning frequency ratio range of the FSS depends upon the excitation frequency and mass ratio of the FSS for a given structure.

Table 3.3 Response reduction at optimal tuning frequency ratios

| Earthquake | Peak displacement of the PS, u_p (m) | | | | |
|---------------------|--|------------|-----|-------------|------|
| | without FSS | with FSS | | % reduction | |
| El Centro (1940) | 0.0405 | β | 1.2 | 0.0228 | 43.7 |
| | | μ_{SS} | 0.5 | | |
| | | β | 0.2 | 0.0253 | 37.5 |
| | | μ_{SS} | 1 | | |
| Kobe (1995) | 0.0767 | β | 0.8 | 0.0315 | 58.9 |
| | | μ_{SS} | 0.5 | | |
| | | β | 0.2 | 0.0456 | 40.5 |
| | | μ_{SS} | 1 | | |
| Chi-Chi (1999) | 0.0927 | β | 0.4 | 0.0479 | 48.3 |
| | | μ_{SS} | 0.5 | | |
| | | β | 0.6 | 0.0458 | 50.5 |
| | | μ_{SS} | 1 | | |

3.3.2 Effect of mass ratio

The structural response is plotted against the mass ratio, μ_{SS} for different tuning frequency ratios (β). The effect of mass ratio on the peak displacement response of the PS is shown in Fig. 3.17. It is observed that, at lower β ($=0.1$) or low-frequency (long) pendulums, the variation in peak displacement response of the PS does not vary much with an increase in the mass ratio for all the three earthquakes. At higher tuning frequency ratios ($\beta=2$), the combined system (PS with FSS) behaves as a modified SDOF structure with an additional mass. Due to this, the structural time period of the modified system increases, and the displacement of the PS varies significantly with the mass ratio. At intermediate tuning frequency ratios, the peak displacement response of the PS varies significantly as mass ratio increases and heavily depends on the type of earthquake excitations. Therefore, it can be

concluded that the mass ratio of the FSS has a significant effect on the response of a PS for all frequencies.

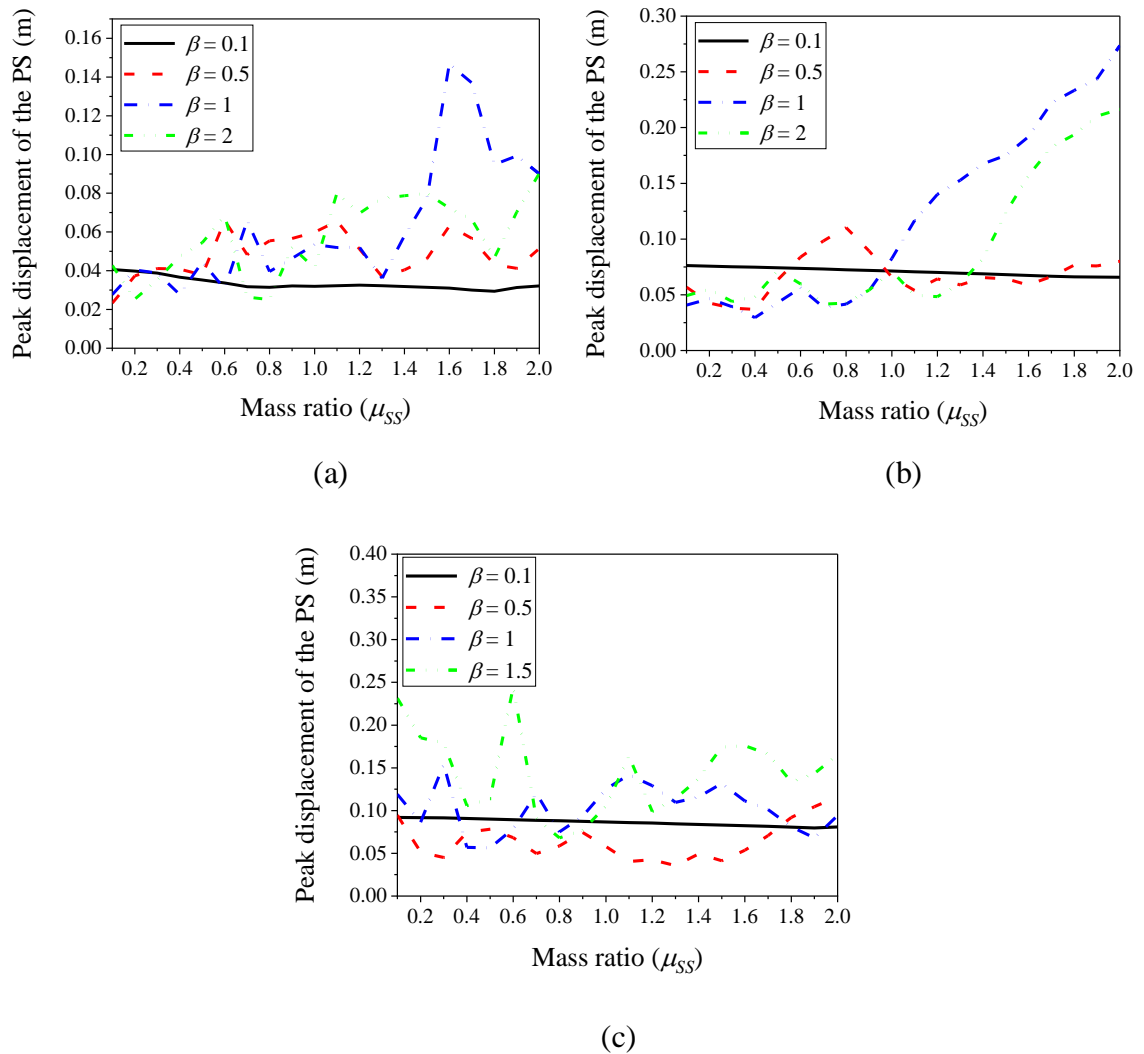


Fig. 3.17 Peak structural response versus mass ratio (a) El Centro (1940); (b) Kobe (1995); (c) Chi-Chi (1999)

3.4 Effect of a hanging NSC on the design response spectrum

From the analysis results above it can be concluded that the effect of suspended/hanging NSC on the seismic response of the primary structure is significant. Therefore, this section tries to incorporate that effect in the design of the structure. The design of the supporting or primary structure is done using the response spectrum method in this study. The calculations of the spectral acceleration of the structure is required for this design. Three

different earthquake excitations have been chosen based upon the shear wave velocity to represent the excitation for hard, medium, and soft soil types from PEER Ground Motion Database (Center 2013). These excitations are made compatible with the design spectra associated with 0% damping. A multiplying factor of 3.2 given in table 3 of IS 1893:2002 (Code 2002) was used to obtain design spectra corresponding to 0% damping from 5% damping design spectra. The design spectra for two seismic zones Zone III and Zone V with respect to different soil types were used in this study. Spectral matching method in the time domain is utilized to generate spectrum compatible earthquake excitations. For this study, the structure is assumed to be fixed on rigid ground. Consideration of soil-structure interaction affects the seismic response and structural period (Ghanbari and Ghanbari 2016). In this study, such soil-structure interaction is neglected. Thus, different excitations with respect to different soil types are considered to represent the different dominant frequencies of the earthquake. The details of the three excitations are shown in Table 3.4. The frequency content for each earthquake excitation can be determined by conducting Fast Fourier Transform (FFT) to each excitation. Table 3.5 summarizes the dominant frequency of each excitation. Fig. 3.18 shows the target IS 1893:2002 spectra for hard, medium, and soft soil conditions for Indian seismic zone III. The corresponding response spectra of the spectrum compatible ground motions are also presented. The target spectra of seismic zone V and corresponding response spectra for the ground motions of different soil types are shown in Fig. 3.19.

Table 3.4 Details of earthquakes

| Event | Station name | Year | Magnitude (M_w) | Shear Wave Velocity, V_s (m/s) |
|--------------------|---------------------|------|---------------------|----------------------------------|
| Kern County | Taft Lincoln School | 1952 | 7.36 | 385.43 |
| Northern Calif-03 | Ferndale City Hall | 1954 | 6.5 | 219.31 |
| Imperial Valley-06 | El Centro Array #3 | 1979 | 6.53 | 162.94 |

Table 3.5 Dominant frequencies of the excitations

| Event | Soil type | Dominant frequency (Hz) |
|--------------------|-------------|-------------------------|
| Kern County | Hard Soil | 2.27 |
| Northern Calif-03 | Medium Soil | 0.63 |
| Imperial Valley-06 | Soft Soil | 0.41 |

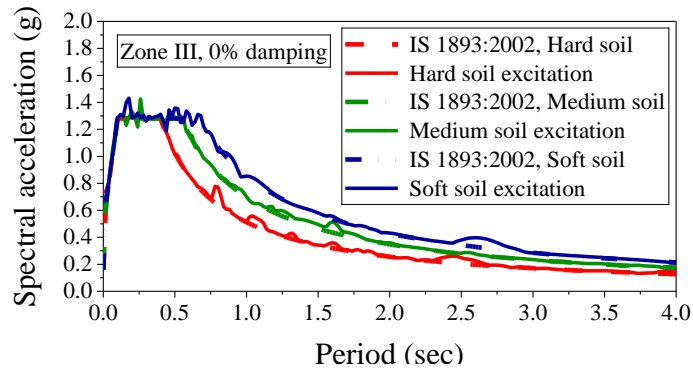


Fig. 3.18 IS 1893:2002 Zone III design spectra and response spectra of the ground motions

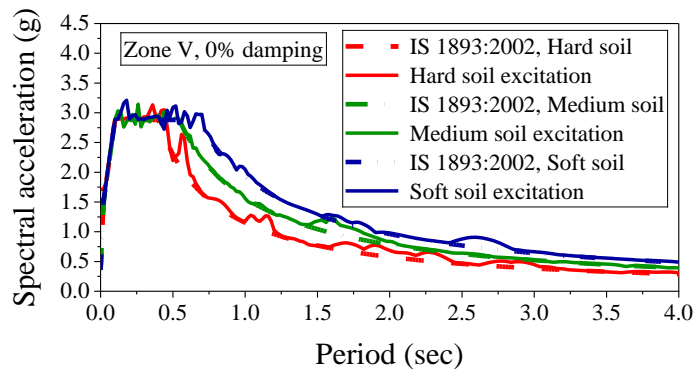


Fig. 3.19 IS 1893:2002 Zone V design spectra and response spectra of the ground motions

Spectrum compatible ground motions in seismic zones III and V for different soil conditions are applied to the combined model to verify the effect of the seismic zone and soil type on the dynamic behavior of a structure with a hanging load. Figs. 3.20, 3.21, and 3.22 display the acceleration response of the PS with and without FSS by solving the system of equations of motion of PS for different earthquake excitations in seismic zones III and V. The structural period of the PS is chosen as 0.8 s. The length of FSS and mass ratio are 0.1 m and 1, respectively.

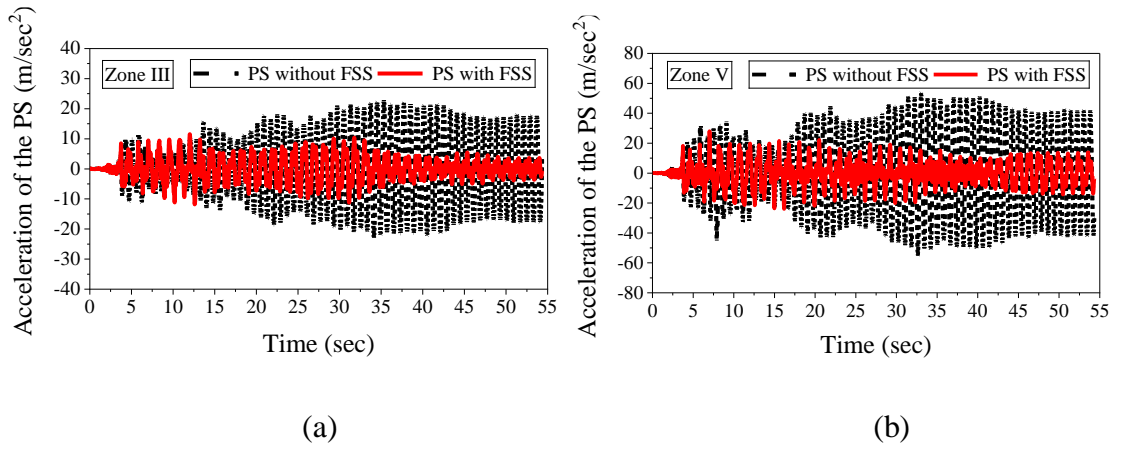


Fig. 3.20 Acceleration response of PS with and without FSS for hard soil excitation (a) Zone III; (b) Zone V

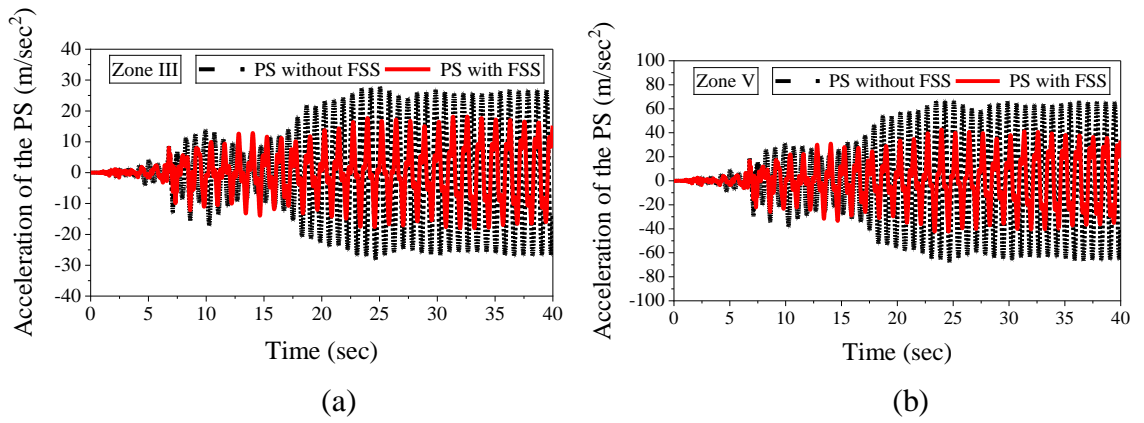


Fig. 3.21 Acceleration response of PS with and without FSS for medium soil excitation (a) Zone III; (b) Zone V

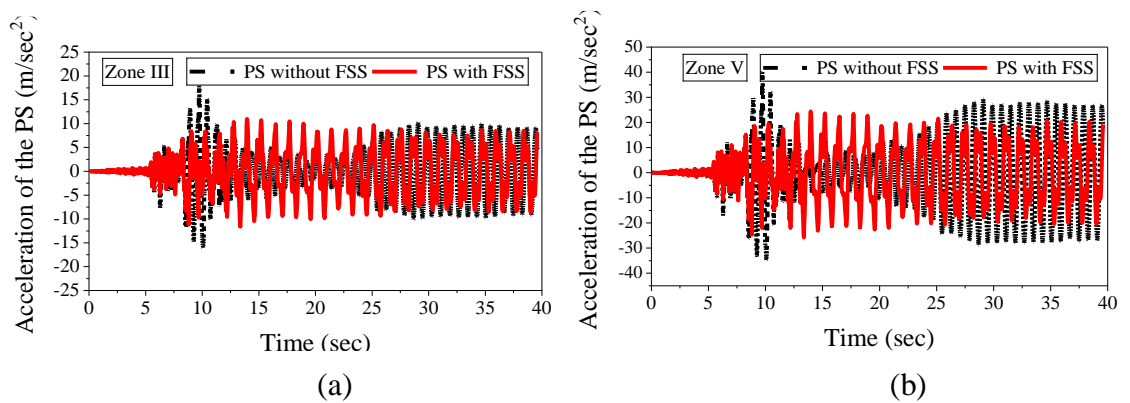


Fig. 3.22 Acceleration response of PS with and without FSS for soft soil excitation (a) Zone III; (b) Zone V

The acceleration response of the PS with FSS on hard soil shows maximum reduction throughout the excitation, as shown in Figs. 3.20a and 3.20b. For medium soil, a reduction in the acceleration of the PS with FSS can be observed. The reduction is not as much as the hard soil condition (Figs. 3.21a and 3.21b). For soft soil, there is a reduction in the acceleration of PS accompanied by amplification at some range acceleration, as shown in Figs. 3.22a and 3.22b. A parameter called *Response Acceleration Reduction Ratio (RARR)* is defined in this study to quantify the effect of FSS as follows:

$$RARR = \frac{a_0 - a_1}{a_0} \times 100 \quad (3.21)$$

where, a_0 is the maximum acceleration of PS without FSS, and a_1 is the maximum acceleration of PS with FSS.

The response of the PS with and without FSS along with *RARR* is shown in Table 3.6. It can be seen that the FSS affects the dynamic response of PS differently under different soil and seismic zone conditions. In all the three soil types, FSS decreases the acceleration response of the PS in both the seismic zones. The maximum value of *RARR* is about 49% on hard soil for both Zone III and V. The minimum value of *RARR* is 35% on soft soil for both Zone III and Zone V. From this preliminary investigation, it can be concluded that the while dynamic response of the PS with FSS depends upon the soil type, dominant frequency of the excitation it is independent of the seismic zone. Hence in this study methodology is developed for the estimation of spectral acceleration of the PS with FSS by incorporating the soil type and seismic zone by varying the vibrational parameters of the FSS.

Table 3.6 Response of PS with and without FSS, and *RARR*

| Soil Type | Maximum acceleration of PS (m/sec ²) | | | | | |
|-----------|--|----------|-----------------|-------------|----------|-----------------|
| | Zone III | | | Zone V | | |
| | Without FSS | With FSS | <i>RARR</i> (%) | Without FSS | With FSS | <i>RARR</i> (%) |
| A | 22.95 | 11.68 | 49.00 | 55.13 | 27.95 | 49.30 |
| B | 28.22 | 18.15 | 35.60 | 67.78 | 42.75 | 36.90 |
| C | 17.91 | 11.56 | 35.45 | 40.10 | 25.78 | 35.70 |

3.4.1 Methodology to determine the modified spectral acceleration for the structure

In this section, a methodology was developed to calculate the spectral acceleration of the PS given the vibrational parameters of the FSS, such as mass ratio (μ_{SS}), length of FSS (L_S), and design spectrum. The design spectra in the seismic design code of India, IS 1893:2002, as shown in Fig. 3.23 are chosen to demonstrate this methodology.

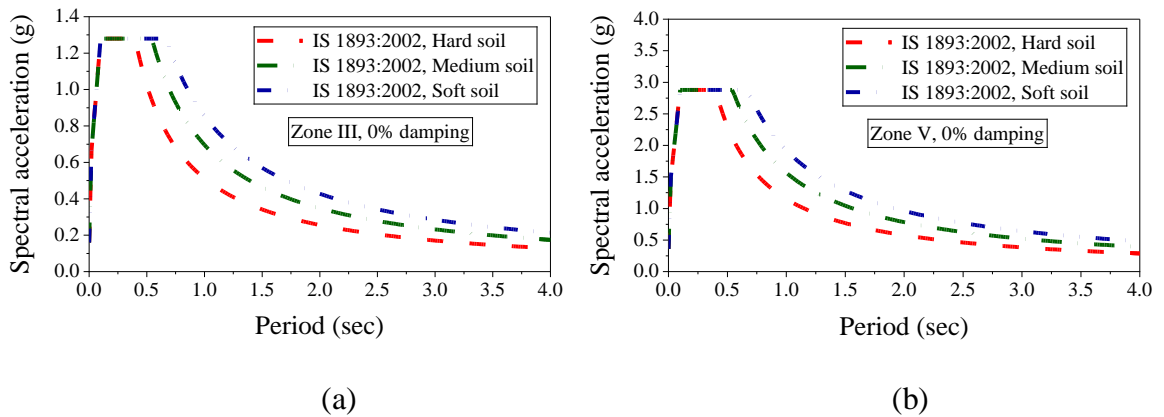


Fig. 3.23 Target design spectra for different soil conditions (a) Zone III; (b) Zone V

It should be noted that this methodology is for any generalized case. The spectral acceleration of the PS with FSS can be calculated through the following steps:

- Consider a PS with an FSS.
- Perform Eigenvalue analysis for the coupled system (PS with FSS i.e. Eqs. (3.19)) and determine modal frequencies.

- Calculate the spectral accelerations (S_{a1} and S_{a2}) from the given spectrum for modal time periods T_1 and T_2 obtained from the above step.
- Find out the inertial forces on PS in two modes and get the total inertial force using Quadratic Combination (QC) method.
- Calculate the new spectral acceleration of PS from the inertial force (obtained in the above step) by dividing it by the mass of the PS.
- Repeat the procedure for different structural periods of PS and construct a new design spectrum.

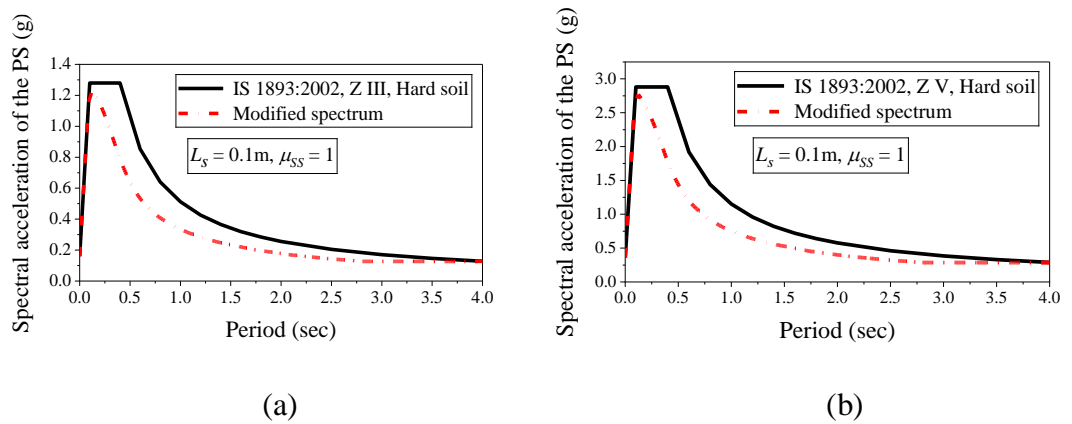


Fig. 3.24 Effect of a smaller length and a higher mass ratio of an FSS on the design spectrum (a) Zone III; (b) Zone V

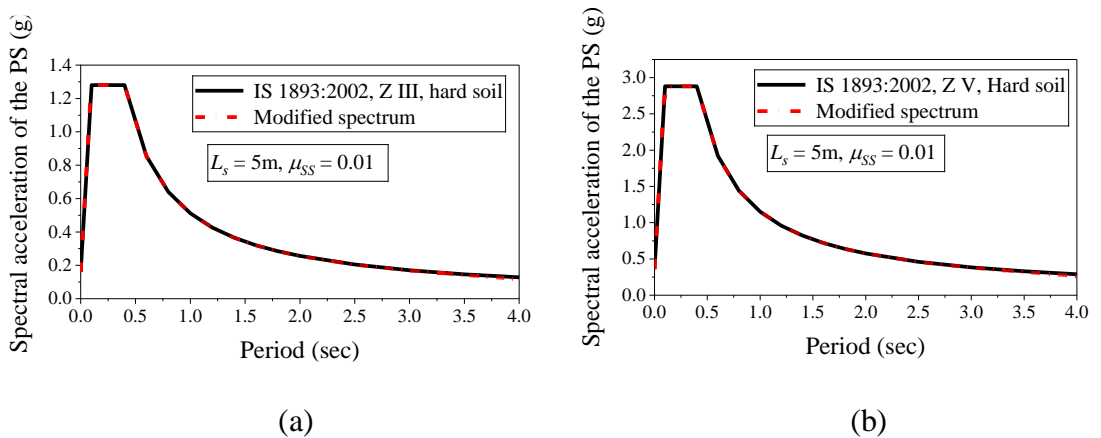


Fig. 3.25 Effect of a longer length and a smaller mass ratio of an FSS on the design spectrum (a) Zone III; (b) Zone V

Design spectra thus produced are compared to existing spectra, as shown in Figs. 3.24 and 3.25. From the figures, it can be observed that the effect of FSS on the design response spectrum is negligible for very long pendulums, while the opposite is true for very short pendulums. In order to quantify the effect of vibrational parameters on the spectral acceleration of PS, a parameter called *Design Acceleration Ratio (DAR)* is defined in this study as follows:

$$DAR = \frac{S_a (modified)}{S_a (original)} \quad (3.22)$$

where, $S_a (original)$ is the spectral acceleration of the PS from the original spectrum (IS 1893:2002 in this case). $S_a (modified)$ is the spectral acceleration of the PS from the modified spectrum (after incorporating the effect of the FSS). The effects of various parameters like μ_{SS} , β , and T_p on *DAR* are studied in the following section. This study is performed on hard soil conditions at seismic zones III and V.

3.4.2 Effect of the mass ratio and tuning frequency ratio on the response

In this section, the effect of mass ratio (μ_{SS}) and tuning frequency ratio (β) on *DAR* are examined. The mass ratio (μ_{SS}) is varied from 0.1 to 1. It should be noted that the mass of the secondary mass is considerable in all these cases. Namely, varying between 10% and 100% of the primary structure. This is only possible for very heavy secondary masses or very light primary structures. The structural periods of the PS are chosen to be 0.5s, 1s, 1.5s, and 2s in line with the most common one-story structures including the scaffolding from Section 3.1.3. Fig. 3.26 shows the *DAR* values in seismic zones III and V with varying mass ratio (μ_{SS}) for different structural periods.

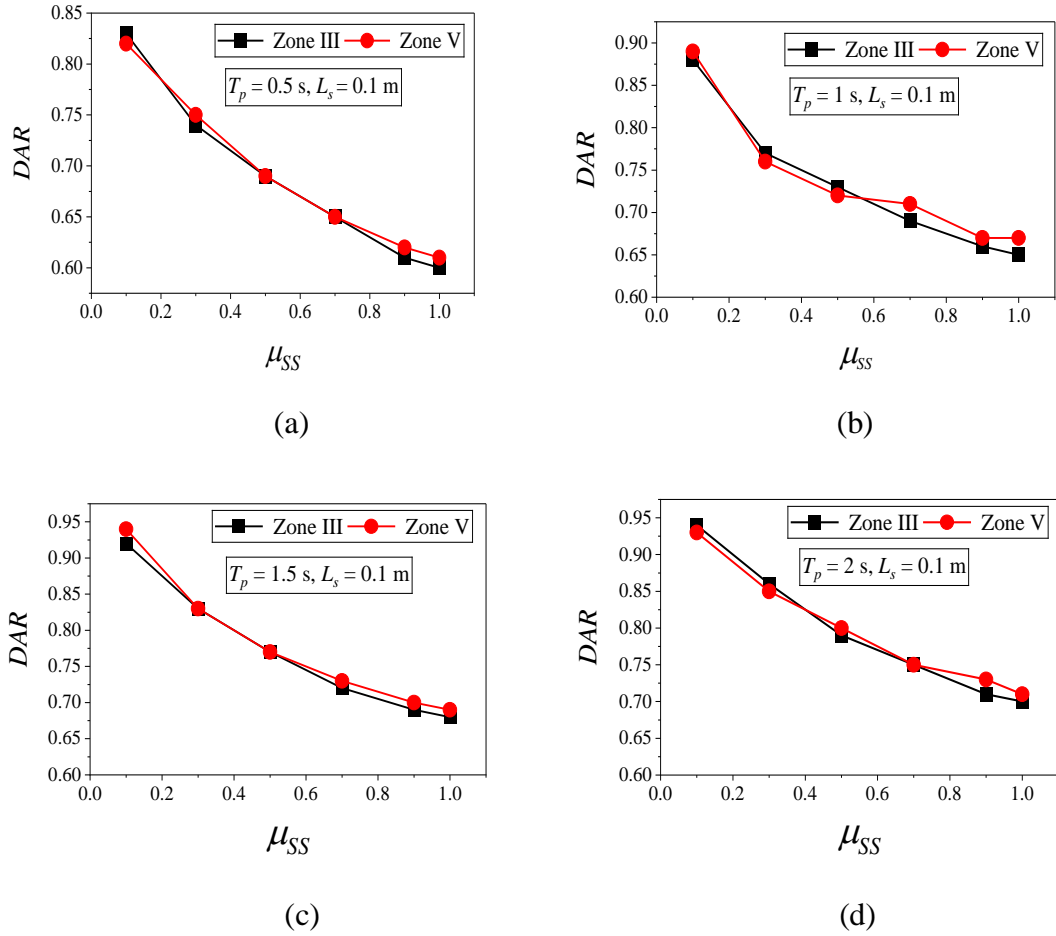


Fig. 3.26 Variation of DAR with mass ratio (μ_{SS}) for different structural periods (T_p)

For a small mass ratio ($\mu_{SS} = 0.1$), the response of the structure reduces by 6-17% with the addition of an FSS. This reduction increases to 30-40% when the mass ratio is high ($\mu_{SS} = 1$). It is important to note that the DAR is not site-specific for a given mass ratio and structural period (Fig. 3.26). While DAR is not site-specific for Indian conditions, it is important to understand independence also for conditions from around the world. In order to understand the variation of DAR in such cases, the values are compared using IS 1893:2016 and ASCE 41-13 (Pekelnicky et al., 2012) for hard soil for 5% damping. Table 3.7 shows the DAR for a given μ_{SS} and L_s as per IS 1893:2016 and ASCE 41-13 codes. It can be observed that DAR is constant with a negligible variation for both the response spectra. This shows that a design expression for DAR can be developed independent of the spectra. In the next section, such a design expression for DAR is developed.

The length of the FSS (L_s) on the modified design spectrum is studied by defining the tuning frequency ratio (β). Tuning frequency ratio (β) is defined as the ratio of secondary system frequency (ω_s) to the primary structure frequency (ω_p). The pendulum frequency ($\sqrt{\frac{g}{L_s}}$) depends upon the suspension length and is independent of the mass ratio. The time period of the structure is set as 0.7 sec. The values of various lengths of FSS and corresponding frequency ratios are shown in Table 3.8.

Fig. 3.27 illustrates the variation of *DAR* with a variation in mass ratio and frequency ratio. The lowest *DAR* value is obtained at the bottom point on the 3D contour plot. In addition to the 3D contour surface, five different lengths of FSS are sampled to better demonstrate the trend in the variation of *DAR* with a mass ratio, as shown in Fig. 3.28. From Fig. 3.28, it can be observed that the *DAR* varies from 0.55 to 0.99, depending on the length and mass of the FSS. It can also be seen that for shorter lengths of FSS and larger mass ratios, the response of the structure reduces with the addition of a secondary system. This variation of response as the length (and hence β) of the secondary system changes can be further explained by performing a Fourier response analysis of these systems with real earthquake ground motions.

For this case, ground motion compatible with Seismic Zone III hard soil excitation is considered, and the structural period (T_p) of the PS is chosen as 0.7 sec (1.42 Hz). The mass ratio (μ_{SS}) is about 0.5. Fig. 3.29 illustrates the effect of the frequency ratio on the acceleration response of the PS with and without FSS. There is only one peak in the Fourier spectra of the acceleration response of the PS without FSS, which is at 1.42 Hz, corresponding to its natural frequency. When the PS is attached with FSS, there exist two peaks in the Fourier response spectra at tuning frequency ($\beta = 1.1$) and un-tuning frequency ($\beta = 1.3$) case. Two peaks are located at both sides of 1.42 Hz, corresponding to the natural

Table 3.7 Variation of *DAR* as per IS 1893:2016 and ASCE 41-13 response spectra (5% damping)

| T_p (sec) | <i>DAR</i> | | | |
|-------------|-------------------------------|------------|-------------------------------|------------|
| | $\mu_{SS} = 0.5, L_s = 0.1$ m | | $\mu_{SS} = 0.5, L_s = 0.5$ m | |
| | IS 1893:2016 | ASCE 41-13 | IS 1893:2016 | ASCE 41-13 |
| 0.1 | 0.94 | 0.98 | 0.94 | 0.99 |
| 0.5 | 0.70 | 0.67 | 0.95 | 0.93 |
| 1 | 0.72 | 0.71 | 0.76 | 0.77 |
| 1.5 | 0.77 | 0.77 | 0.66 | 0.67 |
| 2 | 0.79 | 0.80 | 0.70 | 0.71 |

Table 3.8 Correlations between the length of the FSS and tuning frequency ratio

| L_s (m) | 0.01 | 0.05 | 0.1 | 0.2 | 0.3 | 0.4 | 0.5 | 1 | 2 |
|-----------|------|------|-----|------|------|------|------|------|------|
| β | 3.49 | 1.56 | 1.1 | 0.78 | 0.63 | 0.55 | 0.49 | 0.34 | 0.24 |

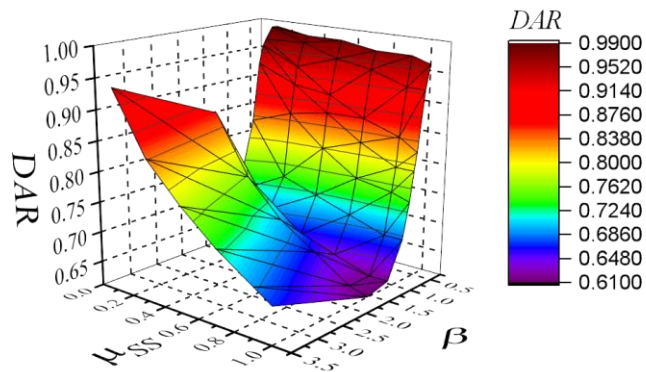


Fig. 3.27 Variation of *DAR* with mass ratio (μ_{SS}) and tuning frequency ratio (β)

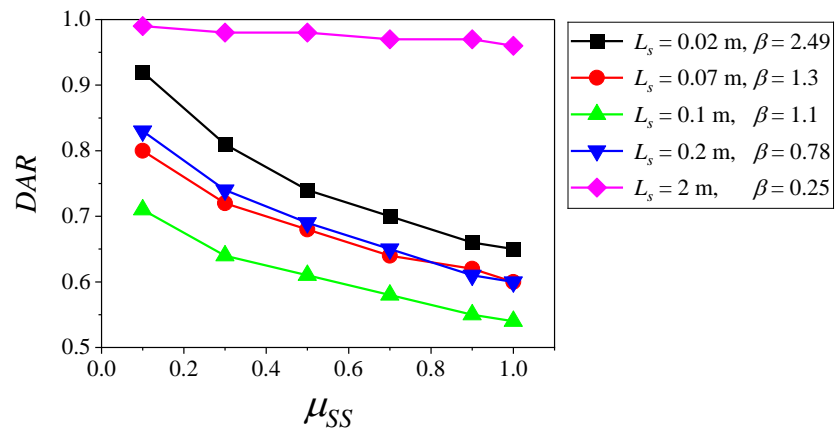


Fig. 3.28 Variation of *DAR* with mass ratio (μ_{SS}) for a selected tuning frequency ratio (β)

frequencies of the PS and FSS, separately. There is also only one peak at 1.42 Hz, at un-tuning frequency ($\beta = 0.25$) case (Fig. 3.29d). For a very high-frequency ratio ($\beta = 2.49$), only one peak is observed at 1.14 Hz, which is the frequency of the PS when the secondary system is rigidly attached. At the tuning frequency case ($\beta = 1.1$), the magnitude of the second peak is greater than the first peak, which shows that response of the FSS is larger than the PS (Fig. 3.29c). Thus, the primary structure's response is transferred to the FSS and resulting in a good reduction effect. In the case of $\beta = 1.3$, the first peak is greater than

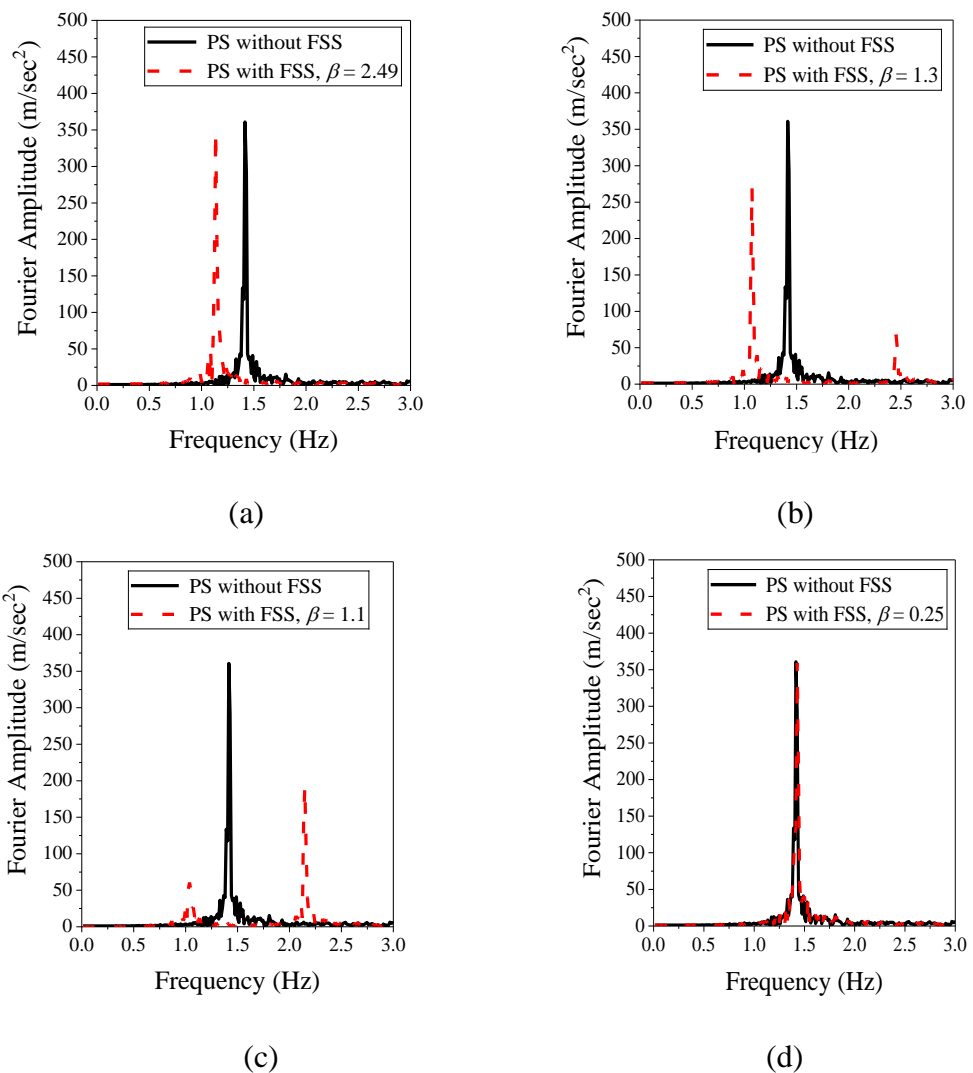


Fig. 3.29 Variation of Fourier amplitude response of PS for different tuning frequency ratios (β)

the second peak, which means that the PS response is more than the response of the FSS. Even though the response of the PS with FSS is less than the PS without FSS, the damping effect of the FSS on the response of the PS is not as good as the former one. For a very low-frequency ratio, $\beta = 0.25$, the moving mode of the FSS is not excited and shows an insignificant effect on the response of the PS. From this, it can also be deduced to the fact that since longer suspension lengths of the FSS leads to low-frequency ratios for a given structural period, such longer length secondary systems show a negligible effect on the PS. Hence, response of the PS with FSS is equal to the response of the PS without FSS at the same structural frequency. Very small suspension lengths of the FSS lead to very high-frequency ratios for a given structural period. Due to small suspension lengths, the stiffness parameter of the FSS becomes very high such that FSS acts as a rigidly attached secondary system. Due to this rigid attachment, a full mass of the FSS participates in the dynamic motion along with PS. This results in an increase of the structural mass, leading to a lower frequency of 1.14 Hz, as shown in Fig. 3.29a.

3.4.3 Validation of the proposed design methodology

To examine the accuracy of the proposed design methodology, the optimum tuning frequency ratios (β_{opt}) of the FSS for a given primary structure are calculated by changing the mass ratio (μ_{SS}). The obtained β_{opt} from the current study is compared with the optimum value obtained by the polynomial equation suggested in the reference study (Yucel *et al.* 2019). For this purpose, the time period of the undamped primary structure is chosen as 0.1 sec. The mass ratios are 0.01, 0.05, 0.1, 0.2 and 0.4. *DAR* values are calculated for each case.

Optimum tuning frequency ratio (β_{opt}) is a tuning frequency ratio where *DAR* is minimum for a given mass ratio. Table 3.9 presents the optimum tuning frequency ratios

of the FSS obtained by using the proposed design methodology in this study and the equations proposed in the reference study. It can be seen that the optimum tuning frequency ratios in both the studies are very close. Therefore, the proposed methodology in this study is validated and can be used to estimate the spectral accelerations of the primary structure with the flexibly attached secondary system.

Table 3.9 Optimal tuning frequency ratios of FSS

| μ_{SS} | β_{opt} | |
|------------|---------------|---------------------------|
| | Current study | Study (Yucel et al. 2019) |
| 0.01 | 1.00 | 1.03 |
| 0.05 | 0.99 | 0.95 |
| 0.1 | 0.92 | 0.92 |
| 0.2 | 0.90 | 0.89 |
| 0.4 | 0.80 | 0.87 |

3.4.4 Design expressions to determine the spectral acceleration of the structure by Non-Linear Regression (NLR) and Artificial Neural Networks (ANN)

In order to design a PS with a given FSS, an expression for *DAR* needs to be developed. In order to develop a design expression, a database has been generated first for the spectral acceleration of PS with FSS for different cases by changing the input parameters mass ratio, length of the FSS, and structural period. The generated database has been used to develop a non-linear regression model and a design expression. For some of the cases, *DAR* can be obtained from Figs. 3.27 and 3.28. In other cases, a design expression will be developed through a parametric study by considering a large number of discrete points correspond to variables T_p , μ_{SS} and L_s . A Non-linear Regression (NLR) analysis of these results produced the following design equation:

$$\begin{aligned}
 DAR = & (1.554 * \mu_{SS} - 2.666 * L_s + 3.091) * e^{(0.629*\mu_{SS}-0.257*L_s-7.697)*T_p} + \\
 & (-0.458 * \mu_{SS} + 1.891 * L_s + 2.753) * e^{(1.268*\mu_{SS}-0.499*L_s-2.885)*T_p} + \quad (3.23) \\
 & LN(0.125 * T_p^2) + 4.336 * e^{(-0.313*T_p-0.235*\mu_{SS}+0.005*L_s-0.083*T_p^2)}
 \end{aligned}$$

Fig. 3.30 shows the correlation between actual and predicted *DAR* values. The actual *DAR* values are obtained by a parametric study using the analytical model, whereas the predicted *DAR* values are obtained by the non-linear regression equation. The Eq. (3.23) best established the dependency among the variables with R^2 of 0.898. In using Eq. (3.23), it must be emphasized that the expression is derived under the following conditions and assumptions: (i) Small displacements of the secondary system, (ii) Length of the FSS from 0.01 m to 2 m, (iii) Mass ratio (μ_{SS}) from 0.1 to 1, (iv) Time period of the PS from 0.1 sec to 4 sec. The proposed design expression can be used for the calculation of spectral acceleration of the PS when it is attached with a flexible secondary system.

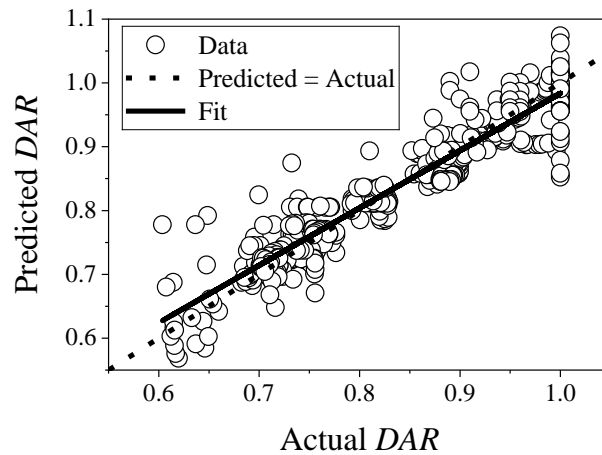


Fig. 3.30 Actual *DAR* vs. Predicted *DAR* by Non-linear Regression

As the design expression obtained by the nonlinear regression is found to be not adequate ($R^2=0.898$), an Artificial Neural Network (ANN) model has been used effectively in this study to predict the spectral acceleration of the PS with FSS, since the output can be obtained from the ANN-based model using simple hand calculations (Shahin et al. 2002). The advantages of modelling of ANN over that of statistical linear and nonlinear regression are: i) the functional design expression or its form need not be assumed a priori as in the case of nonlinear regression, ii) the degree of nonlinearity of independent parameters also need not be assumed a priori, iii) flexibility of varying the network architecture easily for

accurate modelling and prediction which is independent of functional approximation, and iv) the ease of coming up with generalized design expression for the chosen, most accurate simulation and prediction.

A two-layer feed-forward neural network with the tan-sigmoid transfer function for both hidden and output layers has been created in MATLAB R2015a environment to predict the *Design Acceleration Ratio (DAR)*. The network has been trained with Bayesian Regularization (BR) backpropagation learning algorithm. *DAR* values are simulated for 540 cases with input parameters as a mass ratio (μ_{SS}), structural period (T_p), and length of FSS (L_s) for a given seismic design spectrum. The mass ratio varies from 0.1 to 1, with 0.2 intervals. Structural period (T_p) varies from 0.1 sec to 4 sec with 0.5-sec intervals. The length of FSS (L_s) ranges from 0.01 m to 2 m. For a given range of L_s and T_p , the tuning frequency ratio (β) varies in the range of 0.5 to 1.4. Among the whole data, 70% of the data (378 cases) has been allocated to the Training Set, and the remaining 30% of the whole database (162 cases) has been allocated to the Testing Set. Before presenting the input and output variables to the ANN model training, they were normalized between -1.0 and 1.0 to eliminate their dimension and to ensure that all the variables receive equal attention during training (Shahin et al., 2002). The normalized value for each variable x with minimum and maximum values of x_{min} and x_{max} , respectively, is calculated as follows:

$$x_n = \frac{2(x - x_{min})}{(x_{max} - x_{min})} - 1 \quad (3.24)$$

An optimum number of hidden nodes is necessary to ensure the optimal performance of the ANN model. The optimal number of hidden nodes may be taken as the one giving lowest mean squared error (MSE) between 1 to $(2i+1)$, where i is the number of input parameters (Hecht-Nielsen 1992). Since we have three input parameters, ANN models with hidden nodes starting from 1 to 7 have been created and the model having the lowest MSE

has been considered, and the corresponding number of hidden nodes is chosen as an optimum number of hidden nodes which is six in this case as shown in Fig. 3.31. Alternatively, a trial and error method can be used to determine the number of hidden nodes, which is a tedious task. Thus the best performing and optimum ANN model has been obtained by considering six hidden nodes, and the ANN model has been designated as ANN 3-6-1 in this study. An architecture diagram of the model has been shown in Fig. 3.32 for better understanding.

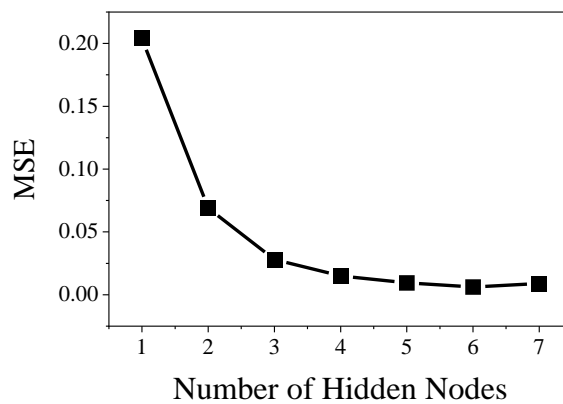


Fig. 3.31 MSE against Number of hidden nodes

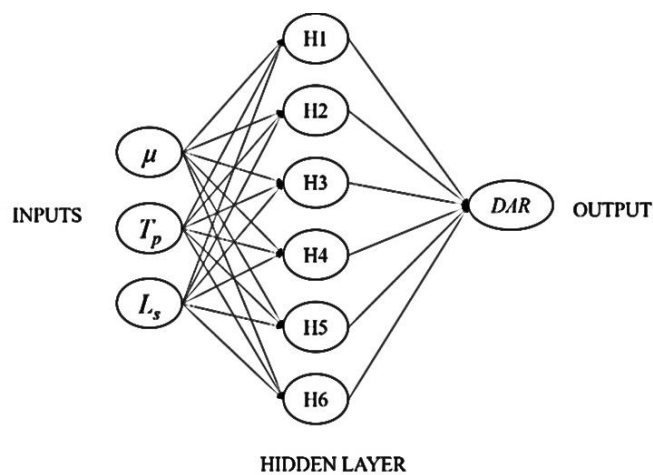


Fig. 3.32 Architecture of the ANN 3-6-1 model

The prediction capability of the ANN model is evaluated by defining the performance measuring functions. In this study, the Coefficient of Correlation (R), Mean Squared Error (MSE), and Mean Absolute Error (MAE) are used as performance measuring functions.

The performance of the model is summarized in Table 3.10. The performance measuring functions are defined as follows:

$$R = \sqrt{\frac{\sum Y_m^2 - \sum(Y_m - Y_p)^2}{\sum Y_m^2}} \quad (3.25)$$

$$MSE = \frac{\sum(Y_m - Y_p)^2}{N} \quad (3.26)$$

$$MAE = \frac{\sum|Y_m - Y_p|}{N} \quad (3.27)$$

where, Y_m and Y_p are the actual target value and predicted output value.

Table 3.10 Performance of ANN-3-6-1 model

| Dataset | R ² | R | MSE | MAE |
|---------------|----------------|-------|--------|--------|
| Training Data | 0.978 | 0.989 | 0.0068 | 0.0612 |
| Testing Data | 0.974 | 0.987 | 0.0059 | 0.0613 |

R-value gives relative correlation and goodness of fit between the actual and predicted values. Therefore, R-value should be as high as possible. MSE and MAE measure errors should be as low as possible (Debnath and Sultana 2019). A strong correlation exists between actual and predicted values if $R > 0.8$ (Smith 1986). Fig. 3.33 shows the correlation between predicted and actual *DAR* in the training and testing phase. The overall correlation between the predicted and actual *DAR* is shown in Fig. 3.33c with R as 0.989. Thus strong correlation achieved between the predicted and actual values using ANN. Fig. 3.34 shows the plot of predicted *DAR* by ANN and Nonlinear Regression against the actual *DAR* values. The results show that ANN model predictions are closer to the line of perfect prediction (zero error line) than those of the nonlinear regression model. In other words, the ANN model has better prediction accuracy than the Nonlinear regression model.

Since the prediction accuracy of the ANN is higher than the non-linear regression model, an attempt has been made in this study to get the model equation for *DAR* from the ANN-3-6-1 model. By using the connection weights of a trained network, a mathematical equation can be developed by relating the input parameters and the output parameter using the following equation (Goh et al. 2005):

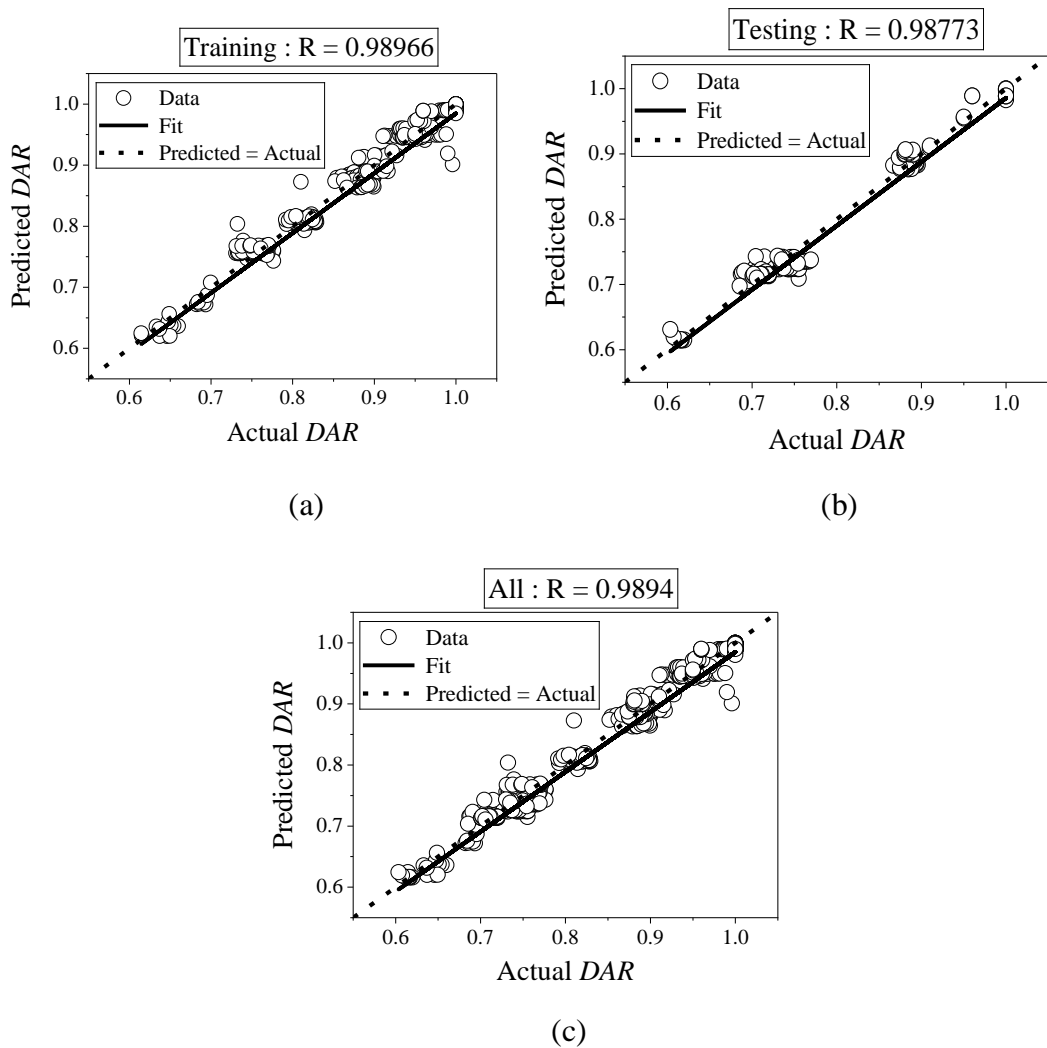


Fig. 3.33 Predicted *DAR* and Actual *DAR* of (a) Training set; (b) Testing set; (c)

Complete database

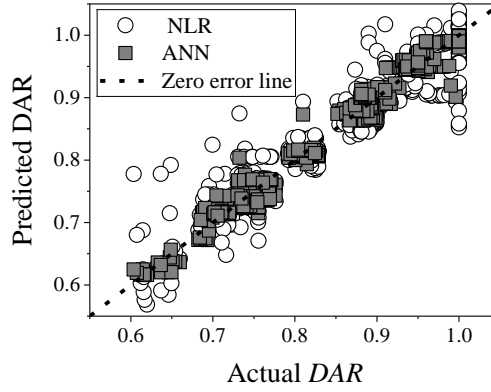


Fig. 3.34 Values of *DAR* predicted by ANN and Non-linear Regression versus the actual *DAR* value

$$Y_n = f_o \left\{ b_o + \sum_{k=1}^h \left[w_k * f_h \left(b_{hk} + \sum_{i=1}^m w_{ik} X_{ni} \right) \right] \right\} \quad (3.28)$$

Where, b_o = output layer bias; w_k = weight connection between neuron k of the hidden layer and single output neuron; b_{hk} = bias at the k th hidden neuron; w_{ik} = weight connection between the input parameter and neuron k of the hidden layer; X_{ni} = input parameter; f_h = transfer function of the hidden layer (Tan-sigmoid function in this case); and f_o = transfer function of the output layer (Tan-sigmoid function in this case). By substituting the values of weights and biases shown in Table 3.11 in the Eq. (3.28) the model equation for the prediction of the *DAR* has been developed. The bias weights, as shown in Table 3.11, make the ANN model more general and robust.

Table 3.11 Weights and biases of ANN-3-6-1 model

| Hidden Node | Input-Hidden weight | | | Hidden output weight | Bias | |
|-------------|---------------------|----------|----------|----------------------|---------|--------|
| | μ_{SS} | T_p | L_s | <i>DAR</i> | Hidden | Output |
| 1 | -0.18646 | -10.7564 | 0.28478 | 2.1987 | -8.0831 | 9.7269 |
| 2 | 0.02614 | -11.2887 | -14.2434 | 1.6868 | 11.7805 | |
| 3 | -0.06059 | 19.75239 | -27.8321 | -1.6673 | 7.8449 | |
| 4 | 0.65939 | 4.93809 | 0.03036 | 1.2847 | -4.5174 | |
| 5 | 0.01072 | 54.37749 | -13.007 | 1.7257 | 27.6945 | |
| 6 | 0.45692 | -0.01439 | -0.00562 | -8.7663 | 1.5647 | |

The following steps can be followed to calculate the *DAR*:

1. Normalize the input parameters μ_{SS} , T_p , and L_s linearly in the range [-1, 1].

2. Calculate the normalized *DAR* using the following expressions:

$$a = -0.18646 * \mu_{SS} - 10.7564 * T_p + 0.28478 * L_s - 8.0831 \quad (3.29)$$

$$b = 0.02614 * \mu_{SS} - 11.2887 * T_p - 14.24345 * L_s + 11.7805 \quad (3.30)$$

$$c = -0.06059 * \mu_{SS} + 19.75239 * T_p - 27.8321 * L_s + 7.8449 \quad (3.31)$$

$$d = 0.659397 * \mu_{SS} + 4.938094 * T_p + 0.03036 * L_s - 4.5174 \quad (3.32)$$

$$e = 0.01072 * \mu_{SS} + 54.37749 * T_p - 13.0071 * L_s + 27.6945 \quad (3.33)$$

$$f = 0.456921 * \mu_{SS} - 0.01439 * T_p - 0.005621 * L_s + 1.5647 \quad (3.34)$$

$$x = 2.198 * \tanh(a) + 1.686 * \tanh(b) - 1.667 * \tanh(c) + 1.284 * \tanh(d) + 1.725 * \tanh(e) - 8.766 * \tanh(f) + 9.726 \quad (3.35)$$

$$\text{Design Acceleration ratio, } DAR \text{ (Normalized)} = \tanh(x) \quad (3.36)$$

3. The Eq. (36) has been de-normalized to get the *DAR* value.

$$DAR = 0.1985 * \tanh(x) + 0.8015 \quad (3.37)$$

The Eq. (3.37) developed for the prediction of the *DAR* should only be applied in the range of dataset for which neural network was trained. The limits for the input parameters with maximum and minimum are given in Table 3.12.

Table 3.12 Limits of Input and Output Parameters of the ANN 3-6-1 Model

| | Limits of Input Parameters | | | | Limits of Output Parameter |
|-----|----------------------------|-----------|-----------|---------|----------------------------|
| | μ_{SS} | T_p (s) | L_s (m) | β | <i>DAR</i> |
| Max | 1 | 4 | 2 | 1.4 | 1 |
| Min | 0.1 | 0.1 | 0.01 | 0.5 | 0.603 |

3.5 Summary

This chapter explores the effect of the hanging or suspended non-structural components on the dynamic response of the supporting SDOF primary structure under harmonic and real earthquake excitations. An extensive parametric study has been conducted on the response of the structure by varying the dynamic properties of the structure and the vibrational parameters of the NSC. The results from the parametric analysis show that the mass ratio and the tuning frequency ratio of the FSS has a significant effect on the response of the structure. A design methodology is proposed to determine the spectral acceleration of the structure with the flexible secondary system by means of the response spectrum method. Finally, design expressions are proposed to calculate the modified spectral acceleration for the structure as a function of the structural period, mass ratio, and length of the FSS by Non-Linear Regression and Artificial Neural Network models. The next chapter investigates the dynamic response of the structure with the sliding NSCs.

CHAPTER 4: SLIDING NON-STRUCTURAL COMPONENTS

This chapter describes the effect of multiple sliding NSCs on the seismic behavior of the structure under earthquake excitations. The analytical model with multiple sliding NSCs is developed, and the implementation of the analytical model will demonstrate the results of the parametric study for a given vibrational and dynamic properties of the NSC and the primary structure, respectively. The effect of the single sliding live load on the dynamic behavior of the supporting structure for a given seismic hazard level was studied in the past literature. The design equation for calculating the portion of the live load that participates in the primary structure inertia was proposed. But in reality, the live load objects can be multiple bodies resting side by side and also one over the other in the form of stacks. The effect of such multiple objects on the dynamics of a PS is still a research gap. Therefore, this chapter explores the effect of such multiple side-by-side and stacked live load objects on the dynamic behavior of the primary structure under earthquake excitations for a given seismic hazard level.

Containers used in pile-supported structures, heavy leads blankets draped on scaffolding structure in the nuclear industry, critical and sensitive laboratory equipment, spent nuclear fuel storage casks, etc., are few examples of such live load objects. These objects can exhibit different modes of motion, such as sliding, rocking, or a combination of sliding and rocking when the supporting structure is subjected to dynamic excitations.

4.1 Mathematical Formulation of Sliding Side-by-Side NSC and SDOF Structure

In this section, the dynamic interaction between a structure and multiple sliding NSCs will be studied. An SDOF structure model shown in Fig. 3.1 is considered as a primary structure

for this problem. Assume there are n number of NSCs resting on the PS. Static (μ_{si}) and kinetic (μ_{ki}) friction coefficients between the structure (m_p) and the i^{th} secondary body (m_{bi}) are assumed as equal and denoted as μ_i . The displacements of the primary structure, i^{th} secondary body, and the ground are denoted as u_p , u_{bi} and u_g , respectively. Sliding secondary bodies are far enough for each other and other obstructions as to not cause impact collision between them. Coulomb's friction model is assumed for deriving the governing equations of motion for primary and secondary masses. Due to the variation in the governing equations depending on the direction of the relative motion between the surfaces, a numerical method is required to solve these equations. Hence, a numerical method, 4th order Runge-Kutta (RK4) is utilized for solving these equations of motion.

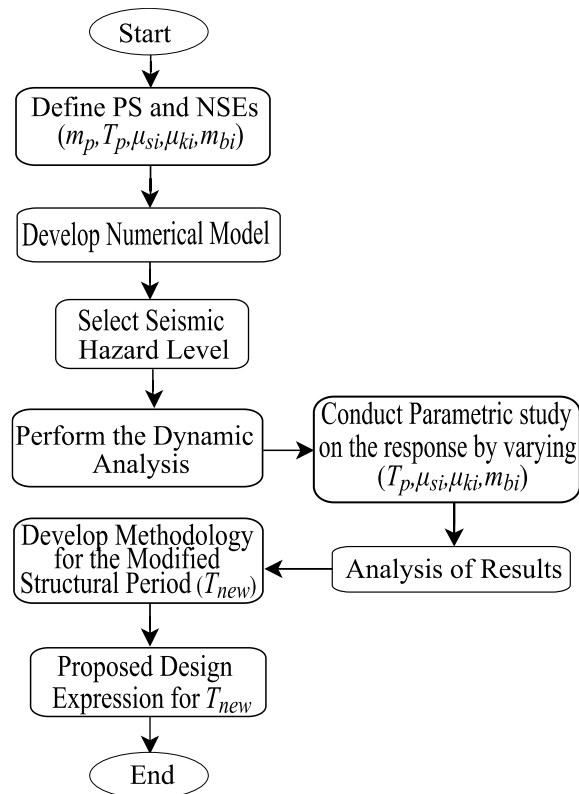


Fig. 4.1 Flow chart showing research methodology

In the RK4 method, all the parameters were considered at $(i - 1)^{th}$ time step to predict the value at i^{th} time step. In order to check the stick and slip conditions, the difference between

velocities of the structure and sliding bodies was calculated for every time step. A tolerance parameter called *epsilon* was defined in the MATLAB platform, set to a relatively very small value (e.g., *epsilon*=0.0001 m/sec) to check the equality of the velocities of the PS and NSCs. The research methodology is seen in Fig. 4.1. The dynamic equations of motion for the system can be written as follows:

The stick/slip behavior between the bodies is verified by defining a function, ***stick***

$$\mathbf{stick}(u_g, u_p, u_b, \mu_s) = (|\dot{u}_p + \ddot{u}_g| < \mu_s g) \& (\dot{u}_p = \dot{u}_b) \quad (4.1)$$

If ***stick*** = 1 (True), then the secondary body sticks to the primary structure.

= 0 (False), the body slides (μ_k is active)

Note that ***stick'*** is defined as the slip condition. Let *n* be the number of secondary bodies placed on the primary structure. The dynamic equations of motion are as follows:

For the primary structure:

$$\left[\left\{ \left(m_p + \sum_{j=1}^n m_{bj} \mathbf{stick}(u_g, u_p, u_{bj}, \mu_{sj}) \right) (\dot{u}_p + \ddot{u}_g) \right\} + c\dot{u}_p + ku_p \right] \quad (4.2)$$

$$= \sum_{i=1}^n \mathbf{stick}'(u_g, u_p, u_{bi}, \mu_{si}) \mu_{ki} m_{bi} g \cdot \text{sign}(\dot{u}_{bi} - \dot{u}_p)$$

sign is the signum function. *sign* equals to +1, -1, and 0 if the relative velocity between the sliding objects and the structure is positive, negative, and zero respectively.

For all the sliding secondary bodies (only when ***stick***($u_g, u_p, u_{bi}, \mu_{si}$) = 0)

$$m_{bi}(\ddot{u}_{bi} + \ddot{u}_g) + \mu_{ki} m_{bi} g \text{sign}(\dot{u}_{bi} - \dot{u}_p) = 0 \quad (4.3)$$

Say, I number of bodies are sliding at a given time step. Then, it should be noted that the total number of equations to be solved is I+1 (Eqs. (4.2) and (4.3)). In subsequent discussions, mass ratio α_i and original structural period (T_p) are defined as follows:

$$\alpha_i = \frac{m_{bi}}{m_p} \quad (4.4)$$

$$T_p = 2\pi\sqrt{\frac{m_p}{k}} \quad (4.5)$$

A mass ratio α is defined as the ratio between the total mass of the secondary bodies to the mass of the primary structure and is given by,

$$\alpha = \sum_{i=1}^n \alpha_i \quad (4.6)$$

The governing dynamic equations of motion of the PS and SBs in stick and sliding/slip mode are solved by the 4th order Runge-Kutta method. For this study, only two secondary bodies are considered (m_{b1} and m_{b2}), as shown in Fig. 4.2.

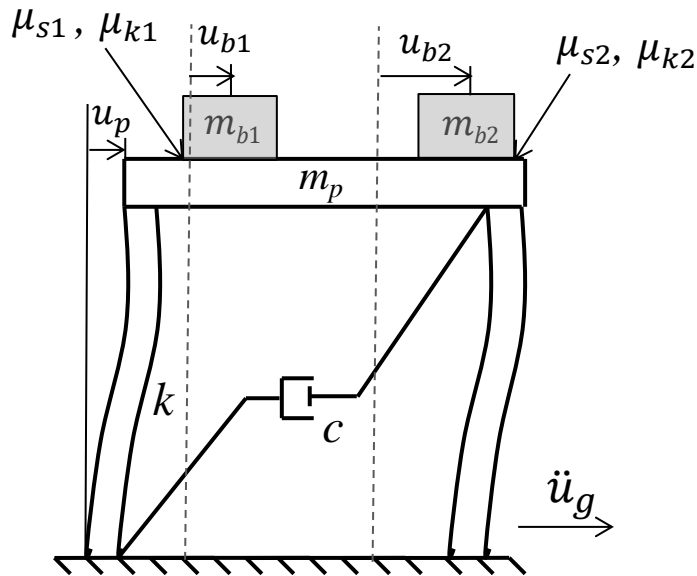


Fig. 4.2 Idealization of primary structure with two sliding SBs

The above formulation is then subjected to spectrum compatible earthquake excitations. Eleven ground motions were selected from the PEER NGA ground motion database (Center 2013), which is the minimum required the number of ground motions as per ASCE 7-16 (ASCE 2016). The moment magnitude (M_w) of the selected excitations is greater than

6. Excitations are made compatible with the design spectrum associated with the two Indian seismic zones III and V, hard soil with 5% damping by the spectral matching method in the time domain. The details of the excitations are shown in Table 4.1. In Fig. 4.3, the 5%-damping mean spectrum of the 11 spectrum compatible earthquake excitations and their target spectra are shown. The average spectrum or mean spectrum does not fall below 90% of the target spectrum in the entire period range as per ASCE 7-16.

Table 4.1 Specifications of the strong ground motions used in the current study

| No. | Event | Year | Station | PGA (g) | Magnitude (M_w) |
|-----|--------------|------|---------------------------|---------|---------------------|
| 1 | Kern County | 1952 | Taft Lincoln School | 0.18 | 7.36 |
| 2 | Loma Prieta | 1989 | Fremont-Mission San Jose | 0.12 | 6.93 |
| 3 | Landers | 1992 | Barstow | 0.13 | 7.28 |
| 4 | Duzce-Turkey | 1999 | Lamont 1059 | 0.15 | 7.14 |
| 5 | Chi-Chi | 1999 | TCU075 | 0.22 | 6.21 |
| 6 | Chi-Chi | 1999 | CHY028 | 0.20 | 6.20 |
| 7 | Chi-Chi | 1999 | CHY046 | 0.12 | 6.22 |
| 8 | San Simeon | 2003 | San Luis Obispo | 0.16 | 6.52 |
| 9 | Parkfield | 1966 | Cholame-Shandon Array #12 | 0.06 | 6.19 |
| 10 | Iwate | 2008 | Semine Kurihara city | 0.16 | 6.91 |
| 11 | Parkfield | 1966 | Temblor pre-1969 | 0.35 | 6.19 |

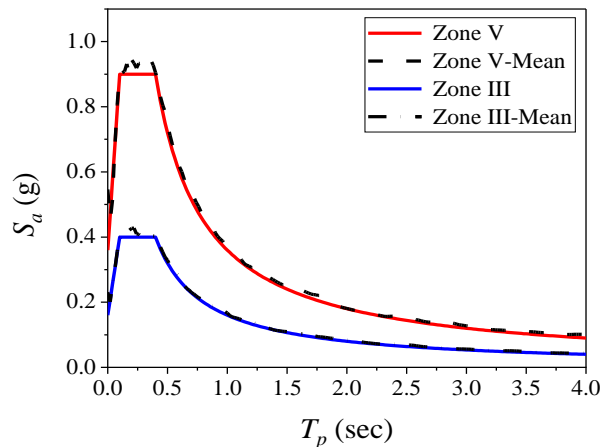


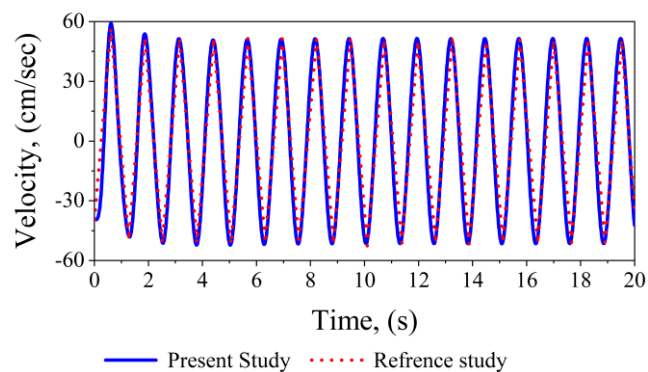
Fig. 4.3 Target and mean acceleration spectra

4.1.1 Validation of Model

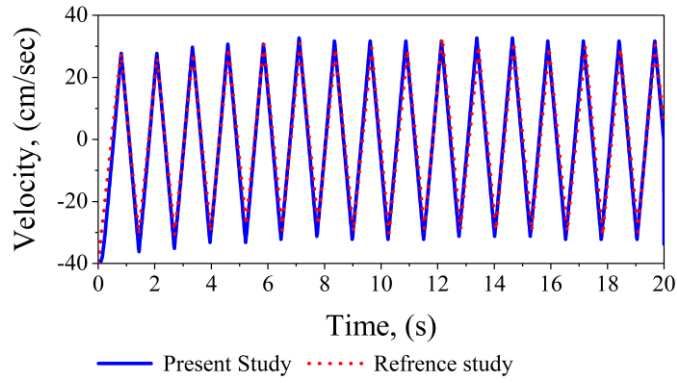
The developed model should be validated before it can be used in further analysis. The validation of the model can be done by comparing the response of the structure with the existing study results and also with the results from the Finite Element (FE) study. The following sub-sections show the validation results.

4.1.1.1 Comparison with the existing study

The validation of the model is done by comparing the velocity responses of the PS and rigid block obtained in this study with the velocity responses of the supporting structure and rigid block obtained by the Nigam-Jennings method based on the exact solutions given in the reference study (Matsui et al. 1991). Hence, the primary structure (m_p) with a single sliding rigid block (m_{b1}) is considered. In the reference study, velocity responses of the structure and rigid block are plotted for stick-stick, stick-slip, and slip-slip conditions. The results for all input conditions were found to qualitatively match with the reference study. For validating the analytical model, the slip-slip condition is arbitrarily chosen. The dynamic structural properties, rigid block parameters, and forcing function parameters used for the slip-slip mode in the reference study are given as input parameters to the model in this study. Fig. 4.4 shows an acceptable correspondence between this study and the velocity responses given in the reference study for slip-slip mode.



(a)



(b)

Fig. 4.4 Velocity responses (a) primary structure; (b) rigid block

4.1.1.2 Comparison with the Finite Element (FE) study

In this section, the displacement response of the PS with multiple sliding SBs is compared with the results of a Finite Element (FE) model. The basic FE model developed consists of a multiple rigid blocks resting directly on a rectangular body that simulates the primary structure. The developed FE model is used to model the response of an SDOF oscillator subjected to base excitation with sliding rigid blocks resting on it. To do so, a horizontal spring element with stiffness and dashpot was attached to this body to simulate the oscillator as shown in Fig. 4.5. Reference point RP_1 is created to simulate the ground point such that one end of the spring element is attached to it and all degrees of freedom (DOF's) of RP_1 are restrained to simulate a fixed point. The other end of the spring element is attached to the rectangular body to simulate the SDOF oscillator.

The motion of the rigid bodies is defined by reference node (REF NODE) assigned to them. A rigid body reference node has both translational and rotational degrees of freedom. In this particular study, RP_2 , RP_3 , and RP_4 are the reference nodes assigned to the structure and rigid blocks, respectively. Masses of the structure (m_p) and rigid blocks (m_{b1} , m_{b2}) are assigned to these nodes as inertia. Coulomb friction model is used to capture friction

and sliding at the contact interface. It is a common friction model used to describe the interaction of contacting surfaces. The model characterizes the frictional behaviour between the surfaces using a coefficient of friction. The DOF's of the reference nodes RP_2 , RP_3 , and RP_4 are constrained in the x-direction and restrained in all other directions.

To capture the sliding of the blocks under base excitation, the contact interface that exists between the blocks and the SDOF oscillator is modelled via an interaction module in ABAQUS. The contact interaction between these bodies is generated by the Surface-to-Surface contact (Explicit) method. The Explicit method is chosen over the implicit method because explicit platform will not encounter convergence problems (Zhang et al. 2017). The 'Hard' contact option is used to define normal behaviour of the contact interaction, while the tangential behaviour used 'Penalty frictional formulation' with a given coefficient of friction to ensure relative horizontal motion between the surfaces. Penalty contact algorithm is used for mechanical constraint formulation (Dassault Systèmes 2016). The finite-sliding formulation, which is the most common and allows for sliding of the surfaces in contact is adopted since small sliding formulation cannot be used for contact pairs using the penalty contact algorithm.

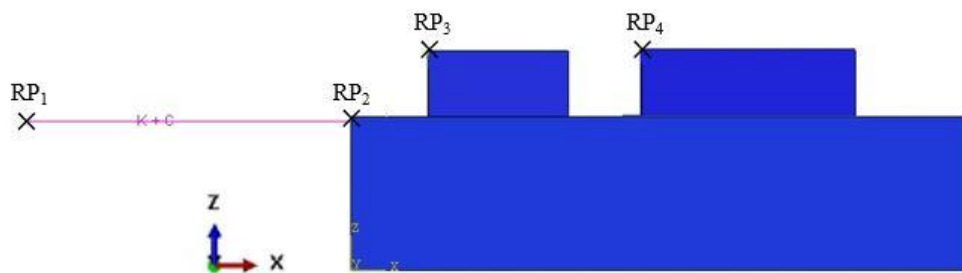


Fig. 4.5 ABAQUS model of a PS with two sliding SBs

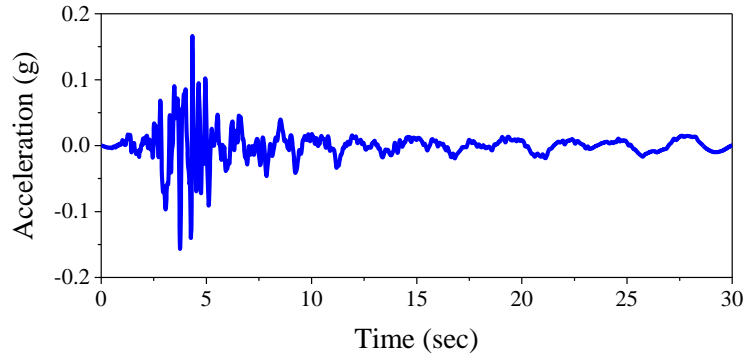
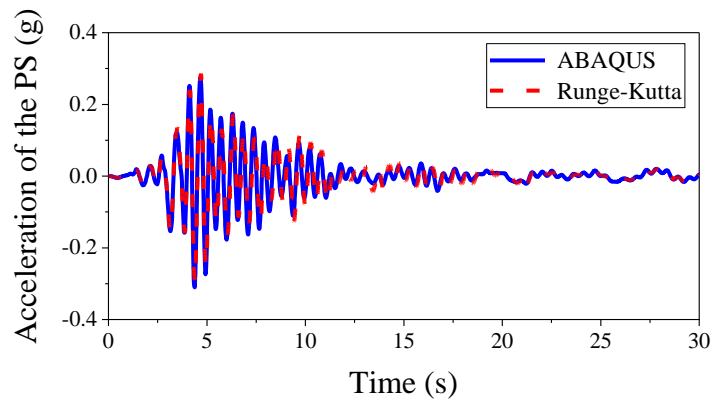
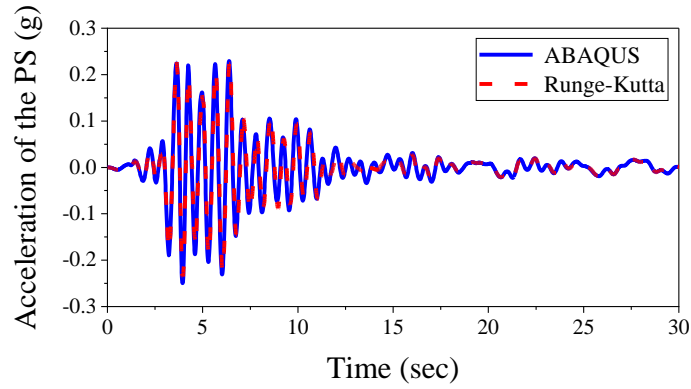


Fig. 4.6 Acceleration time history used for validation of PS with two SBs Model

Horizontal acceleration is applied to the ground point (RP_1) to simulate an earthquake excitation at the base of the SDOF oscillator. The masses of the SDOF structure and rigid blocks were assigned to the reference nodes as inertia. The coefficients of friction values were defined between the structure-rigid blocks interface. A structure with multiple SBs is subjected to a medium seismic hazard level spectrum compatible Parkfield (1966) earthquake recorded at Temblor pre-1969 station. The acceleration time history of the earthquake used in this validation is shown in Fig. 4.6. Fig. 4.7 shows the calculated acceleration response of the PS for selected mass ratios, coefficients of friction, and time period of the structure. It can be observed that the calculated acceleration responses of the PS by utilizing the Runge-Kutta method are identical to those obtained from the FE model.



(a)



(b)

Fig. 4.7 Comparative response of Runge-Kutta Method and FE model for $\alpha_1 = \alpha_2 = 0.5$:
 (a) $T_p = 0.39$ sec, $\mu_1 = 0.2$, $\mu_2 = 0.3$; (b) $T_p = 0.5$ sec, $\mu_1 = 0.2$, $\mu_2 = 0.2$.

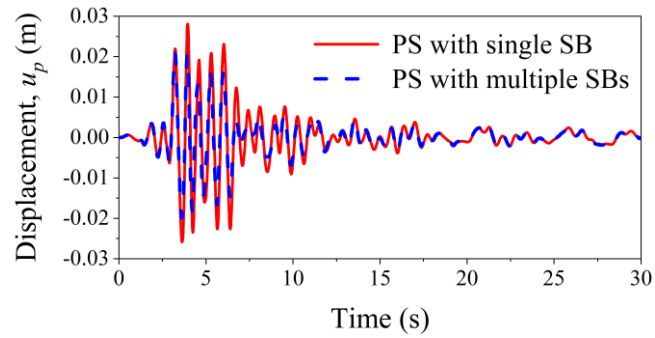
4.2 Dynamic response of a SDOF structure with sliding side-by-side NSCs

This section investigates the dynamic behavior of the supporting structure with multiple sliding NSCs or secondary bodies (SBs) for a given seismic hazard level. This section evaluated the displacement response of the PS with two sliding NSCs and compared against the response of the PS with single sliding NSC for a given seismic hazard level. It also contains an extensive parametric study on the displacement response by varying the dynamic properties of the PS and the interactional properties of the sliding SBs.

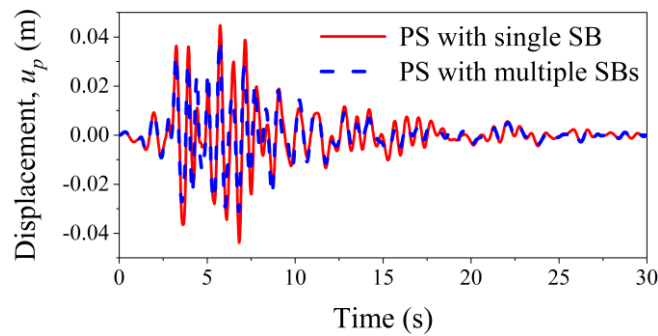
4.2.1 Displacement response

The variation in the behavior of a structure with a single secondary mass versus a structure with multiple masses first needs to be looked at. For this study, the structural period of the PS is chosen as 0.5 sec. In the case of PS with multiple SBs, the mass ratios (α_1 and α_2) are 0.5 and 0.5. The coefficients of friction (μ_1 and μ_2) are 0.3 and 0.1. The mass ratio and coefficient of friction in the case of PS with single SB are 1 and 0.3, respectively.

Earthquake excitation-[#]11 from Table 4.1 is applied to the base of the PS with single and two SBs.



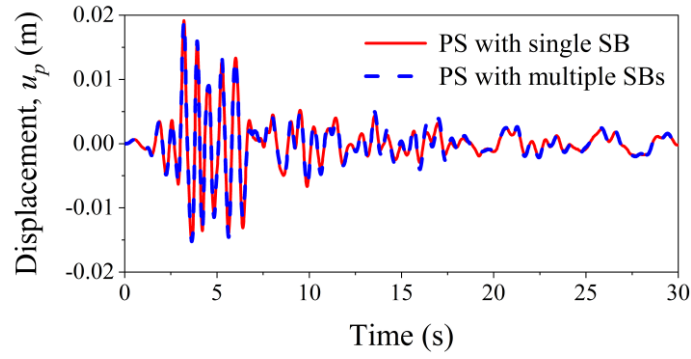
(a)



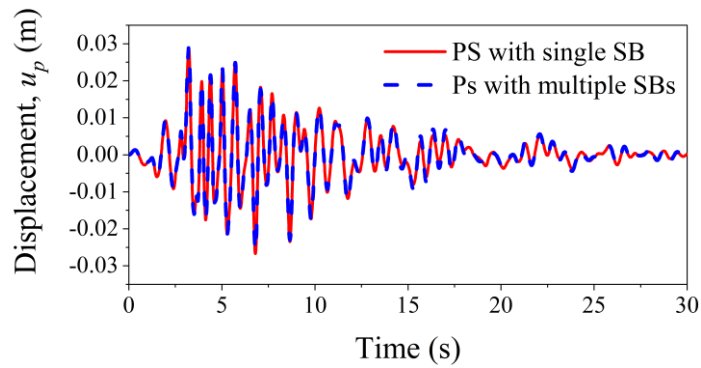
(b)

Fig. 4.8 Displacement of PS with single and two SBs (a) Zone III; (b) Zone V

Fig. 4.8 shows the displacement time histories of the PS with single and multiple SBs. Since the maximum displacement of the PS is of great concern for the design of the structures, maximum displacements of the PS with single and two SBs for a given excitation corresponds to seismic zone III are 0.028 m and 0.021 m respectively. For seismic zone V, those values are 0.044 m and 0.039 m. The maximum displacement of the PS with two SBs is reduced by 25% in zone III, and 11.36 % in zone V compared to PS with single SB, respectively. Hence, seismic behavior of the PS with multiple sliding rigid blocks with different coefficients if friction is not same as structure with a single sliding rigid block.



(a)



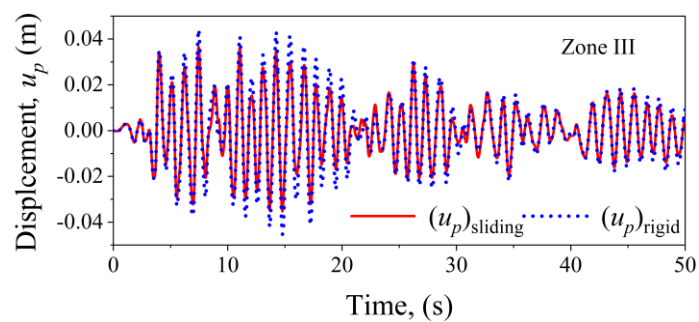
(b)

Fig. 4.9 Displacement of the PS for same coefficients of friction (a) Zone III; (b) Zone V

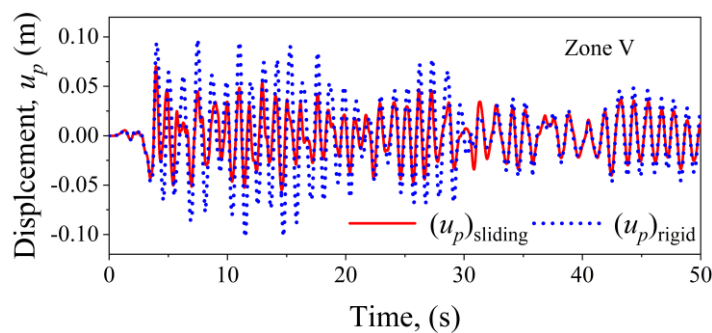
Similarly, Fig. 4.9 shows the displacement time history of the PS with a single ($\mu = 0.1$) and multiple SBs with the same coefficients of friction ($\mu_1 = \mu_2 = 0.1$) between the structure-SBs interfaces. From Fig. 4.9, it should be noted when the coefficients of friction are equal between all the contact surfaces of the model (Fig. 4.2); the secondary bodies act as a single body with combined mass. This conclusion leads to a further discussion on the response of the PS with multiple sliding rigid blocks. In order to verify the effect of seismic hazard level on the response of the structure with multiple SBs, the effect of two rigid sliding blocks (m_{b1} and m_{b2}) on the displacement response of the primary structure in two seismic zones III and V are studied. One ground motion from each seismic hazard level is applied to the PS with SBs. The structural period of the PS is arbitrarily chosen as 0.8 sec.

Mass ratios (α_1 and α_2) are chosen 0.5. Coefficients of friction (μ_1 and μ_2) are chosen as 0.2 and 0.1 between the blocks and structure interface.

The displacement response of the structure with sliding loads ($(u_p)_{sliding}$) is compared against the response of the same structure with rigidly fixed SBs ($(u_p)_{rigid}$). Spectrum compatible earthquake excitation-#11 from Table 4.1 is applied to the base of the PS. From Fig. 4.10, it can be deduced that sliding live loads can mitigate the seismic response of the primary structure. The reduction in displacement is more in zone V (31.4%) compared to zone III (17.3%). Acceleration experienced by the structure is more in zone V, which overcome the static friction between block-structure interface, and hence sliding of the SBs is higher. Due to more sliding of SBs, more energy is dissipated in the highest seismic hazard level when compared to the medium seismic hazard level.



(a)



(b)

Fig. 4.10 Displacement of primary structure (a) Zone III; (b) Zone V

4.2.2 Parametric Study

The displacement response of a structure with multiple sliding bodies on it is different from the response with a single sliding rigid block. This significant-conclusion leads to the following parametric study. The parameters to be varied in this study are: (a) the structural period T_p ; (b) the mass ratios α_1 and α_2 ; (c) the coefficient friction at the interface of SBs. $\mu_1 = \mu_{s1} = \mu_{k1}$ and $\mu_2 = \mu_{s2} = \mu_{k2}$ are assumed for this study. For each seismic damage risk zone, various problems were analyzed. The parameter selected to quantify the effect of SBs on the response of the primary structure in this study is the Displacement Ratio (DR). It is defined as follows:

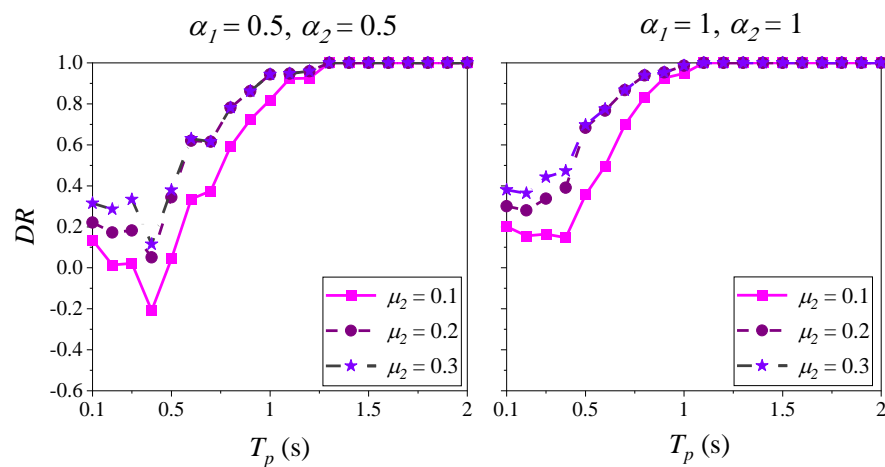
$$DR = \frac{(u_p)_{sliding} - (u_p)_{free}}{(u_p)_{rigid} - (u_p)_{free}} \quad (4.7)$$

Where, $(u_p)_{sliding}$ is the displacement of the PS with sliding rigid blocks. $(u_p)_{rigid}$ and $(u_p)_{free}$ are the displacements of the same structure with rigidly fixed SBs and with no SBs, respectively. SBs behave as rigidly attached bodies to the PS when the DR equals to one. The sliding bodies have negligible effect on the structures response when the DR is close to zero. Sliding rigid blocks reduce the response of the primary structure if the DR is negative. If the DR varies between 0 and 1, then only a fraction of the mass of SBs should be taken into consideration in the analysis and design of the PS. In each run, displacement of the PS was taken as the average value of the maximum displacement resulting from eleven scaled ground motions.

The results for the displacement Ratio (DR) for the medium seismic hazard level (zone III) are shown in Fig. 4.11. It can be observed that DR has a strong correlation with the structural period, coefficients of friction, and mass ratios. From Fig. 4.11, it can be inferred

that rigid sliding blocks behave as rigidly attached to the structures with $T_p > 1.25$ sec regardless of the given mass ratios and coefficients of friction. The DR decreases for structures with periods less than or equal to 0.4 sec for lower mass ratios as observed from Fig. 4.11a. This can possibly be attributed to the increase in acceleration with T_p when $T_p < 0.4$ sec. in the given spectrum (Fig. 4.3). For higher mass ratios, the decrease in DR is very low and increases significantly with the structural period and coefficients of friction. Even for small coefficients of friction, the DR is positive for higher mass ratios. This makes sense since, at higher mass ratios, the limiting static frictional force between the interfaces of PS and SBs is more. Therefore, an effective period of the structure-SBs system increases, which results in the lower absolute accelerations. Such accelerations are not enough to counteract the static friction between the structure and the SBs.

The DR significantly decreases for structures with periods less than or equal to 0.4 sec for lower mass ratios in the highest seismic hazard zone also, as shown in Fig. 4.12. The DR increases significantly with the structural period and coefficients of friction for higher mass ratios. From Figs. 4.11 and 4.12, it can be observed that the DR values in Zone V for given



(a)

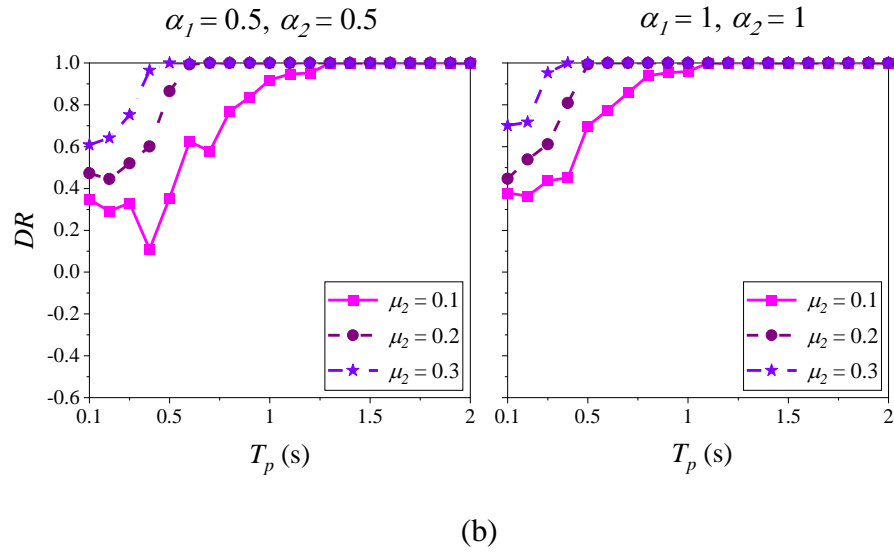
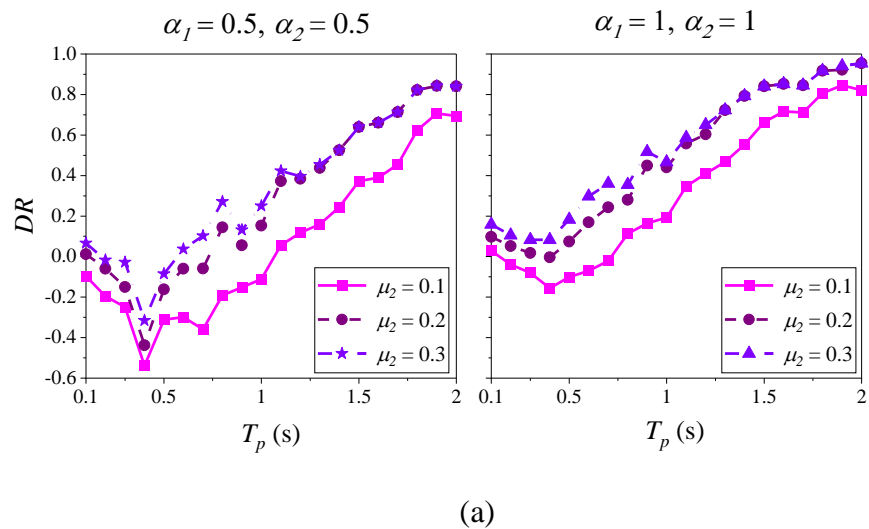


Fig. 4.11 Displacement Ratio (DR) for zone III (a) $\mu_1 = 0.1$; (b) $\mu_1 = 0.3$

mass ratios and coefficients of friction are lower than those in Zone III. Zone V is the highest seismic hazard zone, where the accelerations experienced by the structure are high, which increases the sliding of the SBs and thus dissipates more input energy. From Fig. 4.12, it can be inferred that sliding rigid blocks on structures with $T_p > 0.9$ sec behave as rigidly attached to the PS for higher coefficients of friction regardless of the mass ratios.



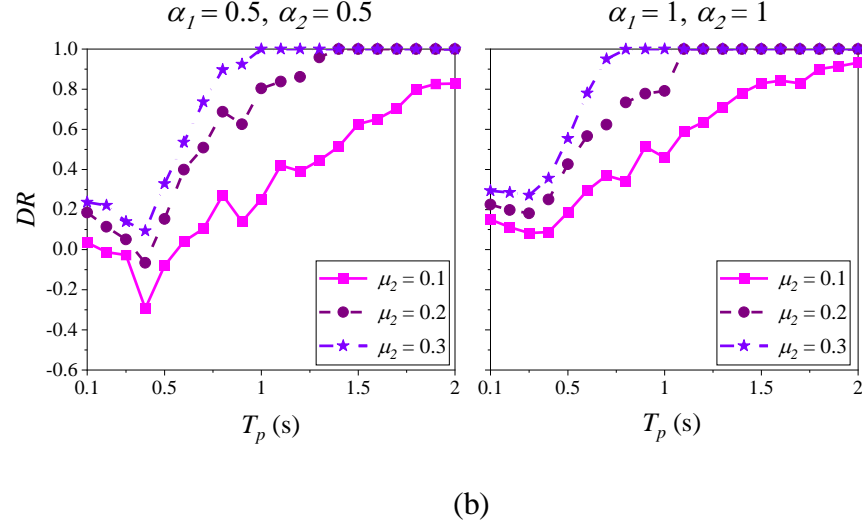


Fig. 4.12 Displacement Ratio (DR) for zone V (a) $\mu_1 = 0.1$; (b) $\mu_1 = 0.3$

Due to sliding secondary blocks, some portion of the mass of secondary blocks participates in the primary structural inertia (Reyes et al. 2016; Smith-Pardo et al. 2015), which in turn modifies the modal characteristics of the primary structure. Hence, an attempt has been made to determine the structural period of the PS when it interacts with multiple sliding rigid blocks.

4.2.3 Modified Structural period due to sliding NSCs

This section explains a methodology to determine the structural period when the SBs are sliding over the PS. This structural period (T_{new}) can be used for the design of a structure by using the corresponding response spectrum. When the SBs are rigidly attached to the PS, the structural period of the PS is given as:

$$T_{rigid} = 2\pi \sqrt{\frac{m_p + \sum_{i=1}^n m_{bi}}{k}} \quad (4.8)$$

Where, n is the number of sliding bodies which equals to 2 in the present study.

Replacing m_{bi} with $\alpha_i m_p$ in the Eq. (4.8), then it becomes

$$T_{rigid} = 2\pi \sqrt{\frac{m_p + \sum_{i=1}^n \alpha_i m_p}{k}} \quad (4.9)$$

The Eq. (4.9) can be rearranged as follows:

$$T_{rigid} = 2\pi \sqrt{\frac{m_p}{k}} \sqrt{\left(1 + \sum_{i=1}^n \alpha_i\right)} \quad (4.10)$$

Replace $2\pi \sqrt{\frac{m_p}{k}}$ in the above expression with T_p and hence Eq. (4.10) becomes

$$T_{rigid} = T_p \sqrt{\left(1 + \sum_{i=1}^n \alpha_i\right)} \quad (4.11)$$

Thus, Eq. (4.11) gives the structural period of the PS when the SBs are rigidly attached to the structure. The following section explains a procedure to determine the structural period of the PS when the SBs are in the sliding phase with the PS. In this study T_{new} is termed as the modified structural period of the PS when it is interacted with sliding SBs. $T_{new} = T_{rigid}$, when SBs are rigidly attached to the structure.

4.2.3.1 Algorithm for determination of modified structural period

The procedure to determine the T_{new} is outlined below for a given set of values of T_p , μ_1 , μ_2 , α_1 and α_2 for the defined ground motions.

1. Calculate the absolute maximum structural acceleration (A_{max}) for the ground motions.
2. Check if $\mu_1 g$, $\mu_2 g > A_{max}$. If yes, conclude $T_{new} = T_{rigid}$. Go to step 3, if no.
3. Calculate the 5%-damping mean displacement spectrum of PS for the ground motions.

4. Calculate the mean of the maximum displacement of the PS with given SBs for the scaled eleven ground motions.
5. Determine the structural period from the 5%-damping mean displacement spectrum (obtained in Step (3)) for the calculated mean displacement (obtained in Step (4)) by linear interpolation.

Fig. 4.13 shows the determination of the structural period of the PS with SBs under scaled eleven ground motions for $T_p = 1$ sec, $\alpha_1 = \alpha_2 = 0.5$, $\mu_1 = 0.2$ and $\mu_2 = 0.05$. The modified structural period of the PS due to the interaction of SBs in this particular case is 1.12 sec.

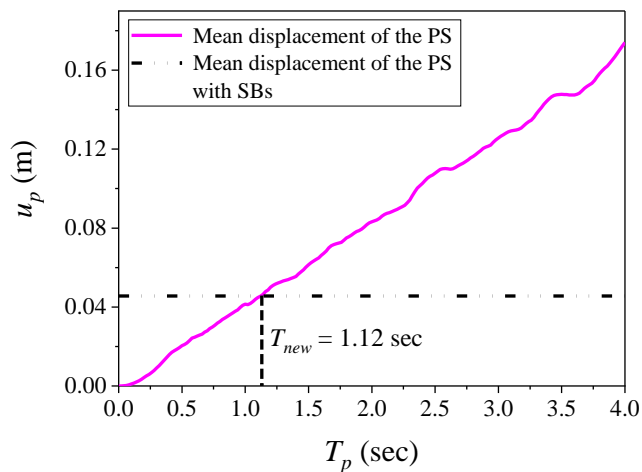


Fig. 4.13 Determination of the modified structural period by proposed algorithm

4.2.3.2 Validation of the proposed algorithm

The proposed algorithm for the calculation of the modified structural period needs to be validated before conducting a parametric study. For such validation, the target spectrum for operating level (OLE) seismic hazard is taken from the report (Earth Mechanics Inc. 2006). Ground motion scenario mentioned in the study (Smith-Pardo et al. 2014) is used for the validation. Since the reference study (Smith-Pardo et al. 2015) is for the structure

with a single live load object, put $m_{b2} = 0$ in the present study to convert the structure with multiple SBs to structure with a single sliding body. Thus, Eq. (4.11) becomes:

$$T_{rigid} = T_p \sqrt{(1 + \alpha_1)} \quad (4.12)$$

The structural period of the PS due to the live load object interaction is given as (Smith-Pardo et al. 2015):

$$T_\lambda = T_p \sqrt{(1 + \alpha_1 \lambda)} \quad (4.13)$$

Where, λ is the portion of live load object participates as inertia in the primary structure. From the example calculation of the live load as inertia for OLE seismic hazard in the reference study, the structural period of the PS for given input parameters is 0.86 sec. In the example calculation, reference study assumed linear range of response. The same input parameters are used (since the present study also deals with the linear analysis), and the structural period is calculated by the algorithm proposed in Section 4.2.3.1 by considering the OLE level mean spectrum as a design spectrum. Thus, the $T_{new} = 0.858$ sec obtained from Fig. 4.14, by using the proposed algorithm, is in agreement with the structural period obtained through a portion of the live load (λ) in the reference study.

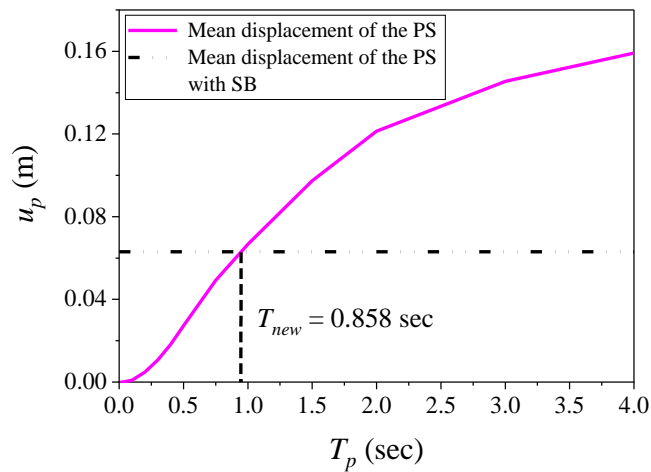


Fig. 4.14 Determination of the modified structural period for OLE hazard level

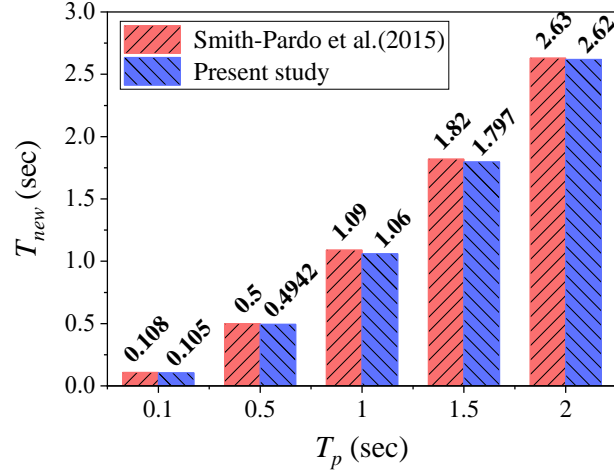


Fig. 4.15 Validation of the proposed algorithm

Fig. 4.15 shows the comparison of the structural period of PS with SBs (T_{new}) obtained by the proposed algorithm with a reference study for input parameters of $\mu_1 = 0.1$, $\mu_2 = 1E-08$, $\alpha_1 = 0.75$, $\alpha_2 = 1E-08$. From Fig. 4.15, it can be observed that T_{new} obtained by the proposed algorithm agrees with the algorithm proposed in the reference study.

4.2.4 Parametric study on modified structural period

A parametric study of T_{new} with the following variables and ranges of values is performed:

(a) the structural period T_p (from 0.1 sec to 2.0 sec, increments of 0.1 sec); (b) the mass ratios α_1 and α_2 (0.1, 0.5, 1.0); (c) the coefficients of friction (from 0.05, 0.1 to 0.5 with increments of 0.1). A total of 4980 analysis runs are tabulated for this study.

Figs. 4.16 and 4.17 show a subset of results from the parametric study for a given set of mass ratios and coefficients of friction. Fig. 4.16 shows that under medium seismic hazard zone, SBs behave as rigidly attached bodies to the structures with a period larger than 1.25 sec regardless of the mass ratios and coefficients of friction corresponding to the plots of displacement ratio (DR) introduced in Section 4.2.2. It can also be observed that T_{new} significantly increases with the original structural period, coefficients of friction, and mass ratios. For small coefficients of friction, T_{new} is nearly equal to T_{rigid} as seen before.

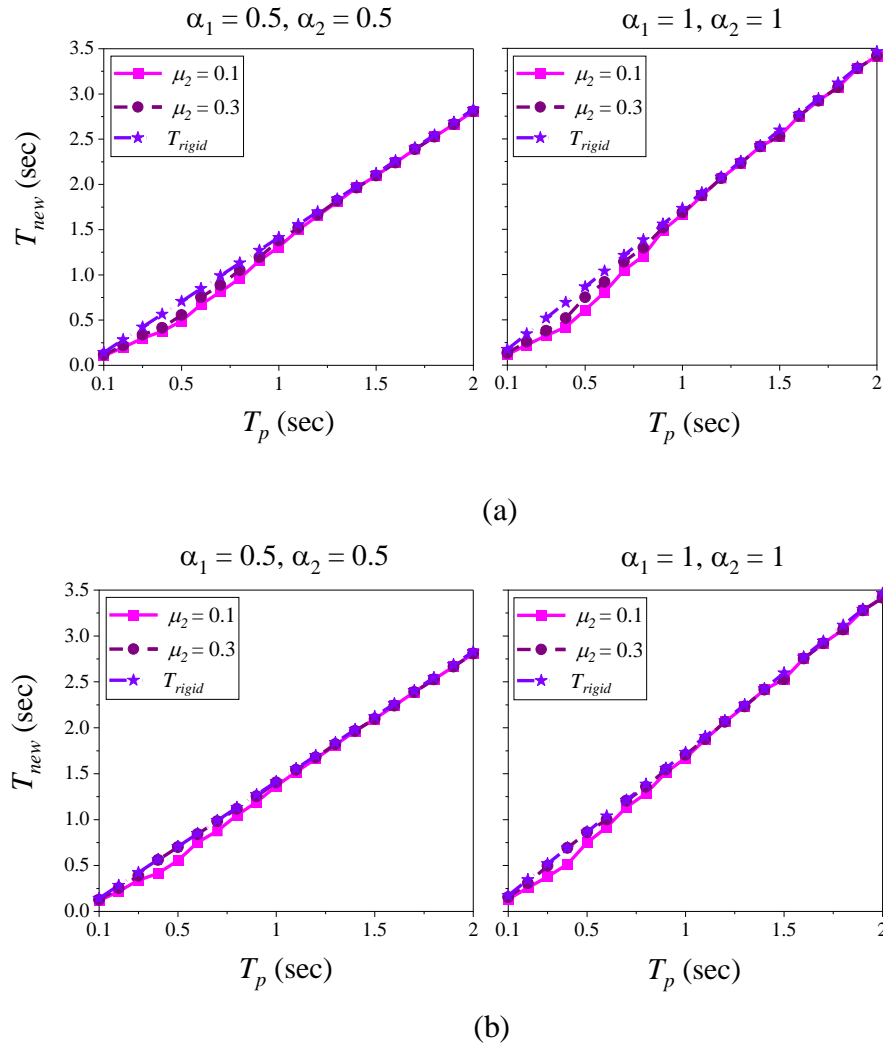
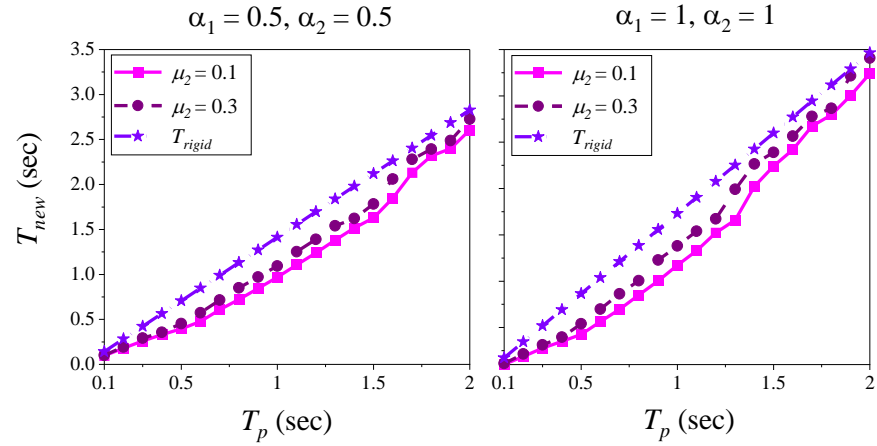
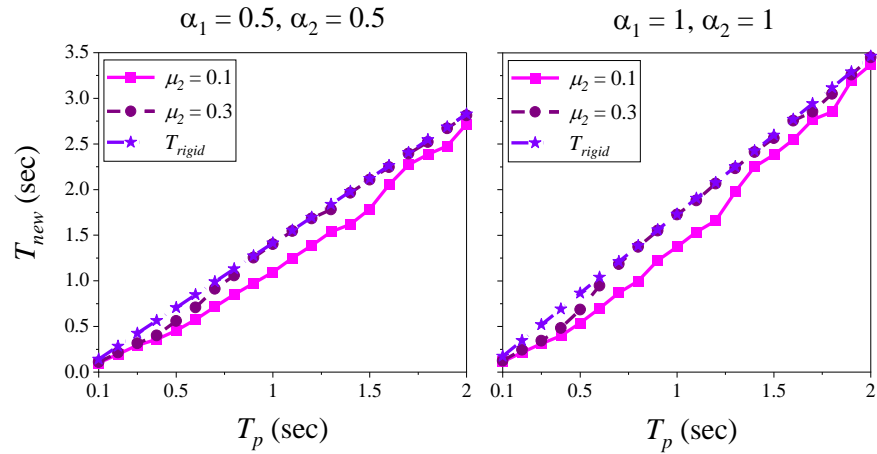


Fig. 4.16 Modified structural period (T_{new}) for zone III (a) $\mu_1=0.1$; (b) $\mu_1=0.3$

Fig. 4.17 shows the variation of T_{new} in the highest seismic hazard zone. It shows that also for the highest seismic hazard zone, the T_{new} significantly increases with the original structural period, coefficients of friction, and mass ratios. The amount of mass participation of SBs in the inertia of the structure is less in this seismic hazard zone compared to the medium seismic hazard zone even for higher coefficients of friction. From Fig. 4.17, it can be inferred that when the coefficients of friction between the PS and two masses interfaces are high, SBs could behave as rigidly attached bodies to the structures with periods larger than 0.9 sec regardless of the mass ratios.



(a)



(b)

Fig. 4.17 Modified structural period (T_{new}) for zone V (a) $\mu_1=0.1$; (b) $\mu_1=0.3$

4.2.5 Design expressions for modified structural period by Non-Linear Regression and Artificial Neural Network

To design a structure with multiple sliding SBs by response spectrum method, an equation for T_{new} needs to be developed. For some of the cases, T_{new} can be obtained from Figs. 4.16 and 4.17. In other cases, a design equation will be developed through a parametric study by considering a large number of discrete points correspond to various variables. This study comprised of the variables and ranges of values, as mentioned in Section 4.2.4.

Non-Linear Regression (NLR) analysis yield the following design equations to calculate T_{new} for each seismic hazard zone:

For Medium Seismic Hazard Zone:

$$T_{new} = \left((-3.613 * T_p) - (0.876s * \mu_1) + (0.041s * \mu_2) - (4.241s * \alpha_1) - (4.188s * \alpha_2) \right) + 0.782s * e^{\left(\frac{(0.053}{s} * T_p) + (0.014 * \mu_1) + (0.002 * \mu_2) \right) + (0.053 * \alpha_1) + (0.052 * \alpha_2) + 4.588} - 76.889s \quad (4.14)$$

For Highest Seismic Hazard Zone:

$$T_{new} = \left((-6.388 * T_p) - (7.589s * \mu_1) - (5.236s * \mu_2) - (5.965s * \alpha_1) - (5.309s * \alpha_2) \right) + 6.365s * e^{\left(\frac{(0.0443}{s} * T_p) + (0.047 * \mu_1) + (0.033 * \mu_2) \right) + (0.036 * \alpha_1) + (0.032 * \alpha_2) + 3.21} - 157.67s \quad (4.15)$$

The prediction capability of the regression models for both the seismic zones are evaluated by defining the various statistical performance functions like Co-efficient of Determination (R^2), Correlation Coefficient (R), Root Mean Square Error (RMSE), Mean Square Error (MSE) and Mean Absolute Error (MAE). The performance of the models is summarized in Table. 4.2.

Table 4.2 Performance of the regression models

| Seismic Zone | R^2 | R | MSE | MAE |
|--------------|-------|-------|-------|-------|
| III | 0.987 | 0.993 | 0.013 | 0.091 |
| V | 0.953 | 0.976 | 0.015 | 0.151 |

An alternate approach, such as machine learning, has been utilized in this study, along with NLR, to derive the design expression for each seismic hazard zone. The machine learning technique (ANN), is used. T_{new} values are simulated for 4980 cases. Of all the data, 70% of the data (3486 cases) were assigned to the training set and the remaining 30%

(1494 cases) to the testing set. The type of the neural network with a learning algorithm and the transfer function for the hidden and output layers were considered the same as the neural network used in Section 3.4.3. The MSE for the nodes 6 to 11 is almost constant for both the seismic hazard zones, as shown in Fig. 4.18, and hence the optimum number of nodes is chosen as six. An architecture diagram of the model has been shown in Fig. 4.19 and is designated as ANN 5-6-1 model.

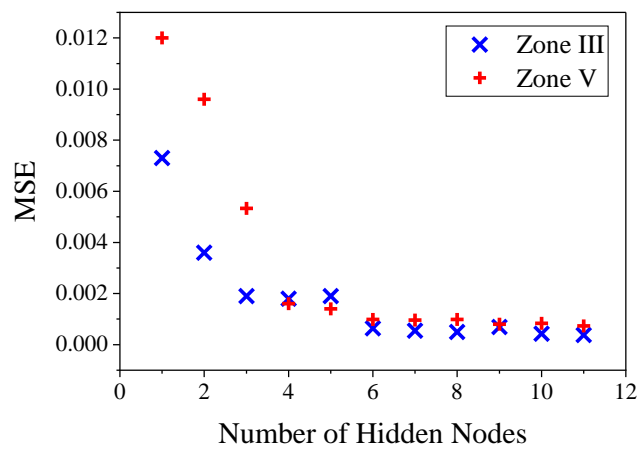


Fig. 4.18 MSE against Number of hidden nodes for both the zones

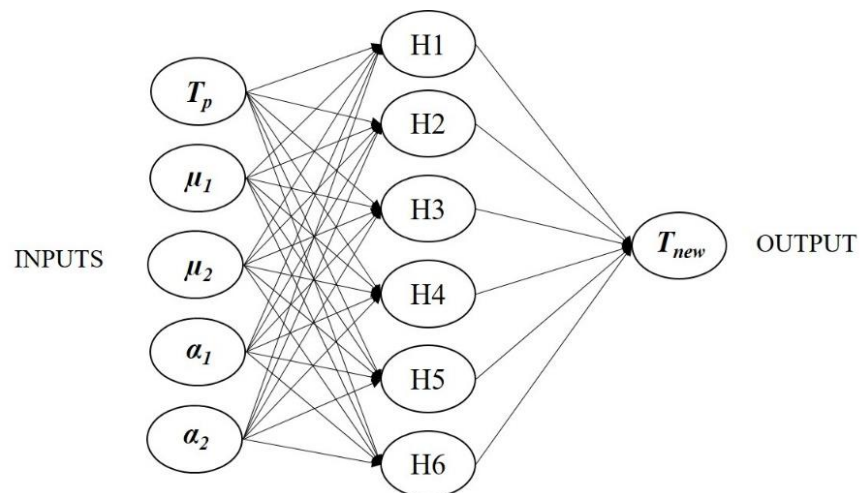


Fig. 4.19 Architecture of the ANN 5-6-1 model.

Using the connection weights of a trained network, a mathematical equation can be developed by relating the input and the output parameters using the Eq.(3.28). Performance measuring functions defined in Section 3.4.3 are used here to assess the capability of the developed ANN model. The performance of the model is summarized in Table 4.3.

Table 4.3 Performance of the ANN-5-6-1 model

| Dataset | MAE | | R | | MSE | |
|---------------|----------|--------|----------|--------|----------|--------|
| | Zone III | Zone V | Zone III | Zone V | Zone III | Zone V |
| Training Data | 0.0321 | 0.0407 | 0.998 | 0.997 | 0.0016 | 0.0027 |
| Testing Data | 0.0375 | 0.0477 | 0.998 | 0.997 | 0.0029 | 0.0043 |

Table 4.4 Weights and biases of ANN-5-6-1 model for Zone III

| Hidden Node | Input-Hidden weight | | | | | Hidden output weight | Bias | |
|-------------|---------------------|---------|---------|------------|------------|----------------------|--------|--------|
| | T_p | μ_1 | μ_2 | α_1 | α_2 | T_{new} | Hidden | Output |
| 1 | -0.0876 | -0.2312 | 2.91433 | -0.1091 | -0.2362 | -0.9377 | 2.725 | 0.1745 |
| 2 | -0.5937 | -0.004 | -0.0076 | -0.1253 | -0.1249 | -12.4309 | 2.106 | |
| 3 | 1.1576 | 0.0196 | 0.0198 | 0.0224 | 0.0229 | 11.16713 | 2.438 | |
| 4 | 0.0083 | 0.2111 | -2.9388 | 0.0896 | 0.2148 | -1.2210 | -2.899 | |
| 5 | -0.1411 | 2.6219 | -0.1769 | -0.2569 | -0.1852 | -0.9648 | 2.642 | |
| 6 | 0.0615 | -2.650 | 0.1590 | 0.2227 | 0.1450 | -1.4075 | -2.866 | |

Table 4.5 Weights and biases of ANN-5-6-1 model for Zone V

| Hidden Node | Input-Hidden weight | | | | | Hidden output weight | Bias | |
|-------------|---------------------|---------|---------|------------|------------|----------------------|--------|--------|
| | T_p | μ_1 | μ_2 | α_1 | α_2 | T_{new} | Hidden | Output |
| 1 | 1.1480 | -0.0779 | -0.0055 | 0.1209 | 0.1939 | 1.1675 | -1.324 | -4.590 |
| 2 | 0.3129 | -2.1858 | 0.04617 | 0.2288 | -0.0023 | -2.3117 | -3.625 | |
| 3 | 0.0129 | 0.3806 | -0.0291 | 0.5551 | 0.0510 | -5.406 | 2.102 | |
| 4 | -0.1629 | 0.3417 | -0.019 | 0.5361 | 0.0968 | 1.4368 | 1.199 | |
| 5 | -0.9235 | -0.0365 | -0.0311 | -0.0307 | -0.0217 | -7.0198 | -1.813 | |
| 6 | 0.4089 | 0.1318 | -3.2302 | -0.1108 | 0.4204 | -0.4825 | -3.918 | |

By substituting the values of weights and biases shown in Tables 4.4 and 4.5 in the Eq. (3.28), the model equations for the prediction of T_{new} for Zone III and Zone V can be developed. For such design expressions, the procedure used for the development of the DAR equation by ANN in Section 3.4.3 is followed. The resultant design equations are as follows:

For Medium Seismic Hazard Zone:

$$T_{new} = 1.6606 * \tanh(x) + 1.7564 \quad (4.16)$$

For Highest Seismic Hazard Zone:

$$T_{new} = 1.6795 * \tanh(x) + 1.7705 \quad (4.17)$$

The Eqs. (4.16) and (4.17) developed for the prediction of T_{new} should only be applied in the range of the dataset for which the neural network was trained. The limits for the input parameters with maximum and minimum are given in Table 4.6.

Table 4.6 Limits of Input and Output Parameters for the ANN 5-6-1 Model

| | Limits of Input Parameters | | | | | | Limits of Output Parameter | |
|----------------|----------------------------|--------|-------------------|--------|-------------------------|--------|----------------------------|--------|
| | T_p (s) | | μ_1 & μ_2 | | α_1 & α_2 | | T_{new} (s) | |
| Seismic Hazard | Zone III | Zone V | Zone III | Zone V | Zone III | Zone V | Zone III | Zone V |
| Max | 2 | 2 | 0.5 | 0.5 | 1 | 1 | 3.417 | 3.45 |
| Min | 0.1 | 0.1 | 0.05 | 0.05 | 0.1 | 0.1 | 0.095 | 0.091 |

4.3 Mathematical Formulation of Sliding Stacked NSCs and SDOF Structure

Heavy components resting on a structure are usually considered to be part of live loads in the design of a structure. Guidelines suggest different percentages of the live loads as masses in the main structure inertia. A close look at these guidelines is required to

understand these inertial masses better. Assuming these components to be rigidly attached to the main structure, the design of the structure becomes too conservative since energy dissipation due to friction between their interfaces is neglected. On the other hand, the design can be unsafe if these components are completely neglected in horizontal excitation. The complexity of the problem arises when the live loads are due to stacked objects. Such stacks are widely seen in docks and storage structures. In these cases, energy dissipation by friction will be seen between various layers of the stack and also between the main structure and the live load objects. While some work has been done on the seismic behavior of main structure with a single live load object, studies on stacked live load objects are needed. By considering the stacks as a single object by neglecting the energy dissipation due to friction between the layers, the response of the structure can be overestimated (Smith-Pardo et al. 2015). This is the main concern of the present study. Therefore, this section presents an analytical model of the structure with stacked sliding live load objects. The live load objects may undergo sliding, rocking, and combined sliding–rocking under external excitations. In the present study, squat container stack (one on the top of the other) of two rigid bodies which show only sliding mode of vibration is considered.

In this study, a combined model is developed by considering the nonlinearity due to the sliding of the blocks. The nonlinearity due to the yielding of the structure is not considered. Static and Kinetic coefficients are equal to each other at each surface of the system. Live load objects considered in this study are sufficiently squat. Squat rigid bodies ($\mu < B/H$), where μ is the coefficient of friction at the rigid block-structure interface, B and H are the width and height of the rigid body, respectively are slip dominant. Because of this condition, rocking mode and slide-rock mode of the rigid blocks cannot occur (Sideris et al. 2014). In this particular study, the width (B) of the rigid body is termed as contact width.

The minimum contact width required for the rigid bodies at the bottom most and within the stack to not occur rocking is given as:

$$B_i > \mu_i \sum_{j=i}^n H_j \quad (4.18)$$

where, n equals to number of secondary bodies.

The mathematical formulation involves the derivation of the dynamic equations of motion of the single-degree primary structure (PS) with n number of secondary bodies (SBs) as a stack counting them bottom to top (1^{st} body is at the bottom of the stack). The following methodology is formulated to derive the equations of motion of the PS and sliding SBs:

1. Start from the top most mass in the stack, i.e., n^{th} body (m_n).
2. Check sliding condition (Eq. (4.19)) at every interface in the stack moving downwards.
3. While moving downwards, find the clusters sticking to each other.
4. Consider each cluster as an individual body, and all such clusters as sliding w.r.t. each other.
5. Derive the dynamic equations of motion for the clusters (Eqs. (4.20) and (4.21)) and solve them.

For the above steps 1 and 2, a sliding condition is to be defined. Note that as the calculation moves from the topmost body downwards, the sliding conditions provide the clusters. Let the q^{th} body be the topmost body of the cluster that the i^{th} body belongs to. Hence there would be $(q - i)$ bodies stuck to the i^{th} body above it.

A function ***slip_i*** is defined to check the sliding behavior between the i^{th} and $(i - 1)^{\text{th}}$ bodies.

$$\mathbf{slip}_i = \left[(\ddot{u}_{i-1} + \ddot{u}_g) \sum_{j=i}^q m_j + \mu_{k_{q+1}} g \cdot \text{sign}(\dot{u}_{q+1} - \dot{u}_q) \sum_{j=q+1}^n m_j \right] \geq \mu_{s_i} g \sum_{j=i}^n m_j \quad (4.19)$$

If $\mathbf{slip}_i = 1$ (True), then i^{th} body slides with respect to $(i - 1)^{th}$ body.

= 0 (False), the i^{th} body sticks to the $(i - 1)^{th}$ body

It should be noted that \mathbf{slip}_i is also used to check the sliding between the bottom-most body of a stack (m_{b1}) and the primary structure (m_p).

Fig. 4.20a shows the primary structure with a n number of SBs in the various levels of the stack. By using the condition for sliding \mathbf{slip}_i , relative motion between the different levels of the stack is verified, and corresponding clusters are defined as shown in Fig. 4.20b.

The dynamic equations of motion can be written as follows:

Assume PS is part of the 1^{st} cluster, and there are C clusters above it.

$$M_0(\ddot{U}_p + \ddot{u}_g) + c\dot{U}_p + kU_p = \mu_{k_1} \left(\sum_{j=1}^c M_j g \right) g \cdot \text{sign}(\dot{U}_2 - \dot{U}_p) \quad (4.20)$$

where, M_0 is the mass of the 1^{st} cluster. μ_{k_1} is the kinetic coefficient of friction between the interfaces of the 1^{st} cluster and the above cluster. U_p, U_2 , are the displacements of the 1^{st} and above clusters, respectively.

The dynamic equation of motion for the l^{th} cluster:

$$M_l(\ddot{U}_l + \ddot{u}_g) = -\mu_{k_l} \left(\sum_{j=l}^c M_j \right) g \cdot \text{sign}(\dot{U}_l - \dot{U}_{l-1}) + \mu_{k_{l+1}} \left(\sum_{j=l+1}^c M_j \right) g \cdot \text{sign}(\dot{U}_{l+1} - \dot{U}_l) \quad (4.21)$$

where, M_l is the mass of the l^{th} cluster. μ_{k_l} is the kinetic coefficient of friction between the interfaces of the l^{th} cluster and the $(l - 1)^{th}$ cluster, whereas $\mu_{k_{l+1}}$ is friction

coefficient between the $(l + 1)^{th}$ cluster and the l^{th} cluster, respectively. U_{l-1}, U_l, U_{l+1} are the displacements of the $(l - 1)^{th}, l^{th}$ and $(l + 1)^{th}$ clusters respectively.

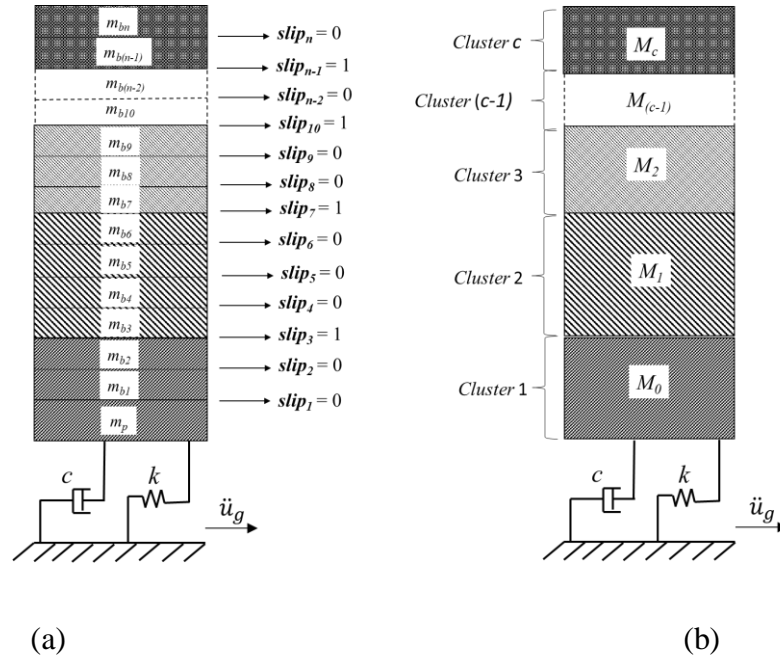


Fig. 4.20 Clusters formation

The numerical analysis procedure is shown as the flow chart in Fig. 4.21. The present study examines the effect of a two-level stack of SBs on the seismic behavior of the structure. The idealization of a single-degree primary structure (PS) with a mass m_p , lateral stiffness k , and viscous damping c with such a stack on it is shown in Fig. 4.22. The mass of the secondary bodies is represented as m_{b1} , and m_{b2} . The bottom secondary body (SB₁) in the stack is considered to interact with the structure with Coulomb friction. Such friction is also present between the bodies (SB₁ and SB₂) in the stack. The static (μ_s) and kinetic (μ_k) coefficients of friction are assumed to be equal and denoted as μ in this study. Let u_p , u_{b1} and u_{b2} be the displacements of PS and SBs, respectively with respect to ground. The combined system is subjected to a ground acceleration of \ddot{u}_g .

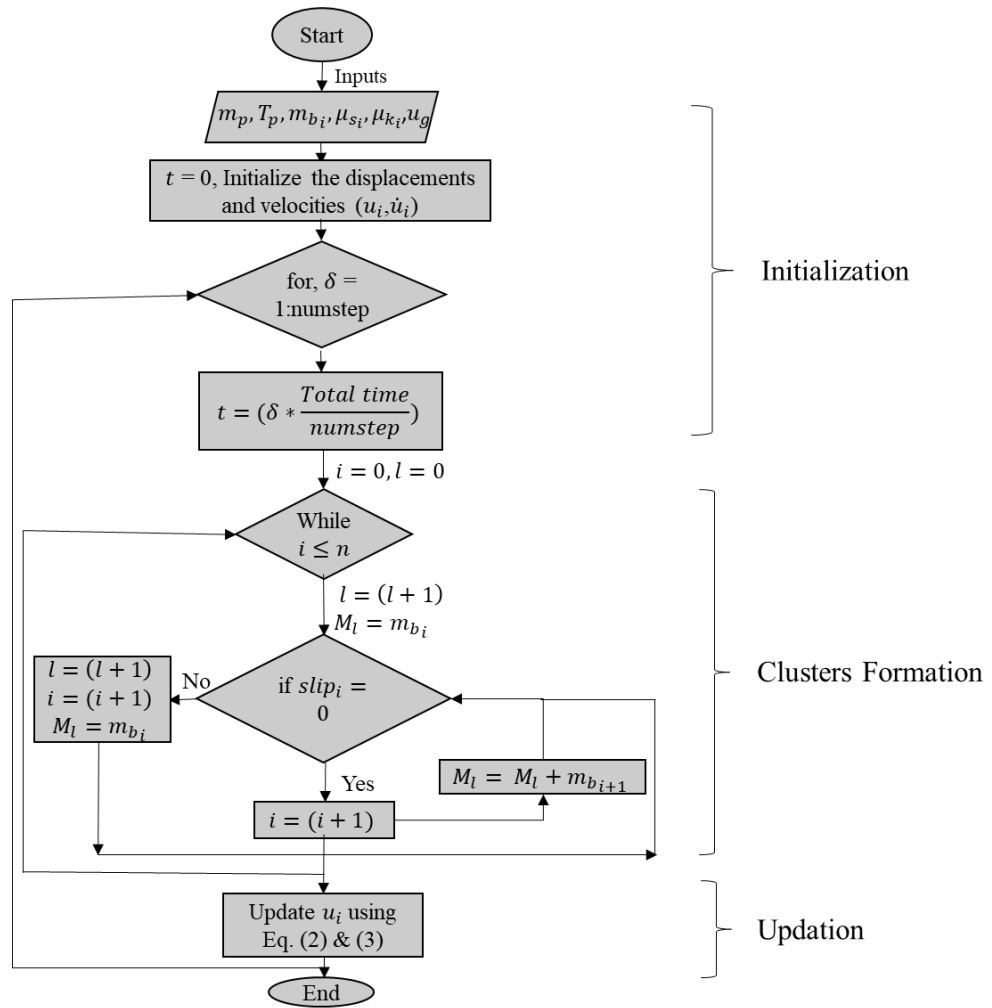


Fig. 4.21 The flowchart of the numerical analysis procedure

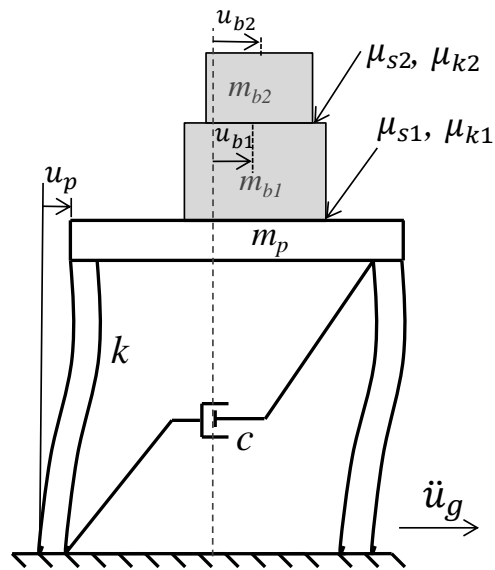


Fig. 4.22 Idealization of single-degree primary structure with two level stack of SBs.

The governing dynamic equations of motion (Eqs. (4.20) and (4.21)) for the structure and the stack in stick and sliding/slip mode are solved by the 4th order Runge-Kutta method. In the subsequent discussion, mass ratios (α_i) of the stack of live load objects, original structural period (T_p), and the mass ratio (α) of single sliding live load objects are introduced and defined by the Eqs. (4.4), (4.5), and (4.6), respectively. The seismic hazard levels and the ground motions used in this section are shown in Fig. 4.3 and Table 4.1 of Section 4.1.

4.3.1 Validation of the Model

A Finite Element (FE) model was developed to validate the above method. In this section, the main features of a FE model developed using ABAQUS/CAE release 6.14 (academic version) are described. The basic FE model developed consists of a rectangular body that simulates the primary structure with sliding rigid blocks resting on it. The rigid blocks and primary structures are modelled as discrete rigid bodies. The developed FE model is used to calculate the response of a single-degree oscillator with sliding rigid blocks resting on it. To do so, a horizontal spring element and dashpot were attached to the rectangular body to simulate the oscillator, as shown in Fig. 4.23.

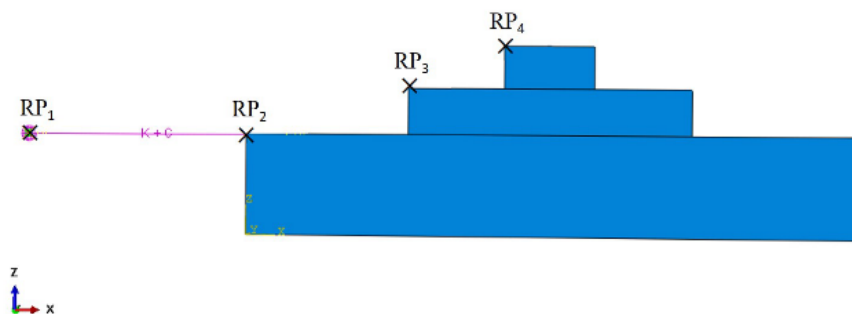


Fig. 4.23 ABAQUS model of a structure with a two-level stack of SBs

The motion of the rigid bodies is defined by reference nodes assigned to them. A rigid body reference node has both translational and rotational degrees of freedom. Reference node (RP₁) is created to simulate the ground point such that one end of the spring is attached to it, and all degrees of freedom of RP₁ restrained to simulate a fixed point. The other end of the spring element is attached to the primary structure to simulate the SDOF oscillator. Masses of the structure (m_p) and rigid blocks (m_{b1}, m_{b2}) are assigned to the reference nodes as inertia. In this particular study, RP₂, RP₃, and RP₄ are the reference nodes assigned to the primary structure and the rigid sliding blocks, respectively.

The Coulomb friction model is used to capture the friction and to slide at the contact surface. The model characterizes the frictional behavior between the surfaces using a coefficient of friction, μ . To capture the sliding of the blocks under base excitation, the contact interface that exists between the blocks and the SDOF oscillator is modelled via an interaction module in ABAQUS. This is defined by two surfaces designated as master and slave surfaces. Generally, if a smaller surface contacts a larger surface, it is best to choose the smaller surface as the slave surface (Dassault Systèmes 2016). The contact interaction between these bodies is generated by the Surface-to-Surface contact (Explicit) method. Explicit method is chosen over the implicit method as the explicit platform converges better (Zhang et al. 2017). The normal interaction of the contact is formulated as hard contact, and the tangential interaction is modelled as penalty formulation. The Penalty contact algorithm is used for mechanical constraint formulation. The finite-sliding formulation, which is the most common and allows for sliding of the surfaces in contact, is adopted since small sliding formulation cannot be used for contact pairs using the penalty contact algorithm.

A horizontal acceleration based on earthquake data is applied to the ground point to simulate an excitation at the base of the SDOF oscillator. The structure with a stack of SBs is subjected to a medium hazard spectrum compatible Duzce-Turkey (1999) earthquake recorded at Lamont #1059 station. The acceleration time history of the earthquake used in this validation is shown in Fig. 4.24.

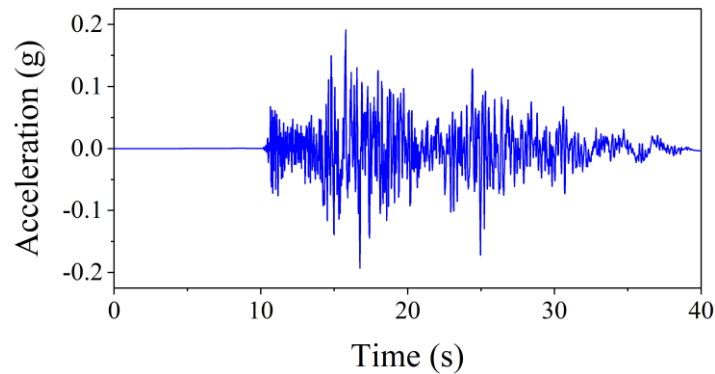


Fig. 4.24 Acceleration time history used for validation

Fig. 4.25 shows the calculated displacement response for selected values of the mass ratios, coefficients of friction, and period of the structure. It can be observed that SB_1 and the structure behave as one since relative sliding displacement between them is zero. The relative sliding displacement of SB_2 w.r.t SB_1 is more in short period structures since the structure accelerates more. Displacement estimates from the developed numerical model match the FE model.

4.4 Dynamic response of a SDOF structure with stacked sliding NSCs

This section investigates the effect of a stack of live load objects on the dynamic response of the structure in comparison to the response of the structure with a single sliding rigid block.

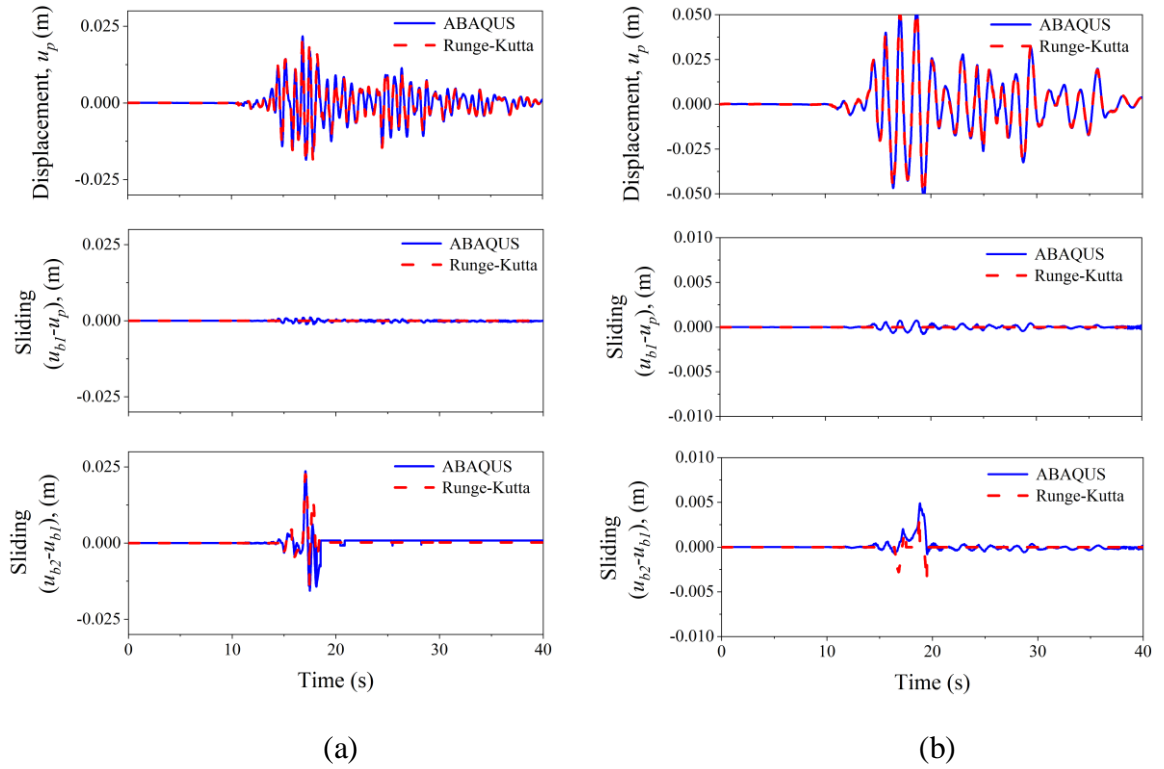
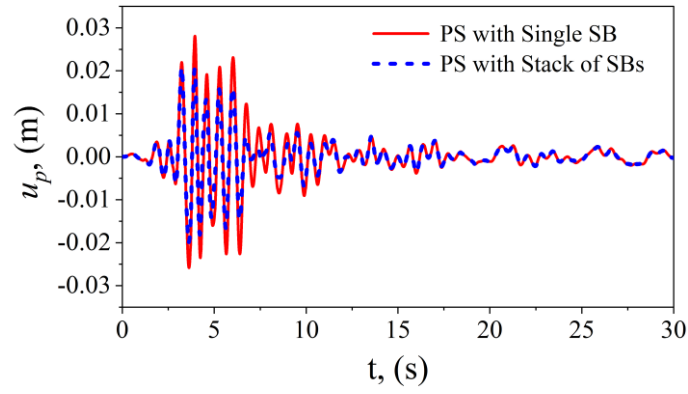


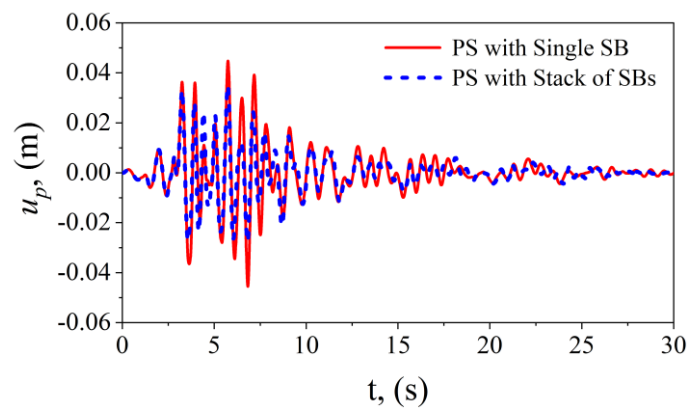
Fig. 4.25 Comparative response of Runge-Kutta method and FE model for $\alpha_1 = \alpha_2 = 0.5$, $\mu_1 = 0.3$, $\mu_2 = 0.1$, and: (a) $T_p = 0.5$ s; (b) $T_p = 1$ s.

4.4.1 Displacement Response

A typical structure of natural period 0.5 sec is chosen. A mass ratio of 0.5 is used for both α_1 and α_2 . Coefficients of friction (μ_1 and μ_2) are 0.3 and 0.1, respectively are chosen to capture the difference in sliding behavior. For the case where the stack is taken as a single mass, the frictional coefficient between the structure and the sliding mass is kept the same (0.3). Spectra compatible earthquake excitation #11 from Table 4.1 is applied to the base of the PS with SBs. The displacement response time histories are shown in Fig. 4.26. Since the maximum displacement of the structure is of great concern for the design of the structures, it is tabulated, as shown in Table 4.7, for both the seismic hazard levels. It should be noted from Fig. 64 and Table. 4.7 that there is considerable dissipation of energy due to sliding within the stack in both the seismic zones.



(a)



(b)

Fig. 4.26 Displacement response of the PS with stacked SBs (a) Zone III; (b) Zone V.

Table 4.7 Maximum displacement of the PS with and without stack

| Maximum displacement of the PS, u_p (m) | | | |
|---|---------------------|------------------------|-------------|
| Seismic Zone | PS with a Single SB | PS with a Stack of SBs | % reduction |
| III | 0.028 | 0.021 | 25 |
| V | 0.046 | 0.035 | 23.91 |

4.4.2 Parametric Study

The displacement response of a structure with a stack of SBs is different from that of a structure with a single sliding rigid block, as seen in the previous section. Hence, a parametric study was performed with the following variables: (a) the structural period T_p ;

(b) the mass ratios α_1 and α_2 ; (c) the frictional coefficients within the stack and between the stack and the PS i.e., μ_2 and μ_1 respectively. Different problems were analyzed for each seismic damage risk zone. For each the mean of the maximum displacement response of the system for scaled eleven ground motions were calculated. A set of parameters is defined to quantify the effect of a stack of SBs on the response of the primary structure and are called *Displacement Response Ratios (DRRs)*.

$$DRR_1 = \frac{(u_p)_{stack}}{(u_p)_{rigid}} \quad (4.22)$$

$$DRR_2 = \frac{(u_p)_{single}}{(u_p)_{rigid}} \quad (4.23)$$

Where $(u_p)_{stack}$ is the displacement of a structure supporting a stack of SBs and $(u_p)_{single}$ is the displacement of the same structure but supporting a single sliding block of the same as whole stack. $(u_p)_{rigid}$ is the displacement of the structure supporting an equivalent rigidly attached block (with the same mass as the stack). DRR_1 or DRR_2 approaching one indicates minimal slippage. If the ratio of DRR_1 to DRR_2 approaches one, it indicates that slippage within the stack is not significant.

Increase in structural period and coefficients of friction shows significant increase in the value of DRR as shown in Fig. 4.27 for medium damage risk zone. From Fig. 4.27, it can be inferred that if $\mu_2 \leq \mu_1$, input energy is dissipated by the relative movement between blocks since $DRR_1 < DRR_2$. For $\mu_2 > \mu_1$, no energy dissipation is observed within the stack ($DRR_1 = DRR_2$). This is due to the fact that when the lower block (SB₁) in a stack is sliding, and upper block (SB₂) is at rest with respect to SB₁, then the resistant force acting on SB₂ is given as $m_{b2}(\ddot{u}_{b1} + \ddot{u}_g) = f_1$. The resistant force f_1 can be obtained from the Eq. (4.21) and is as follows:

$$f_1 = -m_{b2}\mu_{k1}g\text{sign}(\dot{u}_{b1} - \dot{u}_p) \quad (4.24)$$

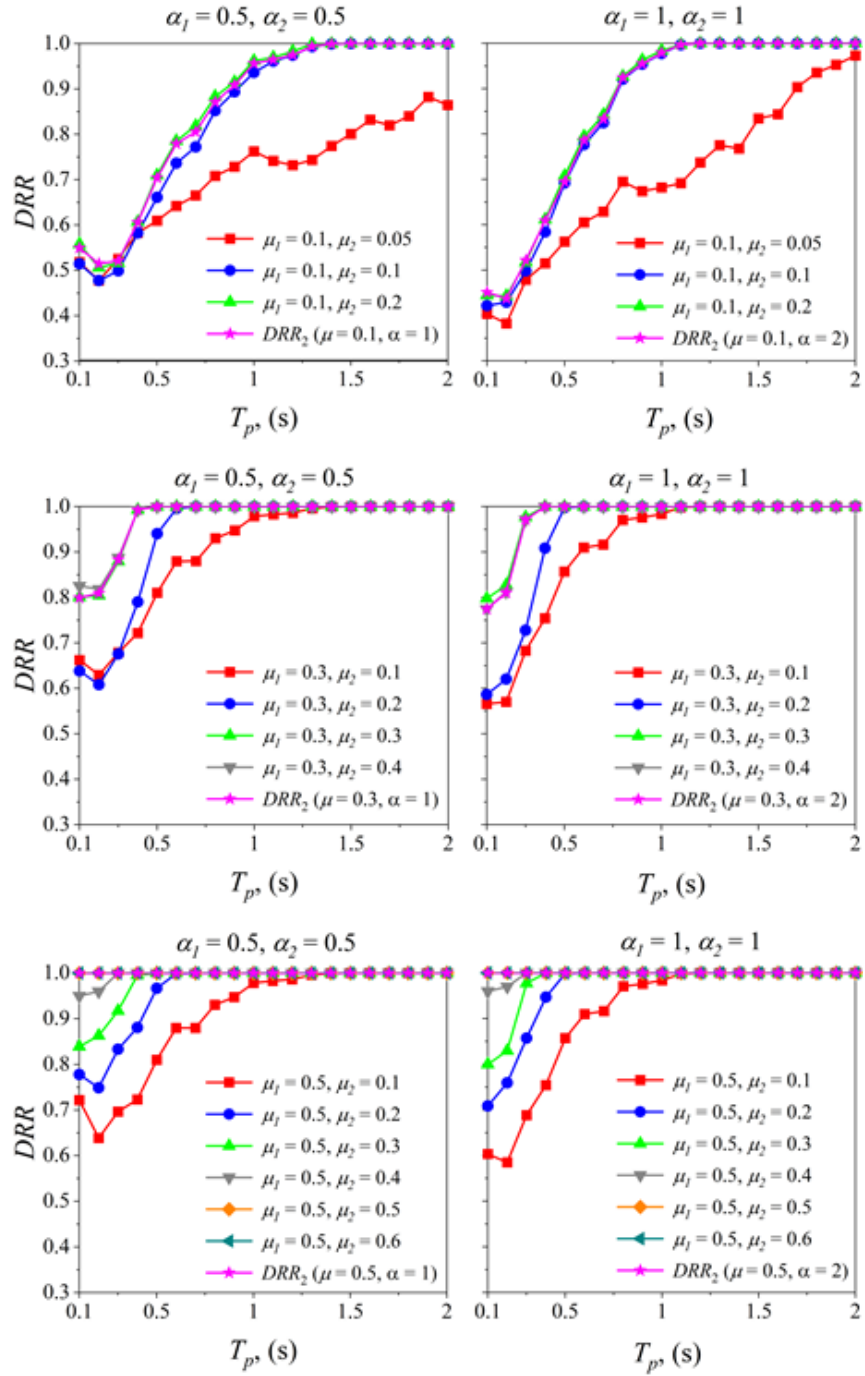


Fig. 4.27 Displacement Response Ratio (DRR) for primary structure under medium seismic damage risk zone (Zone III)

The rigid block on the top m_{b2} , starts sliding only when f_1 exceeds the limiting static frictional force between m_{b1} and m_{b2} i.e., $m_{b2}\mu_{s2}g = f_2$. Since $\mu_{k1} < \mu_{k2}$, f_1 will never reach the value of the limiting frictional force f_2 and hence m_{b2} will not slide when the

lower block (SB_1) slides with respect to the structure. Hence, in this case, the energy dissipation due to friction within the stack is negligible, and the two rigid blocks in the stack behave as a single block ($m_{b1} + m_{b2}$).

From Fig. 4.28, it is observed that DRR increases significantly with an increase in the natural time period of the structure and the coefficients of friction as expected. The same trend is seen for DRR in the highest damage risk zone also. Energy dissipation due to friction between the stack of blocks is negligible when $\mu_2 > \mu_1$ similar to medium damage zone. Hence from Figs. 4.27 and 4.28, it can be concluded that regardless of seismic damage risk zone, mass ratios and friction coefficients if $\mu_2 > \mu_1$, stack of rigid blocks can be considered as a single sliding rigid block.

Due to the sliding of the stack of blocks and within the stack, only a portion of the total mass of the stack participates in the primary structural inertia. This affects the modal characteristics of the primary structure. In this study, an equivalent time period for the structure is evaluated for understanding this behavior.

4.4.3 Modified Structural period due to stacked sliding NSCs

This section explains a methodology to determine the structural period of the primary structure with stacked sliding SBs. The modified structural period is designated as T_{new} and it can be used for the design of a structure by using the corresponding response spectrum. When the SBs are rigidly attached to the PS, the modified structural period of the PS can be calculated using Eq. (4.11). The following proposed algorithm allows determining the modified structural period when the stacked sliding SBs are present on the PS.

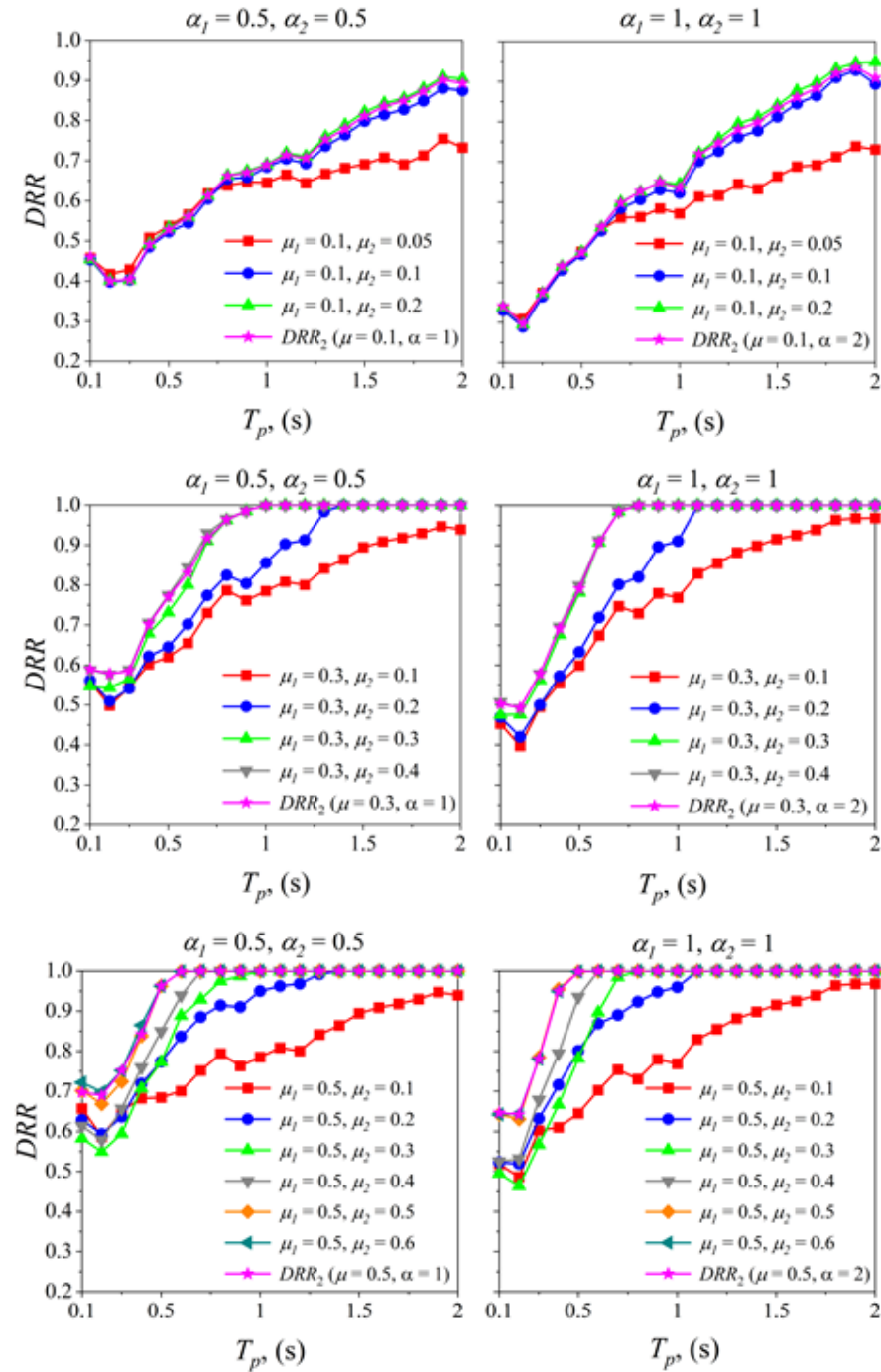


Fig. 4.28 Displacement Response Ratio (DRR) for primary structure $\alpha_2 = 1$ under highest seismic damage risk zone (Zone V).

4.4.3.1 Algorithm for the determination of modified structural period

The algorithm proposed in Section 4.2.3.1 for the determination of the T_{new} in the case of multiple sliding SBs resting on the PS side-by-side can be slightly modified to use the same

algorithm in this case too. A slight modification is required to the step (1) of the proposed algorithm (Section 4.2.3.1). The steps (2), (3), and (4) remain unchanged.

1. Calculate the absolute maximum accelerations of the structure (m_p) and lower body in the stack (m_{b1}) for the eleven scaled ground motions for a given seismic hazard level. If accelerations of m_p and m_{b1} are less than $\mu_1 g$ and $\mu_2 g$ respectively, then the blocks will not slide and, therefore $T_{new} = T_{rigid}$. Otherwise, the sliding will be seen within the stack and below the stack.
2. Calculate the 5%-damping mean displacement spectrum for the set of scaled ground motions.
3. Calculate the mean of the maximum displacement of the PS with a stack of sliding SBs for a given set of scaled eleven ground motions using the numerical procedure shown in Fig. 4.21.
4. Determine the structural period from the 5%-damping mean displacement spectrum (obtained in Step (2)) for the calculated mean displacement (obtained in Step (3)) by linear interpolation.

The process is illustrated in Fig. 4.29. The structural period of the PS with a stack of SBs is evaluated under scaled eleven ground motions for $T_p = 1$ sec, $\alpha_1 = \alpha_2 = 0.5$, $\mu_1 = 0.2$ and $\mu_2 = 0.1$ in this case. The mean displacement of the PS is found out to be 0.0549 m. The corresponding modified structural period of the structure using the above methodology is 1.38 sec.

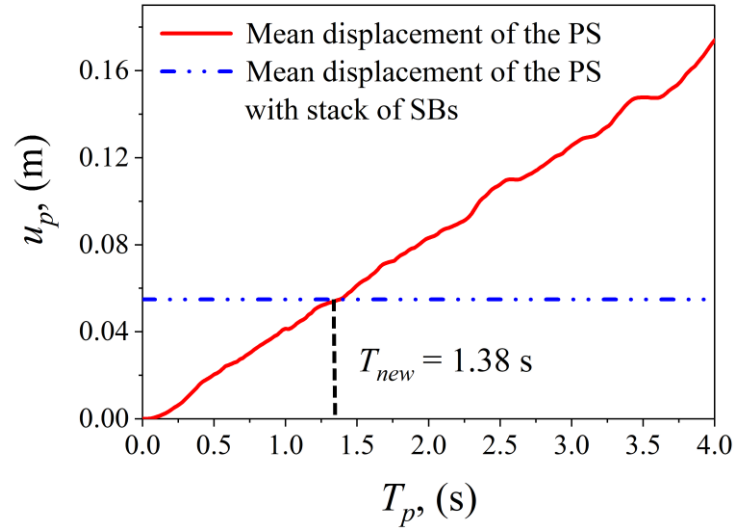


Fig. 4.29 Determination of the T_{new} of a PS with a stack of sliding SBs.

The validation of the proposed algorithm is done with the single live load object from the previous studies. The procedure for validating the algorithm proposed for the structure with the side-by-side SBs (Section 4.2.3.2) was used for this case too. For such validation, the coefficient of friction is considered as very high between the SBs in the stack. The calculated modified structural period of the primary structure with a stack of SBs by the proposed algorithm is successfully validated with the structure with a single sliding live load object.

4.4.4 Parametric study on modified structural period

A parametric study was performed with: (a) the structural period T_p (from 0.1 s to 2 s, increments of 0.1 s); (b) the mass ratios α_1 and α_2 (0.1, 0.5, 1.0); (c) the coefficient of friction within the stack and between the stack and the PS. $\mu_1 = 0.05, 0.1$ to 0.6 (with increments of 0.1) and $\mu_2 = 0.05, 0.1$ to 0.7 (with increments of 0.1). These

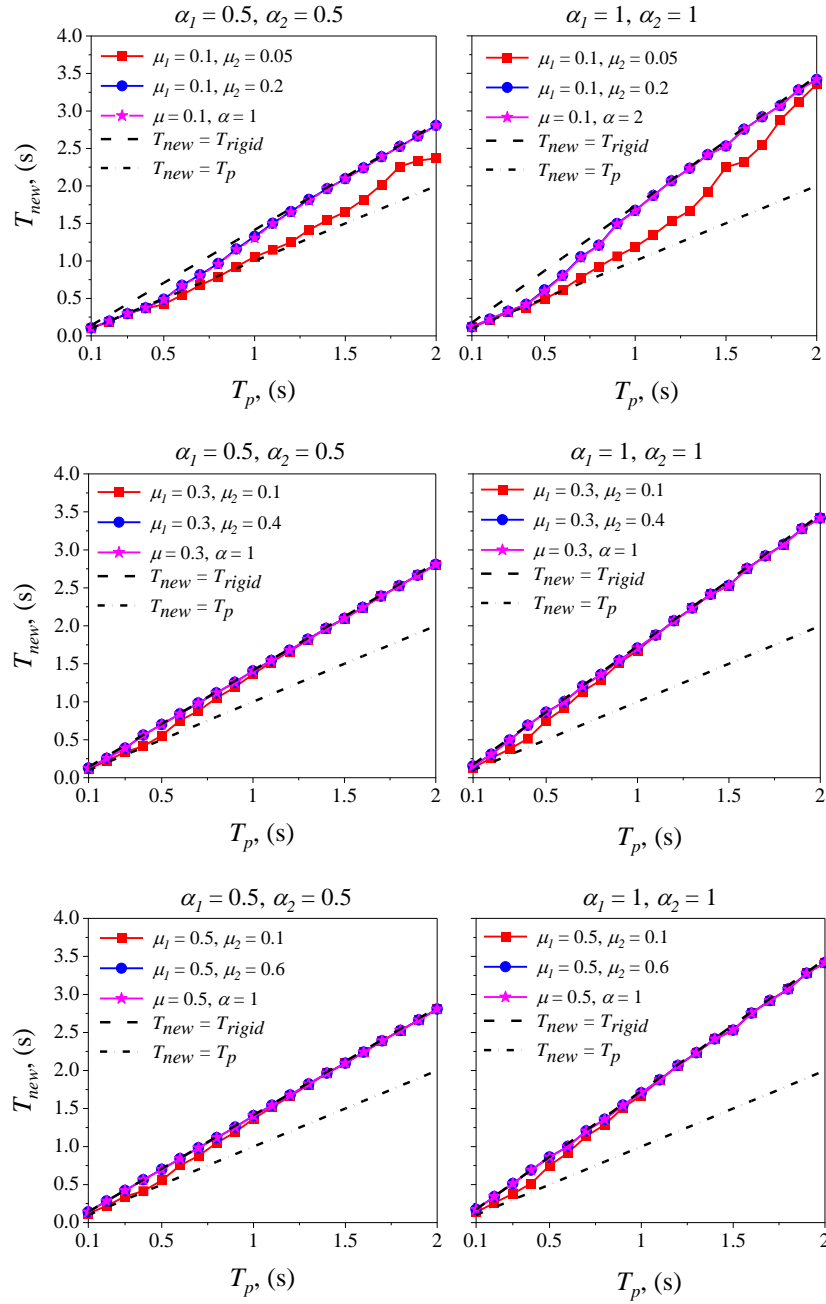


Fig. 4.30 T_{new} against T_p for medium seismic hazard level (Zone III).

ranges are selected based on the most common structural properties. It should be noted that the mass ratios are corresponding to light structures and heavy secondary masses. 6300 runs were analyzed with various permutations for each seismic damage risk zone. Each run involves the calculation of the modified structural period (T_{new}).

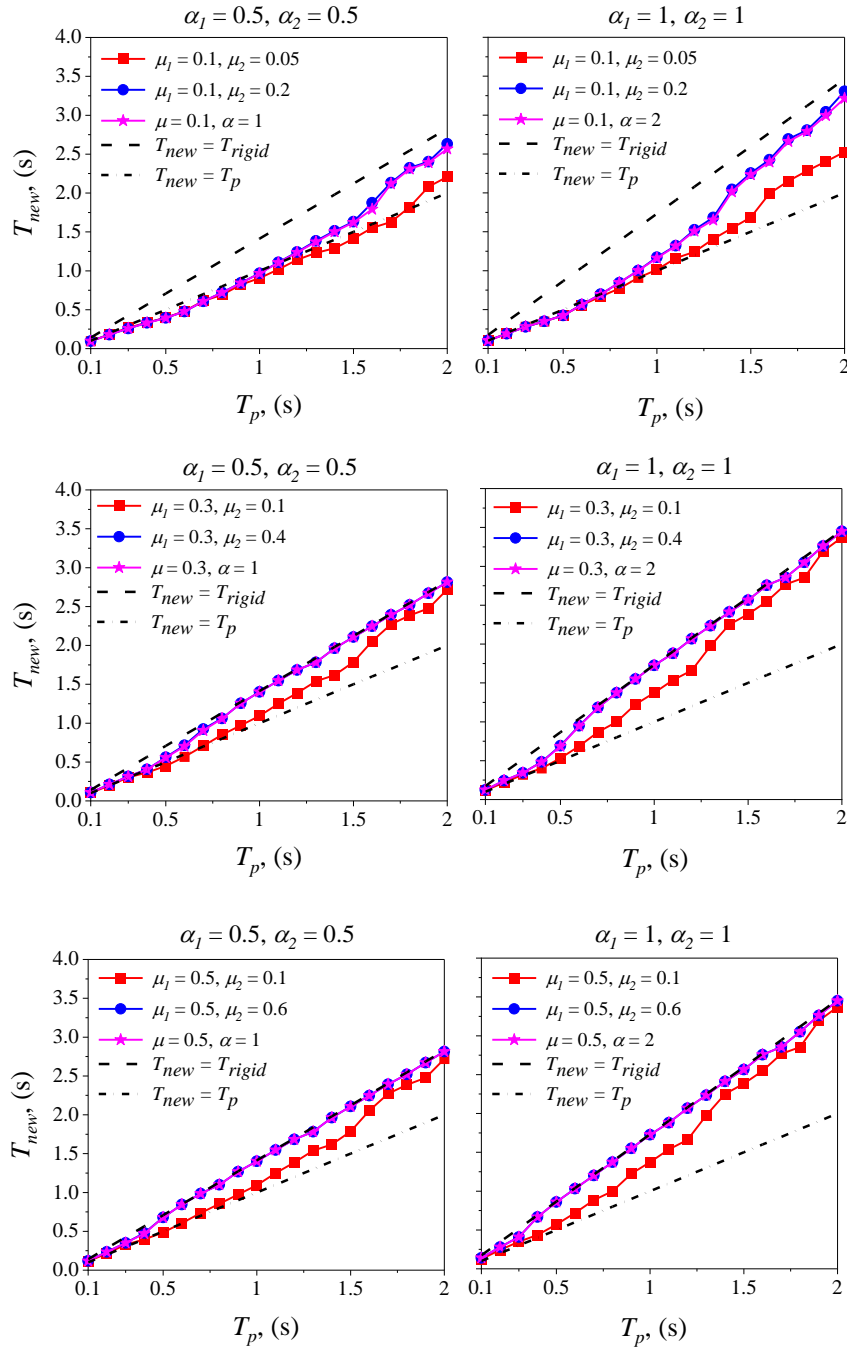


Fig. 4.31 T_{new} against T_p for highest seismic hazard level (Zone V).

Fig. 4.30 shows a subset of results from the parametric study for a given mass ratio and coefficients of friction. It is observed that the structural period of the PS with a stack of SBs (T_{new}) increases with the coefficients of friction and structural period. The increase in structural period (T_{new}) is significant at higher mass ratios. The structural period of the PS with a stack of SBs is equal to the structural period of the PS with a single sliding rigid

block when $\mu_2 > \mu_1$. This is the same as in the case of *DRR* mentioned in Section 4.4.2. It is also observed from Fig. 4.30 that the modified structural period of the PS with a stack of SBs is almost equal to the modified structural period of the PS with single sliding rigid block even for smaller μ_2 values when μ_1 is larger regardless of mass ratios. The structure experiences small total accelerations (since the seismic hazard level is medium), which are not enough to counteract the friction.

The modified structural period (T_{new}) increases with the structural period and coefficients of friction, especially for larger values of mass ratios, as shown in Fig. 4.31 under the highest seismic hazard level also. Energy dissipation associated with the relative movement between blocks can be neglected when $\mu_2 > \mu_1$. From Figs. 4.30 and 4.31, it can be observed that energy dissipation due to friction between the blocks is more in the highest seismic hazard level compared to the medium seismic hazard level.

4.4.5 Design expressions for modified structural period by Non-Linear Regression

In order to design a structure with a given stack of sliding bodies by the response spectrum method, an equation for T_{new} needs to be developed. For some of the cases, T_{new} can be obtained from Figs. 4.30 and 4.31. In other cases, a design equation will be developed through a parametric study by considering a large data set corresponding to large number of variables. Non-Linear Regression (NLR) analyses yield the following design equations to calculate T_{new} for each seismic damage risk zone:

For Medium seismic hazard zone:

$$T_{new} = \left((-4.284 * T_p) - (0.173s * \mu_1) + (0.015s * \mu_2) - (4.365s * \alpha_1) - \right. \\ \left. (4.567s * \alpha_2) \right) + 2.022s * e^{\left(\left(\frac{0.053}{s} * T_p \right) + (0.003 * \mu_1) + (0.002 * \mu_2) \right) + (0.044 * \alpha_1) + (0.045 * \alpha_2) + 3.873} - 97.3s \quad (4.25)$$

For Highest seismic hazard zone:

$$T_{new} = \left((-5.464 * T_p) - (2.268s * \mu_1) - (4.451s * \mu_2) - (5.064s * \alpha_1) - (4.693s * \alpha_2) \right) + 2.197s * e^{\left(\frac{0.052}{s} * T_p + (0.02 * \mu_1) + (0.038 * \mu_2) + (0.041 * \alpha_1) + (0.038 * \alpha_2) + 3.97 \right)} - 116.3s \quad (4.26)$$

The prediction capability of the regression models for both the seismic zones are evaluated by defining the various statistical performance functions like Co-efficient of Determination (R^2), Correlation Coefficient (R), Root Mean Square Error (RMSE), Mean Square Error (MSE) and Mean Absolute Error (MAE). The performance of the models is summarized in Table. 4.8.

Table 4.8 Performance of the models

| Seismic Zone | R^2 | R | RMSE | MSE | MAE |
|--------------|-------|-------|-------|-------|-------|
| III | 0.985 | 0.992 | 0.094 | 0.009 | 0.082 |
| V | 0.969 | 0.985 | 0.1 | 0.01 | 0.09 |

The R-value of the model should be as high as possible since it gives the relative correlation and goodness of the fit between the measured and predicted values. RMSE, MSE, and MAE are errors, and they should be as low as possible. Therefore, from Table. 4.8, it can be observed that the strong correlation exists between the measured and predicted values with minimum errors.

4.5 Summary

This chapter explores the effect of the multiple sliding NSCs on the dynamic response of the supporting SDOF primary structure under spectrum compatible real earthquake excitations. An extensive parametric study has been conducted on the response of the structure by varying the dynamic properties of the structure and the interactional properties (mass ratios and coefficients of friction) of the NSCs. The results from the parametric

analysis show that the mass ratios and the coefficients of friction have a significant effect on the response of the structure. A generalized design methodology is proposed to determine the modified structural period of the primary structure. Finally, design expressions are proposed to calculate the modified structural period of the structure as a function of the structural period, mass ratios, and coefficients of friction by Non-Linear Regression and Artificial Neural Network models. The next chapter investigates the damping effect of NSCs on the structures.

CHAPTER 5: DAMPING EFFECT OF NSCs ON THE RESPONSE OF THE STRUCTURE

5.1 General

From the above chapters (3 and 4), it can be seen that the hanging and multiple sliding NSCs significantly affecting the structural response. The seismic response of the structure is usually reduced due to the dissipation of the energy. This dissipation is caused due to the variable forces between the structure and the NSC. In the analysis and design of damped structures, the energy dissipation technology is proved to be an effective tool to resist earthquakes (Ghaedi et al. 2017). A number of research studies and engineering procedures have found that the mitigation effects of the seismic response resulting from the installation of the dampers can be measured on the basis of an additional equivalent damping ratio (Ramirez et al. 2003; Sadek et al. 2000). The modal-strain-energy approach was used to determine the equivalent damping ratio of structures with viscoelastic dampers (Chang et al. 1993). Lee *et al.* (2004) proposed a new method for evaluating the equivalent damping ratio in the structure with added damping devices. A closed form solution was proposed to obtain an equivalent damping ratio without carrying out numerical analysis (Lee et al. 2004). Diotallevi *et al.* (2012) proposed a new dimensionless parameter called damping index. Based on this dimensionless parameter, they proposed a simplified method for the direct assessment of the additional damping ratio of the structure with dampers. The proposed method is verified using a single-degree-of-freedom (SDOF) system (Diotallevi et al. 2012). Park (2013) investigated the seismic response of SDOF systems through nonlinear time history analysis with added damper. Additional equivalent damping ratio was estimated using the damping correction factors and regression equations (Park 2013). Very recently, Hu *et al.* (2019) proposed a simplified method to estimate the additional damping ratio based on energy dissipation. From their analysis, they concluded that the

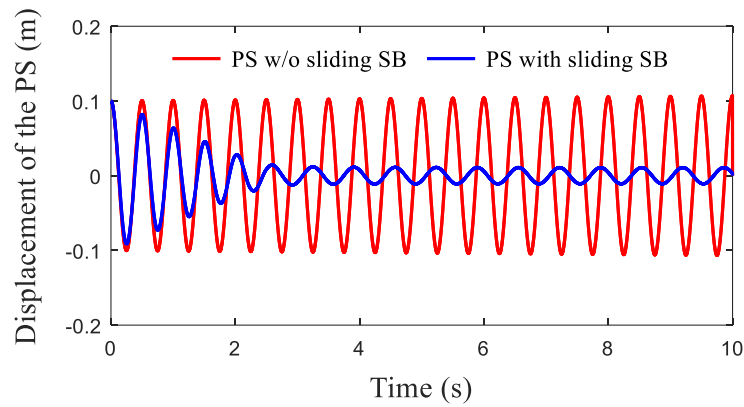
additional damping ratio varies with the time. The proposed method is verified by using a SDOF system (Hu et al. 2019).

The above researcher shows the use of additional equivalent damping ratio of the structure with added dampers. To the author's knowledge, no studies were reported on the additional damping ratio of the structure with flexible NSCs in the literature. Therefore, in this chapter this particular problem is investigated. An additional equivalent damping ratio added to the structure due to these NSCs is evaluated.

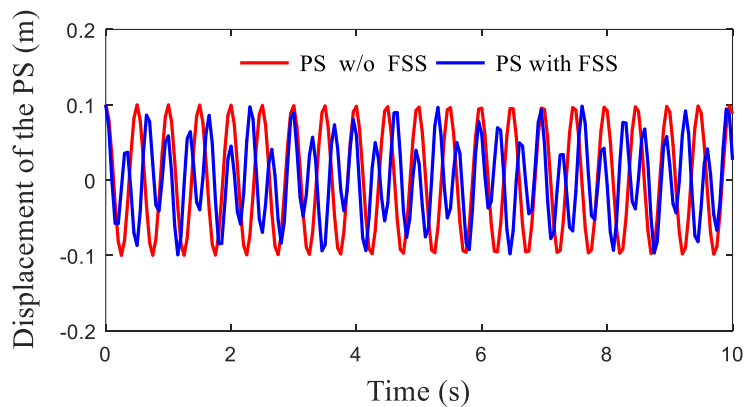
The seismic response of a structure with a hanging mass was varied considerably by external excitations (harmonic and earthquake excitations) and the vibrational properties (mass ratio and length of the pendulum) of the hanging mass. From the analysis results (Chapter 3), the amplitude of the structure's response tends to reduce when the tuning frequency ratio of the hanging mass is nearly equals to one. To understand the energy dissipation of a structure, a SDOF primary structure with a hanging mass and a single sliding secondary body is considered. A free vibration test has been taken on the undamped structure with and without such NSCs. For the analysis, the structural period (T_p) is chosen as 0.5 sec. In the case of sliding SB, the coefficient of friction and mass ratio values are chosen as 0.1 and 0.75, respectively. The tuning frequency ratio and mass ratio in the case of hanging mass are chosen as 0.95 and 0.75, respectively.

Fig. 5.1 shows the displacement response of a structure with a sliding body and a hanging mass. From Fig. 5.1a, energy dissipation in the structure can be seen due to the sliding secondary body. After some duration of the free vibration, the sliding of the secondary body cannot be seen, and the pure steady-state response can be observed. The energy dissipation in the structure with hanging mass is not seen with the hanging mass, even though the response amplitude is observed to be reduced when compared to the structure without a hanging mass (Fig. 5.1b). Therefore, in this study, an attempt has been

made to determine the additional damping ratio added to the structure due to the slide effect as energy dissipation is clearly seen.



(a)



(b)

Fig. 5.1 Displacement of a structure (a) with and without sliding SB; (b) with and without FSS

5.2 Damping effect of the sliding NSCs

Sliding between layers of the secondary mass and the structure will dissipate energy. This energy dissipation can be termed as damping. As observed from Chapter 4, the sliding NSCs can reduce the seismic response of the structure by dissipating the seismic energy due to the slide effect. This energy dissipation can be quantified by the change in equivalent

damping ratio of the structure. Therefore, in this section an attempt is made to determine the additional damping due to the slide effect under earthquake excitations.

For this purpose, the structure with a single sliding live load object is considered. The methodology to determine the additional equivalent damping ratio added to the structure is defined with respect to the rigidly fixed condition (i.e., the additional damping ratio added to the structure due to slide effect is zero when the live load object is rigidly fixed to the structure). The following subsection discusses the methodology implemented to determine the additional damping ratio of the structure. Parametric study results are also presented for a few cases.

5.2.1 Methodology to determine the additional equivalent damping ratio (ξ_a) due to the slide effect

The additional equivalent damping ratio (ξ_a) can be calculated through the following steps:

1. Generate the displacement spectra for an SDOF system for various damping ratios (say, 2%, 5%, 7%, 10%, and 20%) for a given set of spectrum compatible ground motions.
2. Let ξ_{eqf} be the equivalent damping ratio of the structure when the live load object is rigidly fixed to the structure and ξ_{eqs} be the equivalent damping ratio of the structure when the live load object slides.
3. Calculate the mean spectral displacement (S_D) of a given structure (for a given structural period and damping ratio) with a live load object under real earthquake excitations.
4. By using the spectral displacement (S_D) obtained from the above step, and the structural period when the live load object is rigidly fixed (T_{rigid}), ξ_{eqs} can be obtained at the closest intersection point on the displacement spectra

(obtained in Step 1) corresponding to the T_{rigid} on the x-axis and S_D on the y-axis.

5. Finally, additional equivalent damping ratio (ξ_a) due to slide effect can be calculated using the following equation:

$$\xi_a = \xi_{eqs} - \xi_{eqf} \quad (5.1)$$

For the generation of displacement spectra (Step 1), spectrum compatible ground motions are used in this study. The seismic hazard level chosen for this purpose is Indian Seismic Zone V (Hard soil). The response spectrum curve given in the IS 1893 (2016) is for 5% damping ratio. To generate the spectrum compatible ground motions for the damping ratios other than 5% damping ratio, response spectrum curves are needed. Such response spectrum curves for other damping ratios were generated in this study by utilizing the damping modification factors (DMF). The empirical relationship defined in the study (Surana et al. 2019) was used to describe the DMF. The 50th percentile estimated coefficients for the computation of DMFs were used. The resultant displacement spectra are shown in Fig. 5.2.

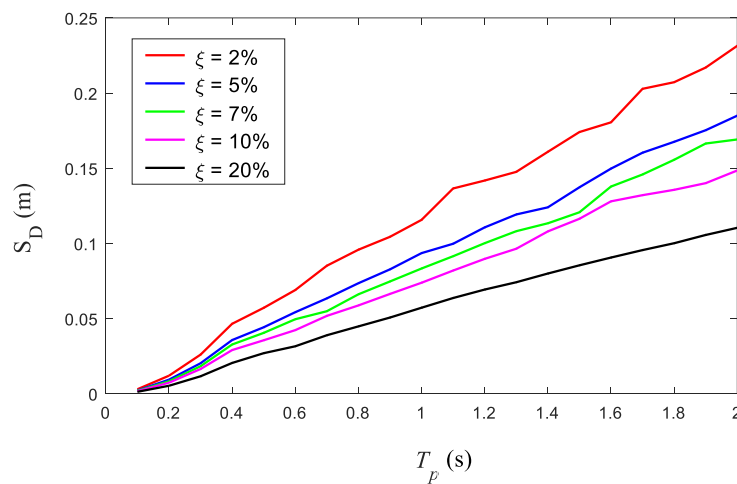


Fig. 5.2 Displacement spectra for various damping ratios.

The methodology is explained through an example. Say, the structural period (T_p) is 0.7 sec and the damping ratio in the structure is 5%. The coefficient of friction (μ) and the mass ratio (α) are chosen as 0.3 and 0.75, respectively. The equivalent damping ratio of the structure is 7%, as shown in Fig. 5.3. The additional equivalent damping ratio can be calculated using Eq. (5.1) and it is 2%. In the following section, a parametric study was conducted for a few cases by choosing the different structural periods, mass ratios, and the different coefficient of frictions to observe the variation in the ξ_a .

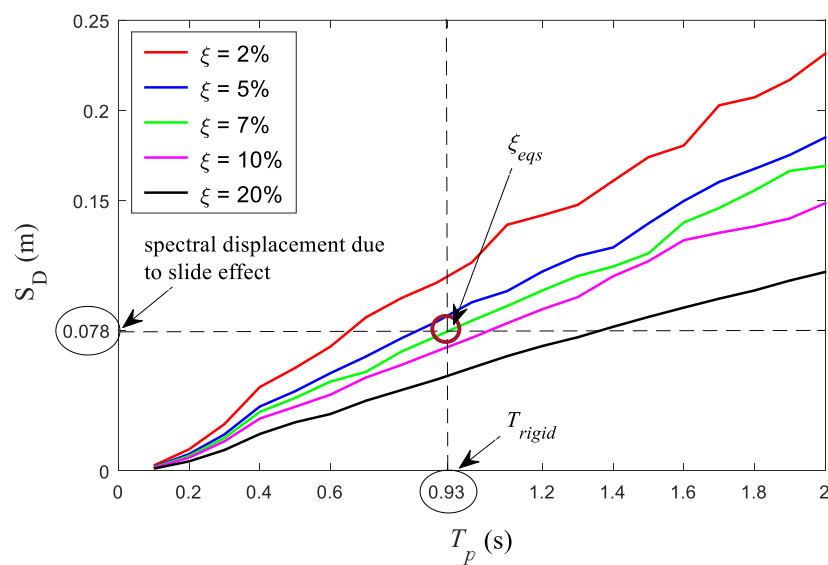


Fig. 5.3 Estimation of additional equivalent damping ratio (ξ_a)

5.2.2 Parametric Study

In the parametric study, the structural periods are chosen as 0.5 sec, and 1 sec to represent the relatively stiff and flexible structures. The mass ratios are chosen as 0.5, 1, 1.5, and 2. The coefficients of friction are varied from 0.1 to 0.6 with 0.1 increments. The variation in the additional damping ratio (ξ_a) with the coefficient of friction for a given mass ratio is shown in Fig. 5.4 for both the stiff and flexible structures.

From Fig. 5.4, it can be observed that the additional damping ratio reduces with the increase in the coefficient of friction irrespective of mass ratio in both the stiff and flexible structures. For the stiff structures (Fig. 5.4a), the energy dissipation in the structure is more, and hence high ξ_a is observed at low coefficient of friction and large mass ratio. At high coefficient of friction, small mass ratios add high ξ_a to the structure. At high coefficient of frictions, the participation of sliding live loads with large mass ratios in the primary structure inertia is more and hence slide effect is less.

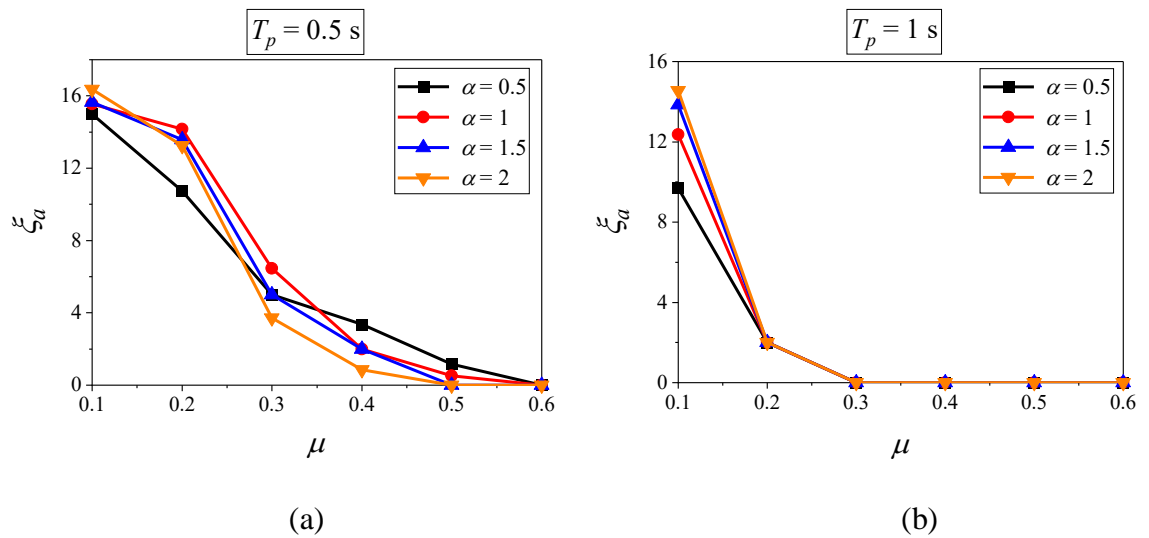


Fig. 5.4 Variation of ξ_a with coefficient of friction for different mass ratios (a) $T_p = 0.5$ s; (b) $T_p = 1$ s

From a given flexible structure (Fig. 5.4b), no energy dissipation in the structure is observed due to the slide effect for $\mu \geq 0.3$ for all the mass ratios considered. Energy dissipation in the structure is high at a lower coefficient of friction for larger mass ratios, and hence high ξ_a was observed in this case similar to stiff structures. Finally, it can be concluded from Fig. 5.4 that for a given coefficient of friction and mass ratio, the additional damping ratio added to the structure due to slide effect is more in stiff structures than that of the flexible structures. The absolute accelerations experienced by the stiff structure are

more compared to the ones experienced by flexible structure, and hence the sliding effect will be high in stiff structures.

The effect of the original structural damping ratio on the additional damping ratio is also studied and shown in Fig. 5.5. Damping ratios (ξ) of 2%, 5%, 7%, 10%, and 20% are chosen. From Fig. 5.5, it can be observed that the additional damping ratio added to the structure due to slide effect decreases with an increase in the damping ratio of the structure for both the stiff and flexible structures. This behavior is expected since the increase in structural damping ratio reduces the absolute accelerations produced in the structure. As shown in Fig. 5.5, the additional damping ratio of the given flexible structure varies between 4% and 0% for a given mass ratio and coefficient of friction. In a stiff structure, additional damping ratio ($\xi_a = 0.6\%$) due to slide effect can be observed even for a high damping ratio ($\xi = 20\%$).

The additional equivalent damping ratio due to slide effect can also be determined from the proposed design equations for a modified structural period for the multiple sliding bodies. For this, the displacement spectra shown in Fig. 5.2 is utilized. ξ_a for the structure with a single sliding live load object and with stacked live loads is calculated and compared.

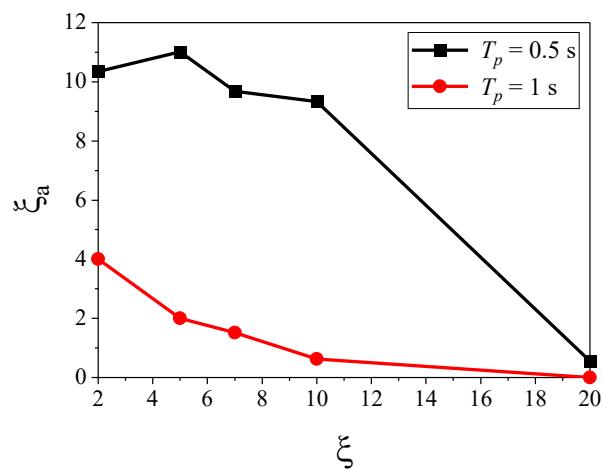


Fig. 5.5 Variation of ξ_a with the damping ratio for $\mu = 0.2$ and $\alpha = 0.75$

This is done so as to qualify the dissipation due to sliding between layers of the live loads. The structural period (T_p) is chosen as 0.5 sec. The damping ratio of the structure is taken as 5%. The mass ratio and the coefficient of friction in the single sliding live load object are 1, and 0.4, respectively. Mass ratios (α_1 and α_2), and coefficients of friction (μ_1 and μ_2) are chosen as 0.5, 0.5, 0.4, and 0.2, respectively for the stacked case. The structural period (T_{rigid}) when the load is rigidly attached to it is 0.71 sec. The ξ_a for the structure with a single sliding live load object can be determined by the methodology shown in Section 5.2.1. For the same structure with stacked live load objects, the modified structural period (T_{new}) was determined using the Eq. (4.26) for a given structural period, mass ratios, and coefficients of friction. The T_{new} is calculated to be 0.53 sec. By using the obtained T_{new} and the 5% mean displacement response spectrum generated from the spectrum compatible ground motions, determine the spectral displacement (S_D). Using this S_D , T_{rigid} and the methodology (Section 5.2.1), the ξ_a can be calculated due to the stacked loads slide effect. Table 5.1 shows the values of ξ_a for both cases. The seismic energy dissipation in the structure is more under stacked sliding loads case than that of the single sliding live load case. And also, from the section 4.5.2, it was concluded that when the $\mu_2 > \mu_1$ for a given seismic hazard level, the energy dissipation due to friction within the stack is negligible and the bodies act as a single sliding live load object. The ξ_a was calculated for this case also and shown in Table 5.1. The ξ_a value when the $\mu_2 > \mu_1$ is approximately equal to that of the structure with a single sliding live load object.

Table 5.1 Additional damping ratio (ξ_a) added to the structure

| | | ξ_a (%) | |
|-------------------------------|----------------------------|---------------------------------|------|
| with single sliding live load | | with stacked sliding live loads | |
| 2 | $\mu_1 = 0.4, \mu_2 = 0.2$ | | 8.05 |
| | $\mu_1 = 0.4, \mu_2 = 0.5$ | | 1.78 |

CHAPTER 6: SUMMARY AND CONCLUSIONS

In this chapter, the summary and conclusions of the study are presented. This is followed by a further scope of work.

6.1 Summary

The major objective of the study presented in this dissertation was to develop a design methodology considering the effect of flexibly attached secondary systems in structural design. Quantification of this effect is first needed for this study. Also, an understanding of the seismic behavior of a structure with such secondary systems was necessary before such an attempt could be made. Hence, the first part of this study focused on assessing the effect of the dynamic and interactional properties of the secondary systems on the seismic behavior of the structure. The second part was focused on developing a design methodology to estimate the design parameters of the elastic structure with such secondary structures. Hanging bodies and sliding secondary systems were considered in this study.

6.1.1 Combined Model for Structure and Hanging NSC

Lead-shielding application in nuclear power plants is the motivation for investigating the effect of the hanging non-structural components on the seismic behavior of a primary structure. Lead-shielding in power plants is primarily provided by lead blankets hanging from or laid on lightweight scaffolding. Due to the high risk associated with the interior of the nuclear power plants, these scaffolding structures need to be designed for seismic loads. Since the lead blankets are considerable in weight with respect to the light frame and are hanging from the scaffolding structure, it is a good example of the problem statement in this study. For simplicity, the scaffolding is assumed to be on the ground and single-storied. Lead shielding of many piping systems in power plants are one-storied.

The governing equations of motion are derived for primary structure and flexible secondary structure by considering small displacements in secondary structure. The analysis was conducted for harmonic and real earthquake excitations. The numerical model of the combined system (primary structure with hanging mass) was validated with an existing study, and seismic response from the model was compared with that of the response from a finite element (FE) model.

The influence of the excitation frequency ratio, tuning frequency ratio, and the mass ratio on the seismic response of the structure was investigated. The excitation frequency ratio is defined as the ratio between the excitation frequency and the natural frequency of the primary structure. The tuning frequency ratio is defined as the ratio between the natural frequency of the hanging mass and the primary structure. The mass ratio is the ratio of the mass of the hanging body to the mass of the primary structure. The inertial forces on the primary structure were considered to understand the secondary mass participation in the seismic behavior of the primary structure under harmonic excitations. A parameter called *Mass Effect Ratio* was defined to quantify such participation.

The effect of the tuning frequency ratio and the mass ratio on the seismic response of the primary structure was investigated under real earthquake excitations. An attempt has been made in this study to assess the effect of the hanging mass on the structure for a given seismic hazard level. Spectrum compatible ground motions were considered. Indian seismic hazard levels, Zone III and Zone V for different soil types were considered. To quantify the effect of the vibrational parameters (length and mass) of the hanging mass on the acceleration response of the structure, a parameter called *Response Acceleration Reduction Ratio* was defined. Finally, a design methodology was developed to determine the spectral acceleration of the structure with a hanging mass. A parameter called, *Design Acceleration Ratio* was defined to quantify the effect of the hanging mass on the spectral

acceleration of the primary structure. The effect of the mass ratio and the tuning frequency ratio on the *Design Acceleration Ratio* was conducted. An expression for the *Design Acceleration Ratio* was developed to determine the spectral acceleration of the structure with hanging mass. Design expressions were developed by means of a Non-Linear Regression and Artificial Neural Networks.

6.1.2 Combined Model for Structure and Sliding NSC

The effect of the multiple sliding non-structural components on the seismic behavior of the primary structure was also investigated in this study. Sliding non-structural components were modelled as a rigid body. In existing literature, the studies were limited to the effect of a single sliding body on the dynamic behavior of the supporting structure. Hence, in this study the effect of the multiple sliding rigid blocks on the seismic behavior of the structure under real earthquake excitations was studied. Multiple sliding bodies resting side by side and also one over the other in the form of stacks were considered.

In this study, the single-story primary structure is assumed to be linear elastic. Sliding secondary bodies are considered to be far enough from each other and other obstructions as to not cause impact collision. A two-level stack of sliding bodies was considered in the case of stacked sliding bodies. Coulomb's friction model was assumed for deriving the governing equations of motion for primary and secondary masses. The 4th order Runge-Kutta method was utilized for solving the equations of motion. The combined system (structure with sliding secondary bodies) were subjected to spectrum compatible earthquake excitations. Two Indian seismic hazard levels (Zone III and Zone V for hard soil condition) corresponds to 5% damping were considered in the analysis. The analysis results from the numerical model were compared against that of the finite element model for validation.

Parameters called *Displacement Ratio* and *Displacement Response Ratio* were defined for both the side by side and stacked cases, for both the seismic hazard levels to study the effect of the interactional parameters (mass and the coefficients of friction) on the seismic response of the structure. An extensive parametric study was conducted on the displacement response of the structure by varying the dynamic properties of the structure and the interactional properties of the sliding bodies. An attempt was made to develop design expressions to determine the dynamic design parameters of the structure with such sliding masses by Non-Linear Regression and machine learning methods for a given seismic hazard level.

6.2 Conclusions

The conclusions for this study were derived from various parametric studies involving structures with hanging masses and multiple sliding rigid bodies subjected to various ground motions.

6.2.1 Combined Model for Structure and Hanging NSC

In this study, for simplicity, the scaffolding is assumed to be on the ground and single storied. The mass is assumed to be lumped at the slab level. The hanging lead blankets are assumed and modeled as a simple pendulum. To simplify the proposed model, small displacements are assumed for the pendulum. Assuming that the primary structure remains in the linear range of response. From this analyses, it was concluded that the effect of a hanging secondary structure on the seismic response of a structure is significant. Hence this mass needs to be considered in the seismic analysis of a structure. Based on the trends and analysis results obtained, the following conclusions were drawn:

- The solution to the analytical model proposed in this study is validated with an existing study and a finite element model. Therefore, this model can predict the

structural response well for such a simple structure and serves as a basic model for further studies.

- As the length of the pendulum is decreased to a very small value, the structure behaves as an SDOF where the mass of the system acts together at all times. For very large lengths the hanging mass is seen not to participate in the vibration and hence not affecting the structure at all. This is in line with earlier studies and design codes. The peak structural response is seen to reduce when the frequency of the secondary mass was in the vicinity of primary structural frequency (similar to PTMDs).
- Under harmonic excitations, if the *mass effect ratio* $\epsilon > 1$, the effect of the pendulum on the structural response cannot be neglected and conversely this effect can be ignored if $\epsilon < 1$.
- An increase in mass ratio doesn't affect the response of the structure at lower tuning frequency ratios (larger lengths of pendulums) for both harmonic and earthquake excitations.
- The displacement response of a structure was observed to reduce significantly due to the presence of such secondary masses in hard soil conditions. On the contrary, for soft soil conditions, the reduction in response was least, with amplification at several peak acceleration points. The effect of the secondary body on the structure was constant in both the seismic Zones III and V for a given soil condition and vibrational properties of secondary mass.
- For a frequency ratio between 0.8 and 1.1, response of the structure was remarkably lower. A hanging mass shows a negligible effect on the structural response when the frequency ratio is less than 0.8 at lower mass ratios (μ). For higher frequency ratios like $\beta > 1.56$, the flexible secondary mass acts as a rigidly attached secondary

mass to the structure. For β between 1.1 and 1.56, the hanging mass shows a reduction in response at higher mass ratios but not as much as the case, when $0.8 \leq \beta \leq 1.1$. This behavior is in line with tuned mass dampers.

- Large values of mass ratio (μ) show a significant effect on the dynamic response of the structure, whether the secondary mass is tuned or un-tuned to the structural frequency.

Based on the above conclusions a design methodology for such structures was formulated.

The highlights of this design methodology and the effect of various parameters on the design are as follows:

- The seismic design of such a structure was found out to be independent of the response spectrum for a given damping level.
- If the value of *Design Acceleration Ratio (DAR)* is nearly one, it implies that there is no effect of the secondary body on the design of the primary structure.
- For a small tuning frequency ratios, the design was independent of the mass ratio (μ).
- For a smaller mass ratio ($\mu = 0.1$), the structural mass in the seismic design can be reduced by 6-17%. For a higher mass ratio ($\mu = 1$), it can be reduced by 30-40%.
- A design expression was developed which allows estimating the seismic response of the structure as a function of T_p , μ and L_s by Non-Linear Regression and Artificial Neural Networks. Neural Networks was proved to be a more effective and powerful tool for predicting the seismic response of the structure with a given secondary system when compared to the regression model.

The limitations of the proposed approach are as follows:

- This particular study is limited to a linear elastic SDOF primary structure. The design methodology proposed in this study can apply to a simple and light structure like a scaffolding structure, as discussed in the introduction section.
- The hanging NSC is modeled as a simple pendulum and limits to a smaller angular displacement.
- The design methodology can be a primary framework for the study of real-life behavior of more complicated structures.

6.2.2 Combined Model for Structure and Sliding NSCs

In this study, the primary structure is assumed to be a single story and linearly elastic. Static and kinetic coefficients of friction between the structure and secondary body are assumed as equal. But in reality, those values are slightly different. In the case of multiple side-by-side condition, sliding secondary bodies are far enough from each other and other obstructions to not cause impact collisions between them. Collisions between them induce forces on the secondary bodies, which are highly non-linear. In stacked bodies, two-level stack is considered with static and kinetic friction values to be the same at each surface. Sliding bodies are assumed as sufficiently squat so they can slide but do not show any rocking failure. The following section shows the conclusions drawn from the structure with side-by-side sliding NSCs and stacked NSCs under earthquake excitations. It also discusses the conclusions drawn from the damping effect of NSCs on the seismic behavior of the structure with such secondary masses.

6.2.2.1 Combined Model for Structure and Side-by-Side Sliding NSCs

- The seismic behavior of a structure is greatly affected by multiple live load objects under real earthquake excitations. Multiple bodies with the same coefficients of friction were shown to behave identical to a single body with their combined mass.

- The seismic behavior of a structure with multiple sliding rigid blocks was found to be different from its behavior with a single sliding rigid block. For a given set of mass ratios and coefficients of friction, the maximum displacement response of the structure was reduced by 25% and 11.36% compared to that of the structure with a single sliding rigid block in the seismic Zones III and V, respectively.
- The displacement response of the structure with multiple sliding rigid bodies was compared with that of the structure with rigidly fixed bodies and found that the reduction in displacement response was more in Zone V (31.4%) compared to Zone III (17.3%) for a given set of mass ratios and coefficients of friction.
- A dimensionless parameter called *Displacement Ratio (DR)* was defined to quantify the effect of the multiple sliding rigid bodies on the seismic response of the structure under earthquake excitations. Under medium seismic hazard level, sliding rigid blocks behave as rigidly attached bodies to the structure if the structural period $T_p > 1.25$ s regardless of the blocks-to-structure mass ratios and coefficients of friction.
- Sliding rigid blocks behave as a set of rigidly attached bodies to the structure if the structural period $T_p > 0.9$ s for higher coefficients of friction regardless of the mass ratios under the highest seismic hazard level.
- A novel methodology has been developed to determine the modified structural period (T_{new}) due to the interaction of secondary bodies. Under both medium and high seismic hazard levels, T_{new} increases significantly with the structural period, coefficients of friction, and mass ratios.
- Design expressions were developed to determine the T_{new} as a function of T_p , coefficients of friction and mass ratios by Artificial Neural Network (ANN) and Non-Linear Regression for both the seismic hazard levels.

6.2.2.2 Combined Model for Structure and Stacked Sliding NSCs

- The seismic response of a structure with a stack of live load objects was found to be different from the response of the same structure with a single sliding live load object with the same combined mass under real earthquake excitations.
- Displacement estimates of the structure were found out to be conservative by neglecting energy dissipation associated with the relative movement of rigid blocks in the stack. Energy dissipation within the stack depends upon the coefficients of friction, mass ratios, and levels of excitation.
- Energy dissipation associated with the relative movement between rigid blocks was more in the highest damage risk zone than the medium damage zone for a given problem.
- For both medium and highest damage risk zones, the displacement response of the structure increases significantly with an increase in the structural period, mass ratios, and coefficients of friction.
- If the surface between the structure and the bottom mass is smoother than the surface between the two bodies in the stack, the energy dissipation within the stack can be neglected regardless of other parameters.
- For structures with $T_p \geq 2$ s, sliding loads would completely stick to the structure regardless of the mass ratios and coefficients of friction under medium seismic hazard zone, except for a very small coefficient of friction between the stacked masses.
- For structures with $T_p \geq 1.25$ s, sliding loads would completely stick to the primary structure for: (i) structure-live load objects with $\mu_1 \geq 0.1, \mu_2 \geq 0.1$ under medium seismic hazard zone; (ii) structure-live load objects with $\mu_1 \geq 0.3, \mu_2 \geq 0.2$ under highest seismic hazard zone.

- A novel methodology was developed to determine the modified structural period (T_{new}) of the primary structure due to the interaction of a stack of sliding rigid blocks. T_{new} increases significantly with the structural period and coefficients of friction, especially for larger mass ratios.
- Design equations were developed to determine the T_{new} as a function of structural period, coefficients of friction, and mass ratios for a given seismic hazard level by Non-Linear Regression (NLR). Since, T_{new} generally, is less than T_{rigid} and more than T_p , the calculation of T_{new} is essential for the design of structures.

The limitations of the proposed approach are as follows:

- This particular study is limited to a linear elastic SDOF primary structure. The proposed design equations can be applied to a simple structure within the elastic range. For the real-life response, the proposed model can be modified by incorporating the yielding in the primary structure.
- The sliding NSCs are limited to squat blocks so that they show only sliding phenomena without any rocking failure.
- The multiple side-by-side sliding NSCs were considered with no collision between them. However, in reality, there might be a chance of collision of multiple blocks.
- The effect of the stack of sliding NSCs on the response of the structure is limited to a two-level stack. It should be noted that, the mathematical formulation is for a stack of n bodies.

6.2.2.3 Damping Effect of Sliding NSCs

The amount of seismic energy dissipation in the structure decides the damping associated with that structure. The sliding NSCs can reduce the seismic response of the structure by dissipating the seismic energy due to the slide effect. This energy dissipation due to the

slide effect adds an additional equivalent damping ratio to the structure. In this study, an attempt has been made to determine the additional damping ratio added to the structure by the sliding live load objects. Based on the trends of analysis results obtained, the following conclusions were drawn:

- The additional damping ratio of a structure due to the slide effect was reduced with an increase in the coefficient of friction irrespective of the mass ratio in both stiff and flexible structures.
- The additional damping ratio added to the structure due to slide effect was more for lower coefficients of friction and higher mass ratios for both stiff and flexible structures. For a flexible structure considered in this study, the additional damping ratio was negligible for $\mu \geq 0.3$. For a given coefficient of friction and mass ratio, the additional damping ratio was more in stiff structures compared to flexible structures.
- Additional damping ratio in the structure due to slide effect was observed to decrease with an increase in the damping ratio of the structure for both the stiff and flexible structures for a given mass ratio and coefficient of friction.
- The additional damping ratio in the structure due to slide effect was more in the case of stacked sliding rigid bodies compared to that of the single sliding rigid body if $\mu_2 < \mu_1$. The energy dissipation in the structure is approximately the same when the $\mu_2 > \mu_1$ and hence nearly the same additional damping ratio was obtained.

6.3 Further Scope of Work

6.3.1 Combined Model for Structure and Hanging NSC

- Further study could investigate the seismic behavior of the structure when the non-linearity of the hanging mass is taken into consideration if it experiences large displacements.
- The proposed design methodology is a step in the direction of developing more generalized design equations for actual complex structures.
- Complex pendulums and their effect on the structure they are attached to is a very complex and interesting problem that can be looked at.

6.3.2 Combined Model for Structure and Multiple Sliding NSCs

- Further studies can include the non-linearity due to yielding of the structure in the developed numerical model.
- More generalized conclusions can be drawn by looking at the actual complex multi-story structures behavior with multiple sliding loads (side-by-side and stacks) at various story levels.
- The present study can be a preliminary study for future studies in this aspect, and the design equations can be modified for multi-story structures whose seismic behavior is affected by the higher modes.

References

- Abdel Raheem, S. E. (2016). "Exploring damping characteristics of composite tower of cable-stayed bridges." *Sadhana - Academy Proceedings in Engineering Sciences*, 41(3), 345–358.
- Amin, M., Hall, W. J., Newmark, N. M., and Kassawara, R. P. (1971). "Earthquake response of multiply connected light secondary systems by spectrum methods." *Proceedings of the 1st National Congress on Pressure Vessels and Piping, American Society of Mechanical Engineers, New York, NY*, 103–129.
- Ardila-Giraldo, O. A., Reyes, J. C., and Smith-Pardo, J. P. (2013). "Contact interface modeling in the dynamic response of rigid blocks subjected to base excitation." *ECCOMAS Thematic Conference - COMPDYN 2013: 4th International Conference on Computational Methods in Structural Dynamics and Earthquake Engineering, Proceedings - An IACM Special Interest Conference*, (June), 3060–3071.
- ASCE. (2016). "Minimum design loads and associated criteria for buildings and other structures (ASCE/SEI 7–16)." American Society of Civil Engineers (ASCE) Reston, VA.
- Aslam, M., Godden, W. G., and Scalise, D. T. (1975). "Sliding Response Of Rigid Bodies to Earthquake Motions." 151.
- Belleri, A., Labò, S., Marini, A., and Riva, P. (2017). "The Influence of Overhead Cranes in the Seismic Performance of Industrial Buildings." *Frontiers in Built Environment*, 3(November), 1–12.
- Biggs, J. M., and Rosset, J. M. (1970). "Seismic analysis of equipment mounted on a massive structure, Seismic Design for Nuclear Power Plants." *Seismic Design for Nuclear Power Plants, RJ Hansen, ed., Cambridge, Mass.*
- Briki, L., and Lahbari, N. (2018). "New plasticity model using artificial neural networks." *International Journal of Structural Engineering*, 9(3), 258–271.
- Center, P. (2013). "PEER ground motion database." *Pacific Earthquake Engineering Research Center, University of California, Berkeley, CA*, <http://ngawest2.berkeley.edu>.
- Challagulla, S. P., Parimi, C., Mohan, S. C., and Farsangi, E. N. (2020). "Seismic Response of Building Structures with Sliding Non-structural Elements." 33(2), 205–212.
- Chandel, V. S., and Yamini Sreevalli, I. (2019). "Numerical study on influence of masonry infill in an RC frame." *Asian Journal of Civil Engineering*, Springer International Publishing, 20(1).
- Chandrasekaran, A. R., and Saini, S. S. (1969). "Live load effect on dynamic response of structures." *Journal of the Structural Division*.
- Chang, K. C., Lai, M. L., Soong, T. T., Hao, D. S., and Yeh, Y. C. (1993). "Seismic behavior and design guidelines for steel frame structures with added viscoelastic dampers, NCEER 93–0009." *National Center for Earthquake Engineering Research, Buffalo, NY*.
- Chaudhuri, S. R., and Hutchinson, T. C. (2005). "Characterizing frictional behavior for use in predicting the seismic response of unattached equipment." *Soil dynamics and earthquake engineering*, Elsevier, 25(7–10), 591–604.
- Chen, Y., and Soong, T. T. (1988). "State-of-the-art review Seismic response of secondary systems." *October*, 10, 218–228.
- Choi, B., and Tung, C. C. D. (2002). "Estimating sliding displacement of an unanchored body subjected to earthquake excitation." *Earthquake Spectra*, 18(4), 601–613.
- Chopra, A. K. (2011). "Dynamics of Structures: Theory and Applications to Earthquake

- Engineering 4th edition Prentice Hall Englewood Cliffs.” NJ.
- Chulahwat, A. (2013). “Structural systems with suspended and self-centered floor slabs for earthquake resistance.” Colorado State University. Libraries.
- Code, I. S. (2002). “IS 1893 (part 1), criteria for earthquake resistant design of structures.” *Bureau of Indian Standards, New Delhi, India.*
- Commission, N. R. (1976). *Development of floor design response spectra for seismic design of floor-supported equipment or components.* Nuclear Regulatory Commission.
- Committee, A. (2010). “Minimum Design Loads for Buildings and Other Structures (ASCE/SEI 7-10).” *Structural Engineering Institute, American Society of Civil Engineering, Reston, Virginia.*
- Dassault Systèmes, D. S. (2016). *Abaqus analysis user’s guide.* Technical Report Abaqus 6.14 Documentation, Simulia Corp.
- Debnath, S., and Sultana, P. (2019). “Prediction of Settlement of Shallow Foundation on Cohesionless Soil Using Prediction of Settlement of Shallow Foundation on Cohesionless Soil Using Artificial Neural Network.” (March).
- Demosthenous, M., and Manos, G. C. (n.d.). “The dynamic sliding response of drums composing free-standing rigid bodies.” 49, 67–77.
- Dhakal, R. P. (2010). “Damage to non-structural components and contents in 2010 darfield earthquake.” *Bulletin of the New Zealand Society for Earthquake Engineering*, 43(4), 404–411.
- Diotalleivi, P. P., Landi, L., and Dellavalle, A. (2012). “A methodology for the direct assessment of the damping ratio of structures equipped with nonlinear viscous dampers.” *Journal of Earthquake Engineering*, 16(3), 350–373.
- Dolšek, M., and Fajfar, P. (2008). “The effect of masonry infills on the seismic response of a four-storey reinforced concrete frame—a deterministic assessment.” *Engineering Structures*, Elsevier, 30(7), 1991–2001.
- De Domenico, D., and Ricciardi, G. (2019). “Dynamic response of non-classically damped structures via reduced-order complex modal analysis: Two novel truncation measures.” *Journal of Sound and Vibration*, Elsevier Ltd, 452, 169–190.
- Earth Mechanics Inc. (2006). “Port-Wide Ground Motion Study Port of Long Beach , California.” *EMI Project No. 01-143*, (01).
- Etedali, S., Hasankhoie, K., and Sohrabi, M. R. (2020). “Seismic responses and energy dissipation of pure-friction and resilient-friction base-isolated structures: A parametric study.” *Journal of Building Engineering*, 29(November 2019).
- Filiatrault, A., Perrone, D., Merino, R. J., and Calvi, G. M. (2018). “Performance-Based Seismic Design of Nonstructural Building Elements.” *Journal of Earthquake Engineering*, Taylor & Francis, 00(00), 1–33.
- Furuta, K., Ito, T., and Shintani, A. (2008). “Rocking and Sliding Motions of a Freely Standing Structure Coupled with Inner Structure.” *ASME 2008 Pressure Vessels and Piping Conference*, American Society of Mechanical Engineers, 97–103.
- Ghaedi, K., Ibrahim, Z., Adeli, H., and Javanmardi, A. (2017). “Invited review: Recent developments in vibration control of building and bridge structures.” *Journal of Vibroengineering*, 19(5), 3564–3580.
- Ghanbari, E., and Ghanbari, A. (2016). “A new criterion for considering soil-structure interaction on analysis of moment frames.” *International Journal of Structural Engineering*, 7(1), 31–47.
- Goh, A. T. C., Kulhawy, F. H., and Chua, C. G. (2005). “Bayesian neural network analysis of undrained side resistance of drilled shafts.” *Journal of Geotechnical and Geoenvironmental Engineering*, American Society of Civil Engineers, 131(1), 84–93.

- Gupta, A., and Bose, M. K. (2017). "Significance of non-classical damping in seismic qualification of equipment and piping." *Nuclear Engineering and Design*, Elsevier B.V., 317, 90–99.
- Hecht-Nielsen, R. (1992). "Theory of the backpropagation neural network." *Neural networks for perception*, Elsevier, 65–93.
- Hu, X., Chen, Q., Weng, D., Zhang, R., and Ren, X. (2019). "Estimation of Additional Equivalent Damping Ratio of the Damped Structure Based on Energy Dissipation." 2019.
- Huang, C., Huo, L., Gao, H., and Li, H. (2018). "Control performance of suspended mass pendulum with the consideration of out-of-plane vibrations." *Structural Control and Health Monitoring*, Wiley Online Library, 25(9), e2217.
- Igusa, T., and Kiureghian, A. Der. (1985). "Generation of floor response spectra including oscillator-structure interaction." *Earthquake Engineering & Structural Dynamics*, 13(5), 661–676.
- Ito, T., Furuta, K., and Shintani, A. (2018). "PVP2008-61086."
- Iwasaki, A., Nekomoto, Y., Morita, H., Taniguchi, K., Okuno, D., Matsuoka, T., and Chigusa, N. (2012). "Experimental study on free standing rack loading full fuel assembly." 8, 251–259.
- Kafali, C. (2006). "Estimation of Kinetic Friction Coefficient for Sliding Rigid Block Nonstructural Components." *Student Research Accomplishments*, 43.
- Kaneko, M., Tamura, K., and Hayashi, Y. (1999). "Evaluation of sliding displacement of furniture during earthquake." *AIJ Journal of Technology and Design*, 8, 73–78.
- Kehoe, B. E. (2014). "Defining rigid vs. Flexible nonstructural components." *NCEE 2014 - 10th U.S. National Conference on Earthquake Engineering: Frontiers of Earthquake Engineering*.
- Kelly, J. M., and Sackman, J. L. (1978). "Response spectra design methods for tuned equipment-structure systems." *Journal of Sound and Vibration*, 59(2), 171–179.
- Konstantinidis, D., and Makris, N. (2010). "Experimental and analytical studies on the response of 1/4-scale models of freestanding laboratory equipment subjected to strong earthquake shaking." *Bulletin of Earthquake Engineering*, 8(6), 1457–1477.
- Konstantinidis, D., and Nikfar, F. (2015). "Seismic response of sliding equipment and contents in base-isolated buildings subjected to broadband ground motions." *Earthquake Engineering & Structural Dynamics*, Wiley Online Library, 44(6), 865–887.
- Larson, B. D. S., and Fafitis, A. (1995). "Friction-damped sdof oscillator." 1226–1233.
- Lee, S., Min, K., Hwang, J., and Kim, J. (2004). "Evaluation of equivalent damping ratio of a structure with added dampers." 26, 335–346.
- Li, B., Duffield, C. F., and Hutchinson, G. L. (2009). "The influence of non-structural components on the serviceability performance of high-rise buildings." *Australian journal of structural Engineering*, Taylor & Francis, 10(1), 53–62.
- Li, B., Hutchinson, G. L., and Duffi, C. F. (2011). "The influence of non-structural components on tall building stiffness." 870(November 2009), 853–870.
- Li, B., Hutchinson, G. L., and Duffield, C. F. (2010). "Contribution of typical non-structural components to the performance of high-rise buildings based on field reconnaissance." *Journal of Building Appraisal*, 6(2), 129–151.
- Lim, E., and Chouw, N. (2014). "Effects of ground motion characteristics on structural response with primary- secondary structure interaction." (April 2015).
- Lim, E., and Chouw, N. (2015). "Review of Approaches for Analysing Secondary Structures in Earthquakes and Evaluation of Floor Response Spectrum Approach." *International Journal of Protective Structures*, 6(2), 237–257.

- Lim, E., and Chouw, N. (2018). "Prediction of the response of secondary structures under dynamic loading considering primary–secondary structure interaction." *Advances in Structural Engineering*, 21(14), 2143–2153.
- Lin, S. L., MacRae, G. A., Dhakal, R. P., and Yeow, T. Z. (2013). "Building contents sliding during earthquakes." *NZSEE Conference, Wellington, NZ*.
- Lin, S. L., MacRae, G. A., Dhakal, R. P., and Yeow, T. Z. (2015). "Building contents sliding demands in elastically responding structures." *Engineering Structures*, Elsevier Ltd, 86, 182–191.
- Lopez Garcia, D., and Soong, T. T. (2003). "Sliding fragility of block-type non-structural components. Part 1: Unrestrained components." *Earthquake Engineering and Structural Dynamics*, 32(1), 111–129.
- Lu, Z., Huang, B., Wang, Z., and Zhou, Y. (2018). "Experimental Comparison of Dynamic Behavior of Structures with a Particle Damper and a Tuned Mass Damper." *Journal of Structural Engineering*, 144(12), 04018211.
- Magliulo, G., Pentangelo, V., Maddaloni, G., Capozzi, V., Petrone, C., Lopez, P., Talamonti, R., and Manfredi, G. (2012). "Shake table tests for seismic assessment of suspended continuous ceilings." *Bulletin of Earthquake Engineering*, 10(6), 1819–1832.
- Martinelli, E., and Faella, C. (2012). "A simplified approach for evaluating seismic-induced actions on non-structural components in buildings." *15th World Conference on Earthquake Engineering*.
- Matsui, K., Iura, M., Sasaki, T., and Kosaka, I. (1991). "Periodic response of a rigid block resting on a footing subjected to harmonic excitation." *Earthquake Engineering & Structural Dynamics*, 20(7), 683–697.
- Matta, E., and De Stefano, A. (2015). "Model calibration in the presence of resonant non-structural elements." *Journal of Civil Structural Health Monitoring*, 5(1), 37–55.
- Medina, R. A., Sankaranarayanan, R., and Kingston, K. M. (2006). "Floor response spectra for light components mounted on regular moment-resisting frame structures." *Engineering Structures*, 28(14), 1927–1940.
- Meersschaert, B., and Chouw, E. L. N. (n.d.). "Influence of multi-directional excitations on the interacting forces at the primary-secondary structure interface."
- Miranda, E., Kazantzi, A., and Vamvatsikos, D. (2018). "New approach to the design of acceleration-sensitive non-structural elements in buildings." *16th European conference on earthquake engineering*, (December), 1–12.
- Mohammadi, M. (2017). "Seismic Behavior of Sliding Base Isolation Systems, Regarding Restitution Factor and Variable Friction Coefficient." *International Journal of Civil Engineering*, Springer International Publishing, 15(2), 287–298.
- Mohammadi, M., Kianian, M., and Kashani, M. (2011). "Sliding Base Isolation Systems , Effects of Vertical Excitation and Restitution Coefficient." *Advances in Structural Engineering*, (September 2011), 18–22.
- Morfidis, K., and Kostinakis, K. (2016). "The role of masonry infills on the damage response of R/C buildings subjected to seismic sequences." *Engineering Structures*, Elsevier Ltd.
- Mostaghel, N., and Tanbakuchi, J. (1983). "Response of sliding structures to earthquake support motion." *Earthquake Engineering & Structural Dynamics*, 11(6), 729–748.
- Murty, C. V. R., Goswami, R., Vijayanarayanan, A. R., Kumar, R. P., and Mehta, V. V. (2012). "Earthquake Protection of Non-Structural Elements in Buildings."
- Myrtle, R. C., Masri, S. F., Eeri, M., and Nigbor, R. L. (2005). "Classification and Prioritization of Essential Systems in Hospitals under Extreme Events." 21(3), 779–802.

- Newmark, N. M. (1965). "Effects of earthquakes on dams and embankments." *Geotechnique*, 15(2), 139–160.
- Nikfar, F., and Konstantinidis, D. (2013). "Sliding response analysis of operational and functional components (OFC) in seismically isolated buildings." *Proceedings, Annual Conference - Canadian Society for Civil Engineering*, 2(January), 1502–1511.
- Nikfar, F., and Konstantinidis, D. (2017). "Peak Sliding Demands on Unanchored Equipment and Contents in Base-Isolated Buildings under Pulse Excitation." *Journal of Structural Engineering (United States)*, 143(9), 1–15.
- Okada, T., and Takanashi, K. (1992). "The resonance responses of steel structure with sliding floor loads." *Proc. 10th World Conf. on Earthquake Engineering, Madrid*, 4419–4422.
- Palermo, Alessandro. (2012). "Experimental and numerical validation of seismic interaction between cladding systems and moment resisting frames." *15th World Conference on Earthquake Engineering (15WCEE)*, (February 2011).
- Paper, C., Bazzurro, P., Universitario, I., and Superiore, S. (2006). "Effects of masonry walls on the seismic risk of reinforced concrete frame." (April 2016).
- Pardalopoulos, S. I., and Pantazopoulou, S. J. (2015). "Seismic response of nonstructural components attached on multistorey buildings." *Earthquake Engineering and Structural Dynamics*, 44(1), 139–158.
- Park, J. H. (2013). "Seismic response of SDOF systems representing masonry-infilled RC frames with damping systems." *Engineering Structures*, Elsevier Ltd, 56, 1735–1750.
- Pekelnicky, R., Engineers, S. E. D., Chris Poland, S. E., and Engineers, N. A. E. D. (2012). "ASCE 41-13: Seismic Evaluation and Retrofit Rehabilitation of Existing Buildings." *Proceedings of the SEAOC*.
- Peng, L.-Y., Kang, Y.-J., Lai, Z.-R., and Deng, Y.-K. (2018). "Optimization and Damping Performance of a Coal-Fired Power Plant Building Equipped with Multiple Coal Bucket Dampers." *Advances in Civil Engineering*, Hindawi, 2018.
- Perrone, D. (2012). "Seismic Demand on Non-Structural Elements : Influence of Masonry Infills on Floor Response Spectra." 1–12.
- Pokhrel, A., Gautam, D., and Chaulagain, H. (2019). "Effect of variation on infill masonry walls in the seismic performance of soft story RC building." *Australian Journal of Structural Engineering*, Taylor & Francis, 20(1), 1–9.
- Qin, Q., and Lou, L. (2000). "Effects of non proportional damping on the seismic responses of suspension bridges." *12th world conference of earthquake engineering*.
- Raheem, S. E. A. (2014). "Analytical and numerical algorithm for exploring dynamic response of non-classically damped hybrid structures." *Coupled systems mechanics*, 3(2), 171–193.
- Ramirez, O. M., Constantinou, M. C., Whittaker, A. S., Kircher, C. A., Johnson, M. W., and Chrysostomou, C. Z. (2003). "Validation of the 2000 NEHRP Provisions' Equivalent Lateral Force and Modal Analysis Procedures for Buildings with Damping Systems." *Earthquake Spectra*, 19(4), 981–999.
- Reyes, J. C., Ardila-Bothia, L., Smith-Pardo, J. P., Villamizar-Gonzalez, J. N., and Ardila-Giraldo, O. A. (2016). "Evaluation of the effect of containers on the seismic response of pile-supported storage structures." *Engineering Structures*, Elsevier Ltd, 122, 267–278.
- Reyes, J. C., Marcillo-Delgado, E., Smith-Pardo, J. P., and Ardila-Giraldo, O. A. (2018). "Assessment of the Effective Seismic Mass for Low-Rise Framed Shear Buildings Supporting Nearly Permanent Live Loads." *Journal of Structural Engineering*, 144(8), 04018098.
- Ryu, Y., Jung, W., and Ju, B. (2016). "Vibration Effects of Nonclassically Damped

- Building-Piping Systems Subjected to Extreme Loads.” *Shock and Vibration*, 2016.
- Sackman, J. L., and Kelly, J. M. (1979). “Seismic analysis of internal equipment and components in structures.” *Engineering Structures*, 1(4), 179–190.
- Sadek, F., Mohraz, B., and Riley, M. A. (2000). “Linear procedures for structures with velocity-dependent dampers.” *Journal of Structural Engineering*, American Society of Civil Engineers, 126(8), 887–895.
- Salman, K., Tran, T. T., and Kim, D. (2019). “Grouping effect on the seismic response of cabinet facility considering primary-secondary structure interaction.” *Nuclear Engineering and Technology*, Elsevier Ltd.
- Saraswat, A., Reddy, G. R., Ghosh, A. K., and Ghosh, S. (2016). “Effects of base excitation frequency on the stability of a freestanding rigid block.” *Acta Mechanica*, 227(3), 795–812.
- Saudy, A., Aziz, T., and Ghobarah, A. (1994). “A new stochastic analysis for multiple supported MDOF secondary systems: I. Dynamic interaction effects.” *Nuclear Engineering and Design*, 147(3), 235–249.
- Shahin, M. A., Jaksa, M. B., and Maier, H. R. (2002a). “Artificial neural network-based settlement prediction formula for shallow foundations on granular soils.” *Australian Geomechanics Journal*, 37(4), 45–52.
- Shahin, M. A., Jaksa, M. B., and Maier, H. R. (2002b). “Artificial neural network based settlement prediction formula for shallow foundations on granular soils.” *Australian Geomechanics: Journal and News of the Australian Geomechanics Society*, Published for the Australian Geomechanics Society by the Institution of ..., 37(4), 45.
- Shao, Y., and Tung, C. C. (1999). “Seismic response of unanchored bodies.” *Earthquake Spectra*, SAGE Publications Sage UK: London, England, 15(3), 523–536.
- Shenton, H. W. (1996). “Criteria for initiation of slide, rock, and slide-rock rigid-body modes By Harry W. Shenton 111, 1 Associate Member, ASCE.” *Asce*, 122(7), 690–693.
- Shie, R. F., Ting, K., Yu, J. S., and Liu, C. T. (2007). “The Sliding and Overturning Analysis of a Free-Standing Cask under Earthquake.” *Solid State Phenomena*, 120, 207–212.
- Shu, Z., Li, S., Zhang, J., and He, M. (2017). “Optimum seismic design of a power plant building with pendulum tuned mass damper system by its heavy suspended buckets.” *Engineering Structures*, Elsevier Ltd, 136, 114–132.
- Sideris, P., Asce, A. M., Filiatrault, A., and Asce, M. (2014). “Seismic Response of Squat Rigid Bodies on Inclined Planes with Rigid Boundaries.” (January), 149–158.
- Singh, B. M. P., Asce, M., Sharma, A. M., and Asce, A. M. (1986). “Seismic Floor Spectra By M O D E.” I(11), 1402–1419.
- Singh, M. P., and Suarez, L. E. (1987). “Seismic response analysis of structure–equipment systems with non-classical damping effects.” *Earthquake Engineering & Structural Dynamics*, 15(7), 871–888.
- Smith-Pardo, J. P., Reyes, J. C., Ardila-Bothia, L., Villamizar-Gonzalez, J. N., and Ardila-Giraldo, O. A. (2015). “Effect of live load on the seismic design of single-story storage structures under unidirectional horizontal ground motions.” *Engineering Structures*, Elsevier Ltd, 93, 50–60.
- Smith-Pardo, J. P., Reyes, J. C., Ardila-Giraldo, O. A., Ardila-Bothia, L., and Villamizar-Gonzalez, J. N. (2014). “Dynamic effect of sliding rigid blocks on the seismic response of structures.” *Second European Conference on Earthquake Engineering and Seismology, Istanbul*, 25–29.
- Smith, G. N. (1986). “Probability and statistics in civil engineering.” *Collins professional and technical books*, 244.

- Sofi, M., Lumantarna, E., Duffield, C., and Mendis, P. (2017). "Effects of interior partition walls on natural period of high rise buildings." *International Journal of Structural Stability and Dynamics*, 17(6), 1–11.
- Surana, M., Singh, Y., and Lang, D. H. (2019). "Damping Modification Factors Observed from the Indian Strong-motion Database." *Journal of Earthquake Engineering*, Taylor & Francis, 00(00), 1–16.
- Swain, S. S., Patro, S. K., and Sinha, R. (2016). "Numerical methodology for dynamic analysis of buildings with friction dampers." *Bulletin of the New Zealand Society for Earthquake Engineering*, 49(3), 245–266.
- Taghavi, S., and Miranda, E. (2004). "Estimation of Seismic Acceleration Demands in Building Components." *13th World Conference on Earthquake Engineering Vancouver, B.C., Canada*, (3199), 3199.
- Taghavi, S., and Miranda, E. (2008). "Effect of interaction between primary and secondary systems on floor response spectra." *14th World Conference on Earthquake Engineering*, 12–17.
- Taniguchi, T. (2002). "Non-linear response analyses of rectangular rigid bodies subjected to horizontal and vertical ground motion." *Earthquake Engineering and Structural Dynamics*, 31(8), 1481–1500.
- Taniguchi, T., and Miwa, T. (2007). "A simple procedure to approximate slip displacement of freestanding rigid body subjected to earthquake motions." *Earthquake engineering & structural dynamics*, Wiley Online Library, 36(4), 481–501.
- Tian, L., Li, W. F., and Wang, Z. L. (2012). "Study on Suspended Mass Pendulums for Vibration Control of Transmission Tower under Seismic Excitation." *Advanced Materials Research*, 446–449, 3323–3327.
- Uva, G., Porco, F., and Fiore, A. (2012). "Appraisal of masonry infill walls effect in the seismic response of RC framed buildings: A case study." *Engineering Structures*, Elsevier Ltd, 34, 514–526.
- Vafai, A., Hamidi, M., and Ahmadi, G. (2001). "Numerical modeling of MDOF structures with sliding supports using rigid-plastic link." *Earthquake Engineering and Structural Dynamics*, 30(1), 27–42.
- Villaverde, R. (1991). "Approximate formulas to calculate the seismic response of light attachments to buildings." *Nuclear Engineering and Design*, 128(3), 349–368.
- Villaverde, R. (1997a). "Seismic design of secondary structures: state of the art." *Journal of structural engineering*, American Society of Civil Engineers, 123(8), 1011–1019.
- Villaverde, R. (1997b). "Method to improve seismic provisions for nonstructural components in buildings." *Journal of Structural Engineering*, 123(4), 432–439.
- Wang, B. S., Ni, Y. Q., and Ko, J. M. (2011). "Damage detection utilising the artificial neural network methods to a benchmark structure." *International Journal of Structural Engineering*, 2(3), 229–242.
- Wang, X., and Liu, H. (2008). "Analysis of seismic response and catastrophic behavior on suspended structure systems." *14th World Conference on Earthquake Engineering*.
- Wang, X., Liu, H., and Ou, J. (2009). "Analysis of seismic response and catastrophic behavior of suspended structure systems." *Journal of Earthquake Engineering and Engineering Vibration*, 29(3), 121–125.
- Wei, W., Dai, A., Pi, Y.-L., and Bradford, M. A. (2016). "Investigations on the Seismic Responses of Structures with a Suspended Mass." *International Journal of Structural Stability and Dynamics*, 16(02), 1550066.
- Welch, D. P., Sullivan, T. J., and Filiatrault, A. (2014). "Equivalent structural damping of drift-sensitive nonstructural building components." *NCEE 2014 - 10th U.S. National Conference on Earthquake Engineering: Frontiers of Earthquake Engineering*, (May

- 2015).
- Westermo, B., and Udwadia, F. (1983). "Periodic response of a sliding oscillator system to harmonic excitation." *Earthquake Engineering & Structural Dynamics*, 11(1), 135–146.
- Whittaker, A., and Soong, T. (2003). "An overview of non-structural components research at three US earthquake engineering research centers." *ATC Seminar on Seismic Design, Performance, and Retrofit of Nonstructural Components in Critical Facilities*, (OCTOBER 2003), 271–280.
- Xiaohang, G. A. O. (1989). "Earthquake responses of structures with sliding floor loads." *Bulletin of Earthquake Resistant Structure Research Center*, University of Tokyo, (22).
- Yao, G. C. (2000). "Seismic performance of direct hung suspended ceiling systems." *Journal of architectural engineering*, American Society of Civil Engineers, 6(1), 6–11.
- Yeow, T. Z., MacRae, G. A., and Dhakal, R. P. (2015). "Incorporating content sliding into seismic building performance assessments." *NZSEE Conference*.
- Yeow, T. Z., MacRae, G. A., Dhakal, R. P., and Bradley, B. A. (2014). "Experimental studies on the sliding behavior of building contents." *NCEE 2014 - 10th U.S. National Conference on Earthquake Engineering: Frontiers of Earthquake Engineering*, (March 2016).
- Younis, C., and Tadjbakhsh, I. (1984). "Response of sliding rigid structure to base excitation." *Journal of engineering mechanics*, 110(3), 417–432.
- Yucel, M., Bekdaş, G., Nigdeli, S. M., and Sevgen, S. (2019). "Estimation of optimum tuned mass damper parameters via machine learning." *Journal of Building Engineering*, Elsevier Ltd, 26(July), 100847.
- Zhai, C. H., Zheng, Z., Li, S., Pan, X., and Xie, L. L. (2016). "Seismic response of nonstructural components considering the near-fault pulse-like ground motions." *Earthquake and Structures*, 10(5), 1213–1232.
- Zhang, M., Jiang, R., and Nie, H. (2017). "A numerical study on the friction and wear predictions of finger lock chuck in landing gear." *Proceedings of the Institution of Mechanical Engineers, Part G: Journal of Aerospace Engineering*, 231(1), 109–123.

Appendices

Appendix 1: Summary of Design Methodology

Structure with a Hanging Mass

To design a structure with a hanging mass, a design equation was developed to determine the spectral acceleration of a structure as a function of the structural period (T_p), length of the attachment of hanging mass (L_s), and mass ratio (μ_{SS}) in the form of *Design Acceleration Ratio (DAR)*. Artificial Neural Network (ANN) produced the following design equation:

$$\text{Design Acceleration ratio, DAR (Normalized)} = \tanh(x) \quad (\text{A-1})$$

$$DAR = 0.1985 * \tanh(x) + 0.8015 \quad (\text{A-2})$$

Where,

$$x = 2.198 * \tanh(a) + 1.686 * \tanh(b) - 1.667 * \tanh(c) + 1.284 * \tanh(d) + 1.725 * \tanh(e) - 8.766 * \tanh(f) + 9.726 \quad (\text{A-3})$$

$$a = -0.18646 * \mu_{SS} - 10.7564 * T_p + 0.28478 * L_s - 8.0831 \quad (\text{A-4})$$

$$b = 0.02614 * \mu_{SS} - 11.2887 * T_p - 14.24345 * L_s + 11.7805 \quad (\text{A-5})$$

$$c = -0.06059 * \mu_{SS} + 19.75239 * T_p - 27.8321 * L_s + 7.8449 \quad (\text{A-6})$$

$$d = 0.659397 * \mu_{SS} + 4.938094 * T_p + 0.03036 * L_s - 4.5174 \quad (\text{A-7})$$

$$e = 0.01072 * \mu_{SS} + 54.37749 * T_p - 13.0071 * L_s + 27.6945 \quad (\text{A-8})$$

$$f = 0.456921 * \mu_{SS} - 0.01439 * T_p - 0.005621 * L_s + 1.5647 \quad (\text{A-9})$$

For given T_p , L_s , and μ_{SS} , *DAR* can be obtained from the above equation (Eq. (A-2)) and the modified spectral acceleration ($S_{a(modified)}$) of the structure can be obtained from the Eq. (A-10).

$$S_a (modified) = DAR * S_a (original) \quad (A-10)$$

Example design problem

A simple example calculation has been provided to explain the process of Design Acceleration Ratio (*DAR*) calculation using the developed equations. A simple one-story primary structure with a flexible secondary system (as shown in Fig. 3.4) is to be designed for the Zone III and V hard soil design spectra shown in Fig. 3.23. The structural period (T_p) of the primary structure is chosen as 0.5 sec. The mass ratio (μ_{SS}) of a secondary system is chosen as 0.5. The effective length of the attachment (L_s) is taken as 0.5 m. Predict the spectral acceleration of the PS with an FSS using ANN and NLR based design equations.

Solution:

Given data: $T_p = 0.5$ sec; $\mu_{SS} = 0.5$; $L_s = 0.5$ m and the design spectra.

Spectral acceleration by ANN:

- Step 1: Normalize the given input parameters in the range of [-1, 1] using Eq. 3.24 and limits of the input parameters given in Table 3.12.
- Step 2: Substitute the normalized data into Eqs. (A-4)-(A-9) and solve for a , b , c , d , e and f .
- Step 3: Calculate the value of x from Eq. (A-3) using the values of a , b , c , d , e and f obtained in Step 2.
- Step 4: Now, calculate the normalized *DAR* from Eq. (A-1) by substituting the value of x obtained in Step 3.
- Step 5: Calculate the de-normalized value of *DAR* from obtained normalized value (Step 4) from Eq. (A-2).

Thus, *Design Acceleration Ratio (DAR)* calculated by ANN is 0.71. By using the obtained *DAR* value, the spectral acceleration of the PS with FSS can be calculated by using Eq. (A-10).

Structure with Multiple Sliding Bodies

The modified structural period (T_{new}) of the primary structure with multiple sliding bodies was determined for the two Indian seismic hazard levels consistent with the medium (Zone III) and highest (Zone V) conditions. The multiple sliding bodies can be side-by-side resting and one over the other in the form of stacks.

Side-by-Side resting sliding bodies:

For Medium Seismic Hazard Zone:

$$T_{new} = \left((-3.613 * T_p) - (0.876s * \mu_1) + (0.041s * \mu_2) - (4.241s * \alpha_1) - (4.188s * \alpha_2) \right) + 0.782s * e^{\left(\frac{(0.053}{s} * T_p) + (0.014 * \mu_1) + (0.002 * \mu_2) + (0.053 * \alpha_1) + (0.052 * \alpha_2) + 4.588 \right)} - 76.889s \quad (A-11)$$

For Highest Seismic Hazard Zone:

$$T_{new} = \left((-6.388 * T_p) - (7.589s * \mu_1) - (5.236s * \mu_2) - (5.965s * \alpha_1) - (5.309s * \alpha_2) \right) + 6.365s * e^{\left(\frac{(0.0443}{s} * T_p) + (0.047 * \mu_1) + (0.033 * \mu_2) + (0.036 * \alpha_1) + (0.032 * \alpha_2) + 3.21 \right)} - 157.67s \quad (A-12)$$

Where, μ_1 and μ_2 are the coefficients of friction at the sliding bodies-structure interface, α_1 and α_2 are the mass ratios of the sliding bodies.

Design Problem

An example design calculation has been shown using the equations A-11 and A-12. A single degree of freedom system (SDOF) as a primary structure (PS) supports sliding secondary blocks (SBs), as shown in Fig. 40. The original structural period and mass of the

PS are chosen as 0.7 s and 200 kg, respectively. The coefficient of friction between PS and SB₁ is assumed as 0.4. The frictional coefficient between PS and SB₂ is taken as 0.2. The mass ratios of SBs (α_1 and α_2) are chosen as 1 and 0.4, respectively. Ground excitations are applied to the PS with SBs that are spectrum compatible with Zone III, and Zone V hard soil IS 1893:2016 spectrum. Assuming that there is no collision between the SBs. Predict the modified structural period of the PS with sliding SBs.

Solution:

Given data: $m_p = 200$ kg; $T_p = 0.7$ sec; $\mu_1 = 0.4$; $\mu_2 = 0.2$; $\alpha_1 = 1$; $\alpha_2 = 0.4$

The values of the new structural period of the PS (T_{new}) obtained from Eq. (A-11) and Eq. (A-12) for Seismic zones, III and V are 1.02 sec and 0.86 sec, respectively. The design spectral accelerations of the PS without SBs in Zones III and V for a given T_p can be obtained from Fig. 4.3 and are 0.22g and 0.52g, respectively. Due to the interaction of SBs, the structural period increases to 1.02 sec and 0.86 sec in Zones III and V, respectively. Thus, the design spectral accelerations of the PS corresponds to T_{new} in medium, and the highest seismic hazard levels are 0.159g and 0.44g, respectively. Therefore, the effective mass of the system is 424.65 kg in Zone III and 301.87 kg in Zone V. These parameters should be used in the seismic analysis/design of the PS in the respective zone.

Stacked sliding bodies:

For Medium seismic hazard zone:

$$T_{new} = \left((-4.284 * T_p) - (0.173s * \mu_1) + (0.015s * \mu_2) - (4.365s * \alpha_1) - (4.567s * \alpha_2) \right) + 2.022s * e^{\left(\left(\frac{0.053}{s} * T_p \right) + (0.003 * \mu_1) + (0.002 * \mu_2) \right) + (0.044 * \alpha_1) + (0.045 * \alpha_2) + 3.873 } - 97.3s \quad (A-13)$$

For Highest seismic hazard zone:

$$T_{new} = \left((-5.464 * T_p) - (2.268s * \mu_1) - (4.451s * \mu_2) - (5.064s * \alpha_1) - (4.693s * \alpha_2) \right) + 2.197s * e^{\left(\frac{0.052}{s} * T_p + (0.02 * \mu_1) + (0.038 * \mu_2) + (0.041 * \alpha_1) + (0.038 * \alpha_2) + 3.97 \right)} - 116.3s \quad (A-14)$$

Where, μ_1 and μ_2 are the coefficients of friction at the bottom sliding body-structure interface and sliding bodies interface within the stack, respectively. α_1 and α_2 are the mass ratios of the sliding bodies.

Design Problem

A numerical example has been provided to explain the process of the structural period calculation using the developed equations.

Problem Statement : Find the modified time period (T_{new}) for a structure with a natural time period of 0.7 sec. and coefficients of friction $\mu_1 = 0.3$ and $\mu_2 = 0.1$ with mass ratios of SBs $\alpha_1 = \alpha_2 = 1$ for Zone III and Zone V seismic hazard levels. The mass of the primary structure (m_p) is chosen as 200 kg.

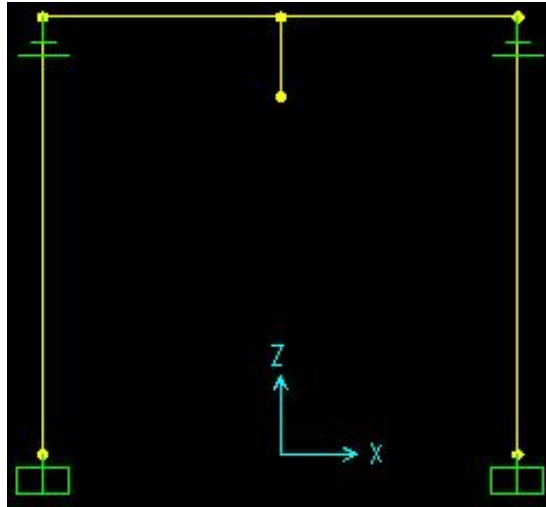
Solution:

Given data: $m_p = 200$ kg; $T_p = 0.7$ sec; $\mu_1 = 0.3$; $\mu_2 = 0.1$; $\alpha_1 = 1$; $\alpha_2 = 1$.

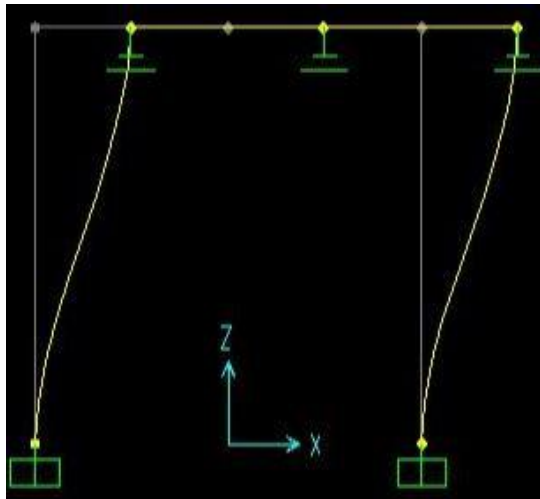
The values of the modified structural period of the PS (T_{new}) obtained from Eq. (A-13) and Eq. (A-14) for Seismic zones, III and V are 1.14 sec and 0.92 sec, respectively.

The design spectral accelerations (S_a) of the PS without SBs in Zones III and V for a given T_p can be obtained from Fig. 4.3 and are 0.22g and 0.52g, respectively. Due to the interaction of the stack of SBs, the structural period increases to 1.14 sec and 0.92 sec in Zones III and V, respectively. Thus, the design spectral accelerations of the PS in medium and highest seismic hazard levels are 0.14g and 0.31g, respectively. Therefore, the effective mass of the system is 530.44 kg in Zone III and 345.46 kg in Zone V. These parameters should be used in the seismic analysis and design of the PS.

Appendix 2: Structure with Hanging NSC (SAP 2000 Model)



SDOF structure with Hanging NSC



SDOF structure

List of Publications and Presentations

Journal Papers accepted/under-review

1. **S.P. Challagulla**, C. Parimi, Jagadeesh Anmala, “Prediction of Spectral Acceleration of a Light Structure with a Flexible Secondary System using Artificial Neural Networks”, *International Journal of Structural Engineering*, 10(4), pp.353-379 2020.
2. **S.P. Challagulla**, C. Parimi, S. Pradeep, Ehsan Noroozinejad Farsangi, “Estimation of Dynamic Design Parameters for Buildings with Multiple Sliding Non-Structural Elements Using Machine Learning”, *International Journal of Structural Engineering*, 2020, in press.
3. **S.P. Challagulla**, C. Parimi, P.K. Thiruvikraman, “Effect of the Sliding of Stacked Live Loads on the Seismic Response of Structures”, *Engineering Journal*, 24(4), pp.97-110, 2020.
4. **S.P. Challagulla**, C. Parimi, S.C. Mohan, E. Noroozinejad Farsangi, “Seismic Response of Building Structures with Sliding Non-Structural Elements”, *International Journal of Engineering*, 33 (2), pp.205-212, 2020.
5. C. Parimi, **S.P. Challagulla**, “Effect of Flexibly Attached Secondary Systems on Dynamic Behavior of Light Structures”, *SN Applied Sciences*, [Under-Review].

Conference Papers

1. **S.P.Challagulla**, Chandu Parimi, “Dynamic Behavior of Primary Structure Attached with Flexibly Connected Secondary Systems”, *REDECON-2016*, Bangalore, India, 9th-12th November, 2016.
2. **S.P.Challagulla**, Chandu Parimi, P.K.Thiruvikraman, A.Naringe, “Stick-Slip Phenomenon of Sliding Secondary Components and its Effect on the Horizontal Seismic Behavior of Single-Story Light Structures”, *International Conference on Structural Nonlinear Dynamics and Diagnosis (CSNDD)*, Tangier, June 25-27, 2018.
3. **S.P.Challagulla**, C. Parimi, A.Naringe, P.K.Thiruvikraman, “Seismic Behavior of Single-Story Light with Sliding Secondary Component Subjected to Near and Far-Field Earthquakes”, *11th Structural Engineering Convention*, Jadavpur University, Kolkata, India, 19th-21th December, 2018.
4. C. Parimi, **S.P.Challagulla**, “Seismic Response of Structures with Stacked and Sliding Live Loads”, *17th World Conference on Earthquake Engineering (17WCEE)*, Sendai, Japan, 13th-18th September, 2020.

Brief Biography of the Candidate

I am Challagulla Surya Prakash, a doctorate research scholar in the Department of Civil Engineering, BITS-Pilani, Hyderabad Campus. My research interests are the Seismic analysis of structures with heavy non-structural components, Seismic hazard analysis and Non-Linear dynamic analysis. Currently, we are working on the dynamic response of the structure with hanging and sliding non-structural components.

Brief Biography of the Supervisor

C.Parimi is working as an assistant professor in the Department of Civil Engineering at BITS-Pilani, Hyderabad Campus. He obtained his Ph.D. from North-western University, Chicago, IL, USA. He has worked as a Senior Structural Engineer in the nuclear power industry in the USA for five years. His research interests are eXtended finite element method (XFEM), computational mechanics, and structural dynamics.